UNIVERSITÀ DEGLI STUDI DI PADOVA

DIPARTIMENTO DI INGEGNERIA INDUSTRIALE

CORSO DI LAUREA MAGISTRALE IN INGEGNERIA ENERGETICA

TECHNISCHE UNIVERSITÄT BERLIN

INSTITUT FÜR ENERGIETECHNIK

Tesi di Laurea Magistrale in Ingegneria Energetica

A MEAN-LINE MODEL TO PREDICT THE DESIGN PERFORMANCE OF RADIAL INFLOW TURBINES IN ORGANIC RANKINE CYCLES

Relatori: *Prof. Andrea Lazzaretto*

Prof.ssa Tatjana Morozyuk (Technische Universität Berlin)

Correlatore: Ing. Giovanni Manente

Laureando: ANDREA PALTRINIERI

ANNO ACCADEMICO 2013/2014

Abstract

This Master Thesis contributes to the knowledge and the optimization of radial inflow turbine for the Organic Rankine Cycles application.

A large amount of literature sources is analysed to understand in the better way the context in which this work is located. First of all, the ORC technology is studied, taking care of all the scientific aspects that characterize it: applications, cycle configurations and selection of the optimal working fluids.

After that, the focus is pointed on the expanders, as they are the most important components of this kind of power production plants. Nevertheless. Their behaviour is not always wisely considered in an organic vision of the cycle. In fact, it has been noticed that mostly literature concerning the optimization of ORC considers the performances of the expander as a constant, omitting in this way an essential part of the optimisation process.

Starting from these observations, in this Master Thesis radial inflow turbines are carefully analysed, performing a theoretical investigation of the achievable performance.

Starting from a critical study of publications concerning the design of radial expanders, a theoretical model is proposed. Then, a design procedure of the geometrical and thermo dynamical characteristics of radial inflow turbine operating whit fluid R-245fa is implemented in a Matlab code.

The variation of turbine efficiency with the main turbine design parameters and working conditions is analysed to search for the optimum designs and extract an efficiency correlation based on operating conditions only. Results show to what extent the thermodynamic properties (volume expansion ratio and the size parameter) influence the turbine efficiency at the design point. The expectation is to address the search for optimum ORC design configuration, working fluid and cycle parameters through the evaluation of fluid properties from a wider perspective that comprises their impact on the real turbine behaviour.

Table of contents

Nomenclature

a	sound speed, m/s
A	area, m^2
AR	area ratio
b	blade height, m^2
bk	blockage factor
C	absolute velocity, m/s
C_p	diffuser pressure recovery factor
d	diameter, m
D_s	specific diameter
E	meridional velocity ratio
h	specific enthalpy, J/kg
i	incidence angle, deg
K	rotor loss coefficient
K_f	friction factor
K_p	nozzle total pressure drop
l	length, m
L	losses, J/kg
m	mass flow rate, kg/s
Ma	Mach number
MFR	fluid-to-hot source mass flow ratio
N	rotating speed, rpm
N_s	specific speed
N_t	typical speed
p	pressure, Pa
P	power, W
PF	performance factor, W/m^2, $PF= P/(2r_{in})^2$
Q	heat power, W
r	radius, m
r_p	pressure ratio
R	degree of reaction
Re	Reynolds number, $Re=U\ r/\nu$
s	specific entropy, J/(kg K)
th	blade thikness, m
T	temperature, K
U	tip speed, m/s
v	specific volume, m^3/kg
V	volumetric flow rate, m^3/s
VH	size parameter, m, $VH=(V_{out})^{0.5}/(\Delta h_{is})^{0.25}$
VR	volumetric flow rate variation, $VR=V_{out}/V_{in}$
$\dot{w}$	specific work, J/kg

W	relative velocity, m/s
Z	number of blades

Greek symbols

α	absolute velocity angle, deg
β	relative velocity angle,deg
β_b	blade angle, deg
γ	specific heat ratio
Δ	differential
ε	effectiveness
ε_h	nozzle static enthalpy loss coefficient
ε_r	radial gap, m
ε_f	axial gap rotor-casing
η	efficiency
λ	inlet blade height to inlet diameter ratio, $\lambda=b_4/d_4$
λ_P	power coefficient
ν	dynamic viscosity
ρ	density, kg/m^3
Φ	flow coefficient
φ_e	fraction of kinetic energy recovery
ψ	load coefficient
ω	rotating speed, rad/s

Subscripts and superscripts

0	total thermodynamic state
1	turbine nozzle inlet
2	turbine nozzle outlet
4	turbine rotor inlet
41	turbine rotor inlet after incidence losses
6	turbine rotor outlet
7	diffuser outlet
calc	calculated
Eu	Euler
F	friction loss
H	hub
HOT	relative to the hot source
HR	heat recovery
HX	heat exchanger
i	incidence loss
k	kinetic energy loss
in	inlet
is	isentropic
L	leakage loss
lm	log mean
m	meridional
ORC	relative to the Organic Rankine Cycle
out	outlet
p	passage loss
rms	root mean square
s	shroud

ts	total-to-static
tt	total –to-total
th	throat section
W-B	Whitfield-Baines

Denket auch daran, dass die Techniker es sind, die erst wahre Demokratie möglich machen. Denn sie erleichtern nicht nur des Menschen Tagewerk, sondern machen auch die Werke der feinsten Denker und Künstler, deren Genuss noch vor kurzem ein Privileg bevorzugter Klassen war, der Gesamtheit zugänglich und erwecken so die Völker aus schläfriger Stumpfheit.

Think also about the fact that are engineers who make true democracy possible. They facilitate not only the daily work of the people but also make the works of the finest thinkers and artists accessible to the public. The pleasure of these works had recently still been a privilege of the preferred classes. Thus the engineers wake the peoples from their sleepy bluntness.

Albert Einstein

Opening of the 7th German Radio and Audio Show
August, the 22nd 1930 in Berlin-Charlottenburg

Chapter 1

Introduction

Energy: a source of power, such as a fuel, used for driving machines providing heat etc. (from Oxford Dictionary).

From this short definition, it is not easy to understand the fundamental role that energy plays in shaping the human condition. People need energy to survive and to thrive, so it should be not surprising that energy production and consumption are some of the most important activities of the human life.

International institution as the World Bank, the United Nations and the European Union consider energy as a fundamental aspect to guarantee basic services as lightning, drinking water access, health services, education and communications. For these reasons, the non-equal distribution of energy sources is probably the main cause of civilisation inequity that characterise the contemporary world panorama. As a matter of fact, a large number of conflicts of the last forty years can be seen as a consequence of this aspect, especially related to access to fossil sources.

Standards of living and quality of civilisation for a long time have been considered proportional to the quantity of energy that a society use. This idea is nowadays not completely true anymore.

The increasing climate changes and the awareness that in non-far future fossil sources are going to end, suggest a new idea: a more sustainable use of energy.

In its first report in 2007, the IPCC (International Panel on Climate Change) formulated the following statement: “Most of the observed increase in global average temperatures since the mid-20th century is very likely due to the observed increase in anthropogenic greenhouse gas concentrations”. 84% of the greenhouse gases emissions are attributable to the energy sector, mainly in the form of carbon dioxide emissions. These emissions are mainly due to industrialized countries: the ten first emitting countries generate two thirds of the world emissions. It can be feared that the actual development of least-industrialized countries will be accompanied by a dramatic increase in CO_2 emissions.

In this context, a new idea of efficiency in energy use and production gains a social role, which has never had before. The struggle that the most developed countries started is felt as need widespread among a large part of the population.

This change requires massive investments in the Research and Development effort for renewable energies and for heat recovery technologies. Fortunately, an increasing number of industries sees this aspect as positive business: achieving a more efficient use of energy, they can save economical sources and gain a better role in terms of market image.

In this framework, the Organic Rankine Cycle is a technology that is achieving a large consensus, as it shows many advantages:

- It has a beneficial effect on energy intensity of several industrial processes, recovering waste heat that otherwise would be lost;
- It can convert renewable heat sources into electricity, as geothermal, biomass and solar heat;
- It is an reliable technology, as it uses the same components of a conventional steam Rankine plant;

The main difference between ORC and steam Rankine cycles lays in the typology of utilised working fluids: to guarantee a better thermal coupling with low-medium temperature heat sources, organic fluids are preferred to water. These fluids in fact are characterized by lower ebullition temperature then water, allowing a more efficient power generation from non-traditional heat sources (oil, coal, methane).

This Master Thesis refers to the main component of this power generation technology: the expander. In particular, radial inflow turbines are analysed, as they are a technology commercially utilised in the range from a few kilowatt to 2-5 MW.

A model is created to investigate the achievable performance, in order to show the correlation between turbine characteristics and operative conditions. Indeed, this feature is a missing aspect of many publications concerning system optimization: usually turbine efficiency is considered as constant value, leading to incorrect evaluation.

This Master Thesis has been developed in collaboration between the Università degli Studi di Padova, and the Technische Univerität Berlin. Thanks to “Erasmus” program, and to the agreement between Prof. Lazzaretto and Prof. Tsatsaronis, I had the possibility to spend six months in Berlin. In this period, under the supervising of Prof. Morozjuk, Ing. Manente and Prof. Lazzaretto, I developed the main part of the work at the “Institut für Energietechnik” of TU-Berlin.

Chapter 2

The Organic Rankine Cycle

The technology related to Organic Rankine Cycles is here introduced, giving an overview on the current state of the art. The main cycle layouts are presented in the first part, focusing on the basic, the regenerative and the supercritical ones. The main indexes used to study and compare different solutions are introduced. Then the most common and suitable applications of ORC are presented, focusing the main advantages that ORCs can bring in energy exploitation of several sources: geothermal, solar, biomass, heat recovery from industrial process and internal combustion engines. Lastly, an overview on the most utilised working fluids is carried out, analysing their characteristic and the main advantages that several authors found out.

2.1 Introduction

The Organic Rankine Cycle is a well-known technology since from the early 70s. A large amount of ORC plants have been built mainly for geothermal, waste heat recovery and combined heat and power applications. This technology shows a number of advantages over the traditional steam Rankine cycle, making it more profitable for power plants with a limited electrical power output (generally lower than 1MWe), even if they are able to achieve a lower efficiency. The temperature limitations of the heat sources, and the lack of constraints regarding the vapour quality at the end of the expansion, comport a different method of optimization [1].

The use of low and medium temperature energy, which is vast but often undeveloped topic, has been seen as one of the solutions to alleviate the energy shortage and environmental pollution problems. In this optic, the ORCs can use various types of heat sources including industrial waste heat, solar

energy, geothermal energy, biomass energy, etc. [2], which in the past have been considered as "lower quality" heat sources, if compared with hydrocarbons as oil, methane and coal.

In Figure (2.1) the utilization fields for ORC and micro ORC technology as a function of the electric power output and of the temperature of the hot sources are suggested [3]: the ORC technology gains large importance in low-medium temperature sources exploitation (range 100-450°C), for a power output between 100kW and 4MW.

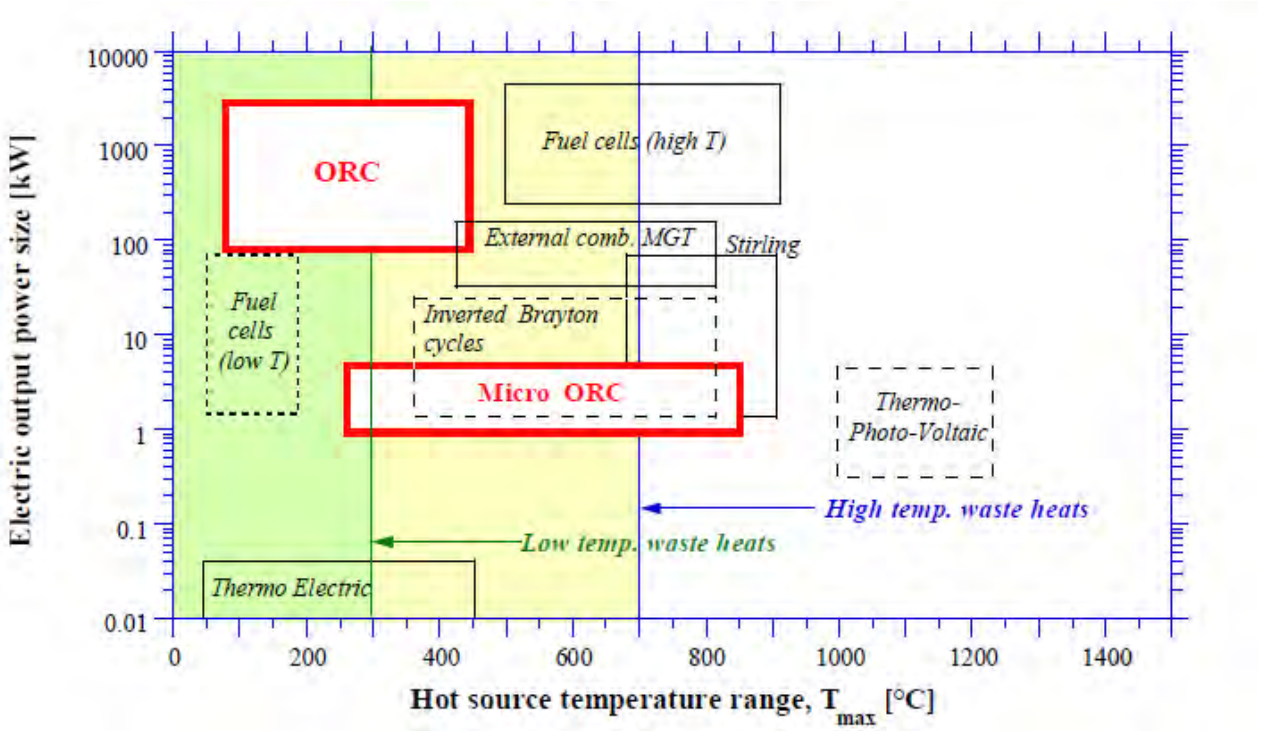

Figure 2.1 Comparison between ORC and other micro-small size power systems, as function of hot source temperature and power output [3].

The particularity of the ORCs over the traditional cycle lays in the working fluid. In fact, an organic component is here used instead of water. The organic compound used is generally a refrigerant, a hydrocarbon (butane, pentane, etc.), a silicon oil, a perfluorocarbon, etc. The particularity of these fluids is to have a boiling point lower than that of the water, and this feature allows recovering heat at lower temperature than in the traditional steam cycles [1].

Nowadays, more than 200 ORC plants are identified, with over 1800MWe installed, and the number is growing at a faster pace than ever before. [1]. The largest number of plant is installed for biomass and Combined Heat and Power applications, followed by geothermal and Waste Heat Recovery plants. Anyway, the first application in terms of installed power is geothermic [1].

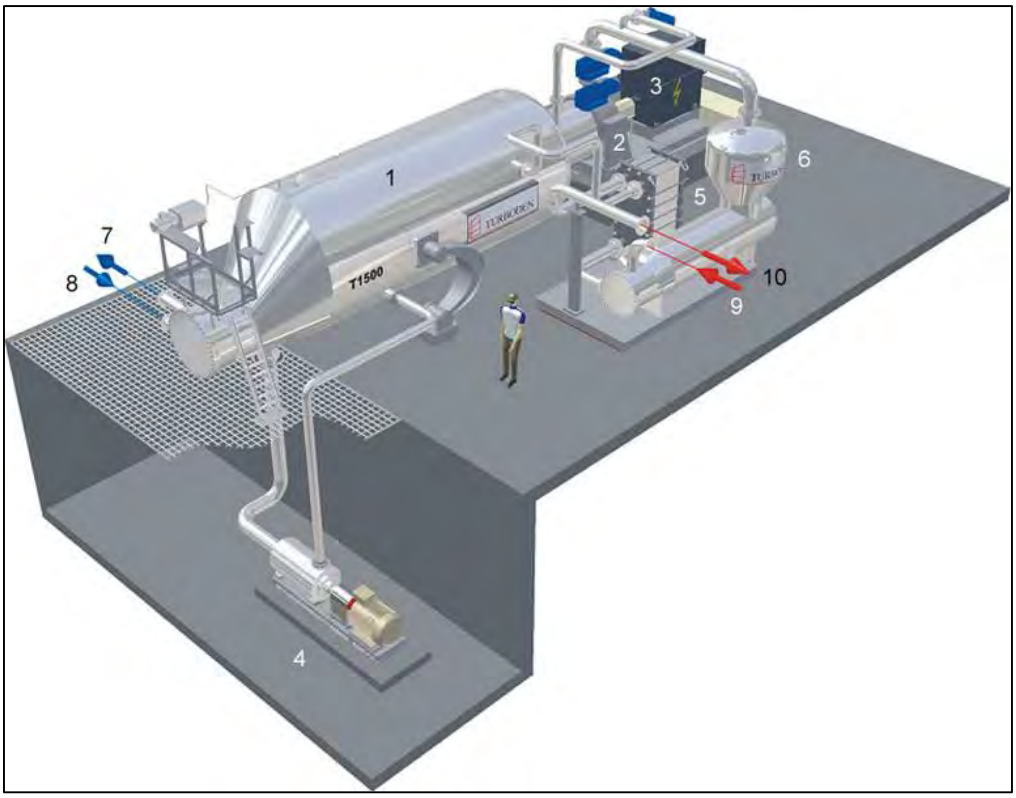

Figure 2.2 *Schematic representation of a 3MW ORC plant, [4]*

2.2 Cycle configurations and performance parameters

The layout of the Organic Rankine cycle is usually simpler than the traditional steam Rankine cycle. In fact, there is no water-steam drum connected to the boiler, and one single heat exchanger can be used to perform the three evaporation phases: preheating, vaporization and superheating [1].

As turbine bleeding and reheating are generally not suitable solutions for ORC, the variations on the cycle architecture are quite limited. It can be installed a heat recuperator as a liquid preheater between the pump outlet and the boiler inlet.

The basic cycle configuration is showed in Figure (2.3), and is very similar to the traditional steam cycle. The main phases can be summarized as:

- The fluid is heated up by the hot source in the evaporator (2-3). This process can be direct, as in a boiler where the organic fluid goes through the heater device, or indirect. In this case another fluid is utilised as heat vector from the hot source to an heat exchanger where the working fluid flows;
- The fluid is expanded in the expander device until the condensing pressure, producing mechanical work (3-4);

- The fluid is cooled down in the condenser (4-1) until the condensing temperature, changing from a gaseous phase to a liquid one;
- The liquid is pumped at the evaporation pressure back to the evaporator (1-2);

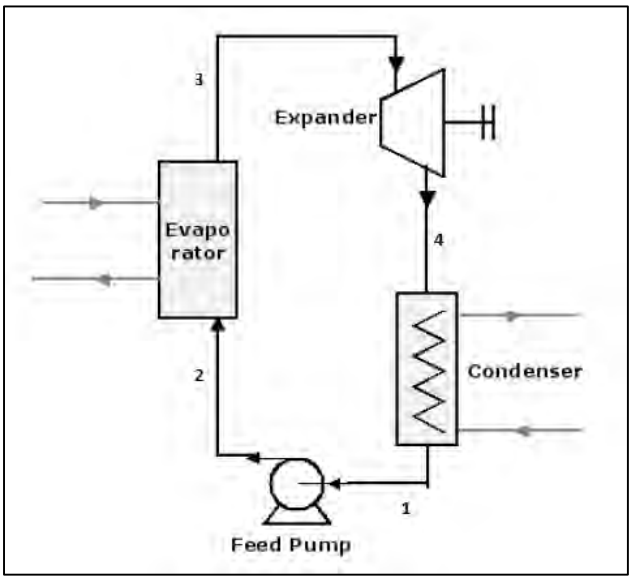

Figure 2.3 *Layout of the basic ORC [1]*

Moreover, the operative condition of the working fluid at the turbine inlet can comprehend a saturated or an overheated vapour. This condition requires the installation and the design of one more device: a super-heater after the evaporator. The difference in inlet condition is showed in the *T-s* diagrams of Figure (2.4).

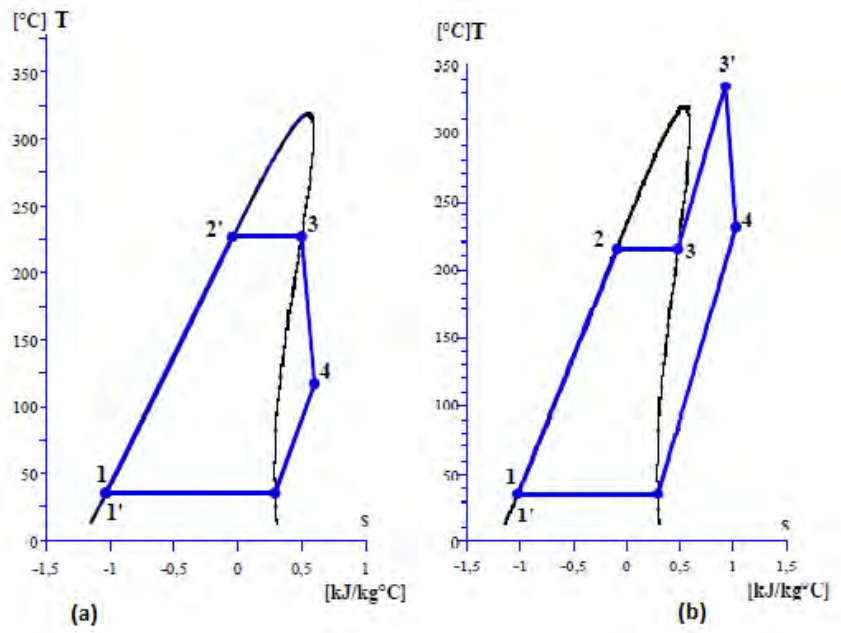

Figure 2.4 *Comparison on T-s diagram of a basic ORC (a) and an overheated one [5].*

A simple modification on the standard configuration leads to the regenerative cycle configuration. This design comprehends now the use of a heat exchanger, whose aim is to transfer heat from the turbine outlet to the evaporator inlet. The layout of the cycle is represented in figure (2.5a).
This internal heat exchange unit allows the heat input to be recovered at higher temperature, in order to achieve a higher cycle efficiency. In fact, referring to Figure (2.5b), the hotter fluid coming out from the expander (state 4) is able to be cooled down until the thermodynamic state 5, and in the meanwhile the fluid in 1 is heated up to state 2. If other parameters are constant, this simple modification of the cycle layout (only one heat exchanger is added) allows to recover a considerable amount of hot and cold sources.

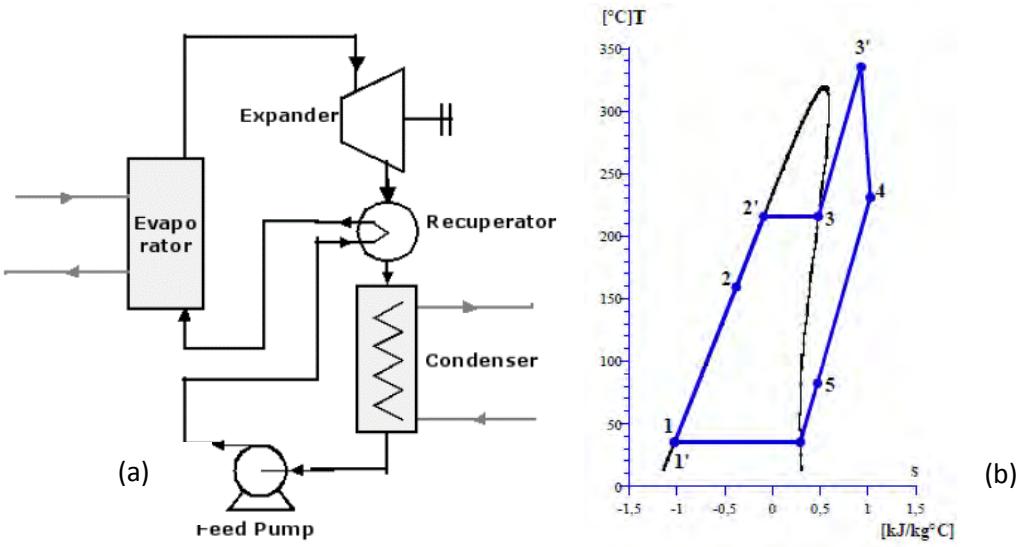

Figure 2.5 *Layout of ORC with heat regeneration (a). The regenerative cycle on T-s diagram (b) [5].*

The main aim of a large amount of literature about ORC is to quantify, discuss and compare the performances of various ORC solutions, in terms of cycle configurations, adaptability to a certain heat source, utilised working fluids.
In order to perform these tasks, is important to have useful comparison based on indexes, which should ideally be simple, aggregated and easy to obtain [3].
Branchini et al. in [3] propose six performance indexes as key indicators of ORC potential:

- ORC cycle efficiency:

$$\eta_{ORC} = \frac{P_{ORC}}{Q_{in,ORC}} \tag{2.1}$$

- ORC specific work:

$$W_{ORC} = \frac{P_{ORC}}{m_{ORC}} \tag{2.2}$$

- Turbine volumetric expansion ratio:

$$VR = \frac{V_{out}}{V_{in}} \tag{2.3}$$

- ORC fluid-to-hot source mass flow ratio:

$$MFR = \frac{m_{ORC}}{m_{HOT}} \tag{2.4}$$

- Recovery efficiency:

$$\eta_{rec} = \frac{P_{ORC}}{Q_{HOT}} = \frac{m_{ORC} W_{ORC}}{m_{HOT} \Delta h_{HOT}} = MFR \frac{W_{ORC}}{\Delta h_{HOT}} \tag{2.5}$$

- ORC heat exchangers surface:

$$\Sigma UA = \frac{1}{m_{HOT}} \Sigma_{HX} \left(\frac{\mathrm{Q}_{HX}}{\Delta T_{lm}} \right) \tag{2.6}$$

Where P_{ORC} is the ORC power output considering mechanical and electrical efficiency equal to 1; $Q_{in,ORC}$ is the ORC input thermal power, W_{ORC} is the specific work per unit of ORC mass flow rate at the turbine inlet, m_{ORC}; Q_{HOT} is the available thermal power from the hot source; Q_{HX} is the heat exchanged at the generic heat exchanger and ΔT_{lm} is the corresponding logarithmic mean temperature difference.

The first three indexes are mainly related to the bottoming cycle thermodynamics. η_{ORC} measures the conversion into useful power of $Q_{in,ORC}$, which is provided as input to the cycle in the evaporator. W_{ORC} affects the amount of fluid required for a design power output, and thus is related to the size of the system. VR is an indicator of turbine characteristic, which will be carefully analysed in §3.7. [5]

The other three considered parameters strongly depend on the decrease of temperature of the heat source, due to the heat exchange with the organic fluid. The *MFR* provides the amount of organic fluid required per unit of hot source mass flow. The parameter ΣUA is related to the sum of heat exchangers surfaces and can be considered as an indirect indicator of the cost of the heat exchangers. η_{rec} is a parameter that is proportional both to the cycle efficiency and to the efficiency of the heat recovery process, as expressed in equation (2.7):

$$\eta_{rec} = \frac{P_{ORC}}{Q_{in,ORC}} \cdot \frac{Q_{in,ORC}}{Q_{HOT}} = \eta_{ORC}\varepsilon_{HR} \tag{2.7}$$

Quoilin in [1] reported the evolution of the three parameters of Equation (2.7), as functions of the evaporation temperature of the cycle, using R-245fa. The heat is available at 180°C, and both the mass flow rate of the heat source and of the cooling water were fixed. It can be seen that the optimum for cycle efficiency does not correspond to the optimum overall efficiency $\eta_{rec,}$ due to the effect of $\varepsilon_{HR.}$

Anyway, the six identified indexes should provide a comprehensive information on energetic and size-economic performance of ORC systems [5].

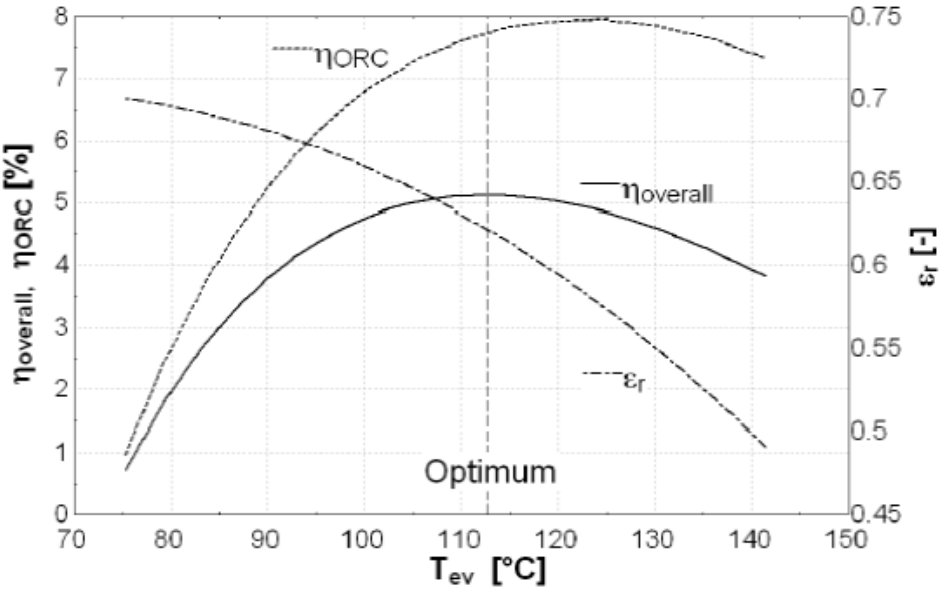

Figure 2.6 *ORC efficiency, heat recovery efficiency and overall efficiency as function of the evaporation temperature, in a waste heat recovery application [1].*

In the state-of-the-art applications, which are discussed nowadays, saturated or slightly superheated vapour is expanded in the turbine. However, the investigation of supercritical fluid parameters is of high importance, since it may lead to higher efficiencies making these plants even more attractive for waste heat applications.

Figure (2.7) shows the process of a subcritical (points 1, 2. 3, 4, 5) - and supercritical (points 1, 2', 3', 4' , 5') ORC in a *T*-*s*-Diagram for a constant superheated vapour temperature.

Even for constant temperature of the superheated vapour, the heat input occurs at a higher average temperature level in the case of supercritical vapour parameters, compared to subcritical. In reality, such high superheating of the subcritical vapour as shown in the diagram could not be realized due

to the tremendous heat exchange area needed due to the low heat-exchange coefficient of the gaseous phase [6].

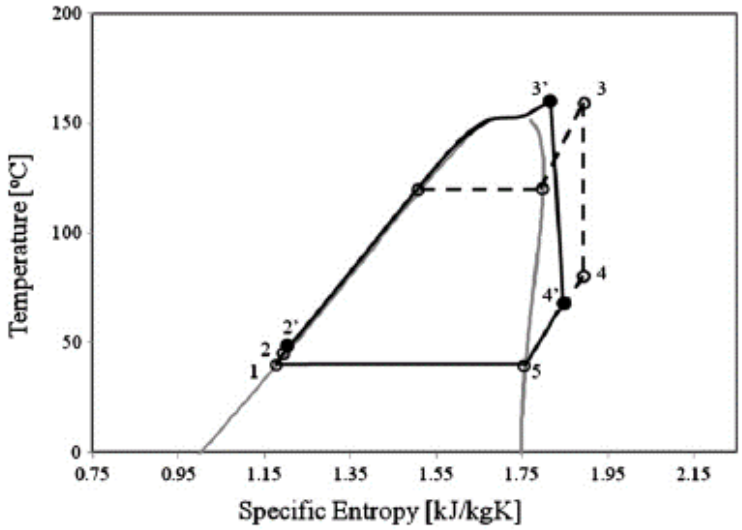

Figure 2.7 *Supercritical (continuous line) and subcritical (dashed line) ORCs on T-s diagram, fluid R-245fa [6].*

As the system efficiency is directly linked with the efficiency of the heat exchange system, as also expressed in Equation (2.7), it is obvious that the aim is to maximise the transferred heat [6].

The exploitation of the heat source in a supercritical ORC can be seen in the diagrams shown in Figure (2.8), which presents the characteristic *T-Q* diagrams of a heat exchanger under subcritical and supercritical parameters. On the diagram, it is possible to have an overview of the whole procedure from the inlet to the outlet point of the heat exchanger of the two flows, the heat source and the organic flow. The closer the two curves are, the lower the exergy destruction of the heat transfer procedure is. Another important characteristic is the pinch point, which is defined as the point of the procedure where the temperature difference between the two flows is minimum [6].

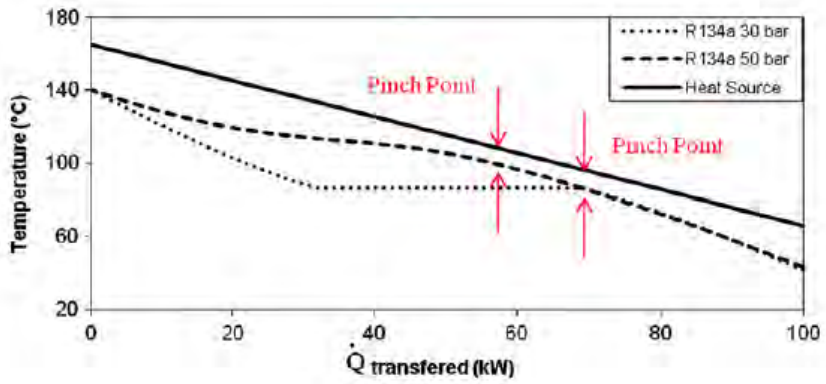

Figure 2.8 *T-Q diagram of heat exchange, fluid R134a. Live vapour parameters: 30 bar, 140°C (subcritical), 50 bar, 140°C (supercritical).*

As can be seen in Figure (2.8), in the supercritical cycle, there is no evaporation range, the state changes from liquid to vapour when the pseudo-critical temperature is reached. On the other hand, in the subcritical cycle the evaporation takes place under constant temperature, which is represented by the horizontal part of the fluid curve. As a result, the two curves are much closer in the case of supercritical conditions and therefore the exergy destruction during the heat exchange is much lower compared to subcritical conditions.

However, when the two curves are close, the logarithmic temperature difference (ΔT_{lm}) between the heat source and the organic fluid in each point is smaller and therefore a lower heat exchanger thermal efficiency is expected.

So in order to achieve the same heat flux and live vapour temperature, and thus the same heat exchanger efficiency as it happens in both cases of Figure (2.8), a much larger heat transfer area is required in the case of supercritical conditions.

Although the above considerations, cycle efficiency is not improved by supercritical conditions, which can nevertheless have a positive effect on the overall system performance.

Anyway, it has already been shown that cycle efficiency does not fully represent the overall system performance because of its negative affection on heat recovery effectiveness.

As a conclusion, it can be said that the application of supercritical fluid parameters in ORCs seems to raise the efficiency without disproportioned rise of installation costs [6]. However, it is very important to further investigate the heat transfer mechanisms in partial loads and transient procedures, and all the results should be verified by experiments and tests in actual ORC installations [6].

2.3 Applications

2.3.1 Biomass combustion

The use of ORCs process for Combined Heat Power production from biomass combustion is nowadays widespread, as many plats has been built in the last two decades [7].

Biomass is widely available in a number of agricultural and industrial process, such as woody industry or agricultural waste. It is as best used in local application for two main reasons [1]:

- The energy density of biomass is low, if compared to that of fossil fuels, which increase the transportation costs;
- Heat and electricity demand are usually available on site, which makes a biomass plant particularly suitable in case of off-grid conditions.

The ORC technology appears nowadays as the only proven one for decentralized applications for the production of power up to 1MWe from solid fuels like biomass [7].

The working principle of such a cogeneration system is showed in figure (n); heat from the combustion is transferred from the flue gases to the heat transfer fluid in two heat exchangers, at a temperature that generally varies between 150°C and 320°C, depending on the biomass quality. The heat transfer fluid (usually a thermal oil) is then directed to the ORC loop, in order to evaporate the working fluid, at a temperature slightly lower than 300°C [1]. Than the working fluid in the ORC follows the process also described in §2.2.

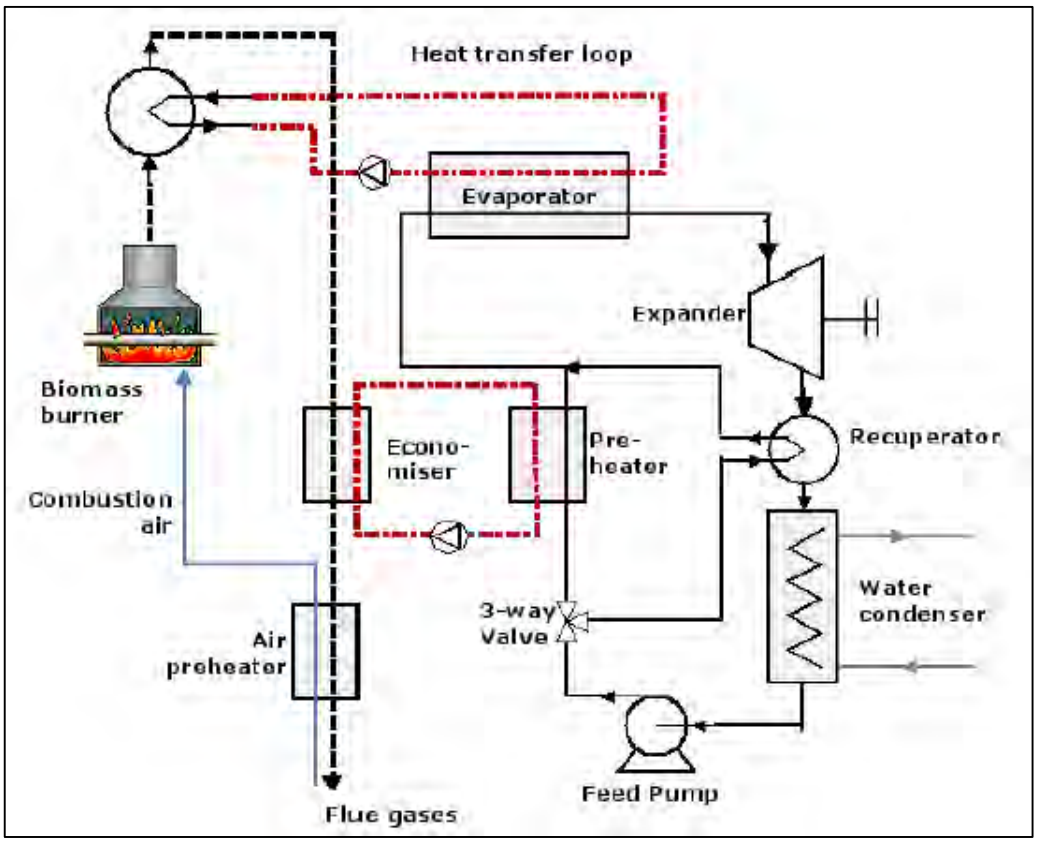

Figure 2.9 *Working principle of a biomass ORC and Combined heat and Power plant [1].*

Even if the efficiency of this kind of systems is low (meanly around 18%, decreasing for small-scale units), some advantages should be underlined [7]:

- The plant design is simple and standardized ;
- The system can work without maintenance , which leads to very low personnel costs;

2.3.2 Geothermal energy

Geothermal energy is a renewable form of energy originating in the heat that is naturally present in the deepest layers of the Earth (the average geothermal gradient in the Earth's crust is approximately 3 °C for every 100 metres towards the centre). This energy resource can be exploited by drilling deep wells and conveying the hot fluids (water and/or steam) trapped in the subsoil to the surface [4].
Geothermal heat sources are available over a broad range of temperatures, from a few tens of Celsius degrees up to circa 300°C. The actual lower bound is about 80°C, and below this temperature the energy conversion process efficiency becomes too small, so that geothermal plants are not economical anymore [1].
The typical scheme of a binary plant is showed in Figure (2.10). The geothermal hot fluid is pumped out from the boreholes, in order to heat up the organic fluid of the ORC. After the heat exchange, the geothermal fluid is re-injected in the wells.

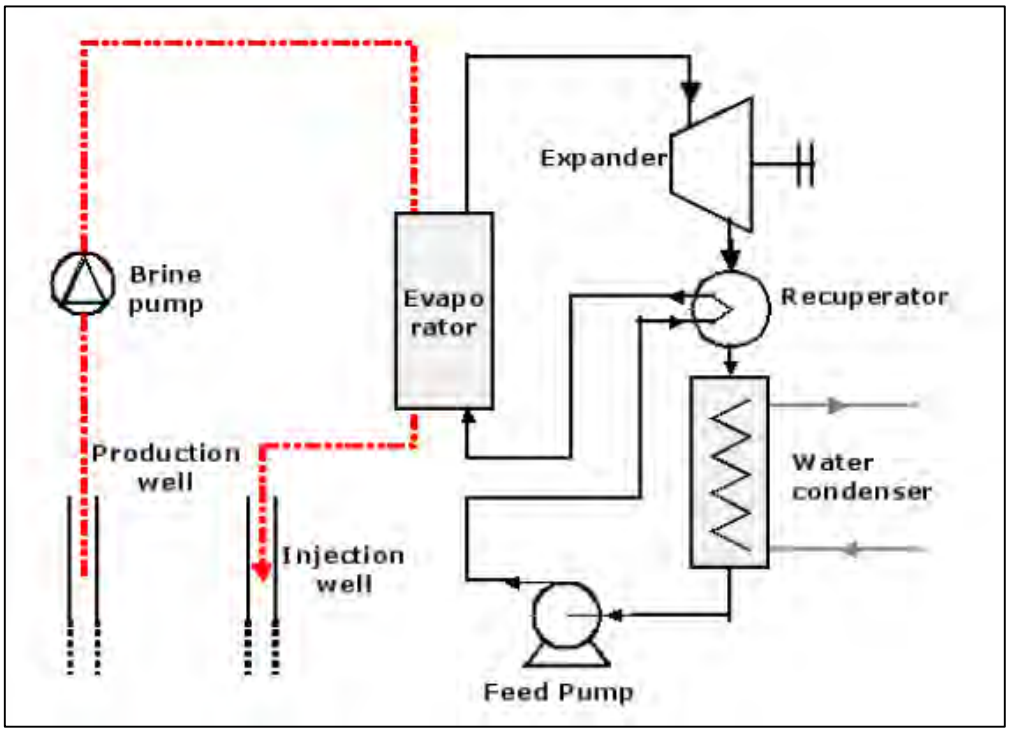

Figure 2.10 *Working principle of a geothermal ORC plant [1].*

Depending on the geological configuration, boreholes can be several thousand meters deep, requiring long periods of continuous work. This aspect lads to high investment cost of this kind of plants, in which drilling costs can reach 70% upon the total [1].

Low-temperature geothermal ORC plants are also characterized by a relatively high auxiliary consumption: the pumps consume from 30 up to more than 50% of the gross output. The main consumer is the brine pump that has to circulate the brine on large distances and with an important flow rate. The working fluid pump consumption is also higher than in higher temperature cycles, because the ratio between pump consumption and turbine output power ("back work ratio") increases with a decreasing evaporating temperature [1].

2.3.3 Solar power plants

The ORC technology is being used coupled with medium temperature solar collectors for commercial applications, thanks to its excellent results in terms of reliability. In fact, concentrating solar power is a well-proven technology: the sun is tracked and reflected on a linear or on a punctual collector, transferring heat to a fluid at high temperature. A specific solar collector in a region with a definite direct solar irradiance can maintain temperatures within restricted limits [1]. Therefore the highest allowed temperature for a working fluid in the ORC is not necessarily achievable through solar heat source. The hot fluid is then transferred to the ORC power plant, in order to heat up the organic fluid that will expand in the turbine. The basic scheme of this kind of plant is showed in Figure (2.11).

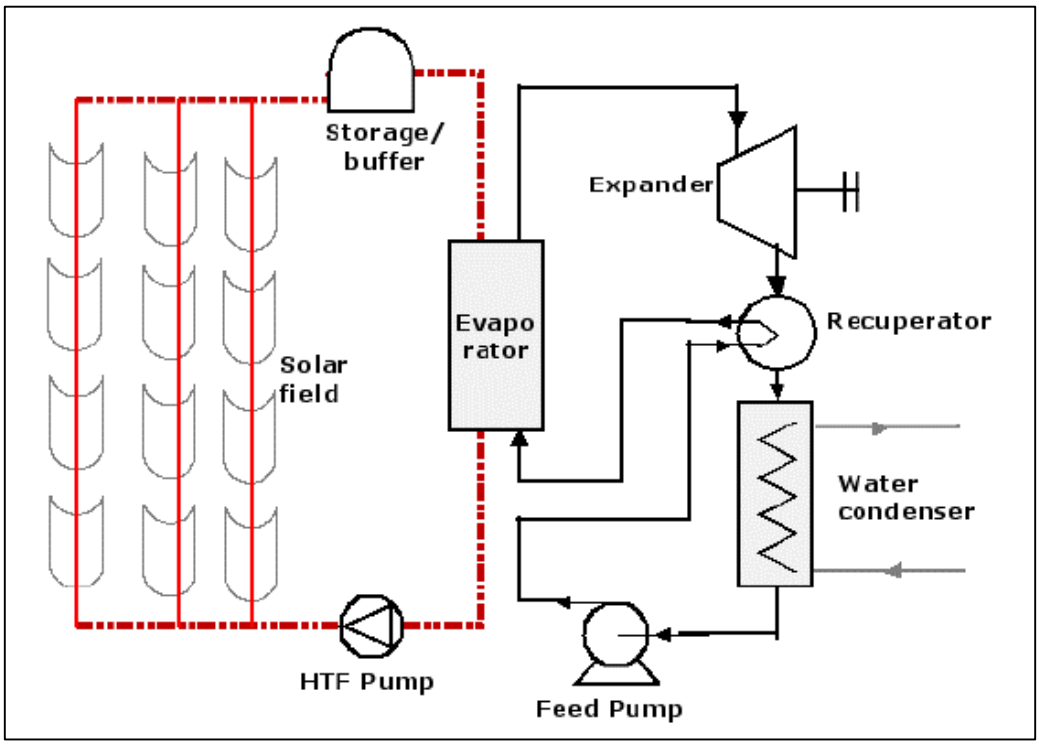

Figure 2.11 *Working principle of a solar thermodynamic ORC plant [1].*

The concentration technology that are nowadays mainly used are:

- Parabolic dish;
- Solar tower;
- Parabolic trough;

Parabolic dishes and solar towers are punctual concentration technologies, leading to a higher concentration factor and to higher temperatures [1]. Parabolic troughs instead work at a lower temperature range (300°C to 400°C). They were mainly coupled to traditional steam Rankine cycles for power generation, but the same limitation as in geothermal or biomass power plants remains: steam cycles require high temperatures, high pressures, and therefore high installed power to be profitable.

Organic Rankine cycles seem to be a promising technology to decrease investment costs at small scale: they can work at lower temperatures, and the total installed power can be reduced down to the kW scale.

2.3.4 Heat recovery from industry process and internal combustion engines

Many applications in manufacturing industry reject hat at relatively low-medium temperature. This heat has been seen for long time as a waste product of the productive processes, and for this reason largely unemployed, because overabundant [8]. The heat is therefore rejected to the atmosphere causing increase of pollutants concentration and affecting the environment of the close districts.

Heat recovery through the coupling of an ORC is a solution that is going to increase in the last years. Anyway, despite their large potential and low cost (circa 1000 to 2000€/kWe), waste heat recovery ORC only account for 10% of the installed ORC in the world in 2011, far behind biomass Combined Heat and Power and geothermal units [1].

Waste heat streams are typically in the form of liquid or gas. Their heat is transferred to the ORC working fluid, either directly or indirectly (with an intermediate medium closing loop), depending upon the characteristics of the waste heat source and other constrains.

Given the importance of the original industrial process over the heat recovery system, the heat recovery plant must be conceived as a “fail safe” device; this is to say that if the heat recovery system fails, the primary process will not be affected. This is usually achieved by having the heat exchanger with the primary heat stream in a bypass line, with the possibility of excluding this line whenever necessary [8]

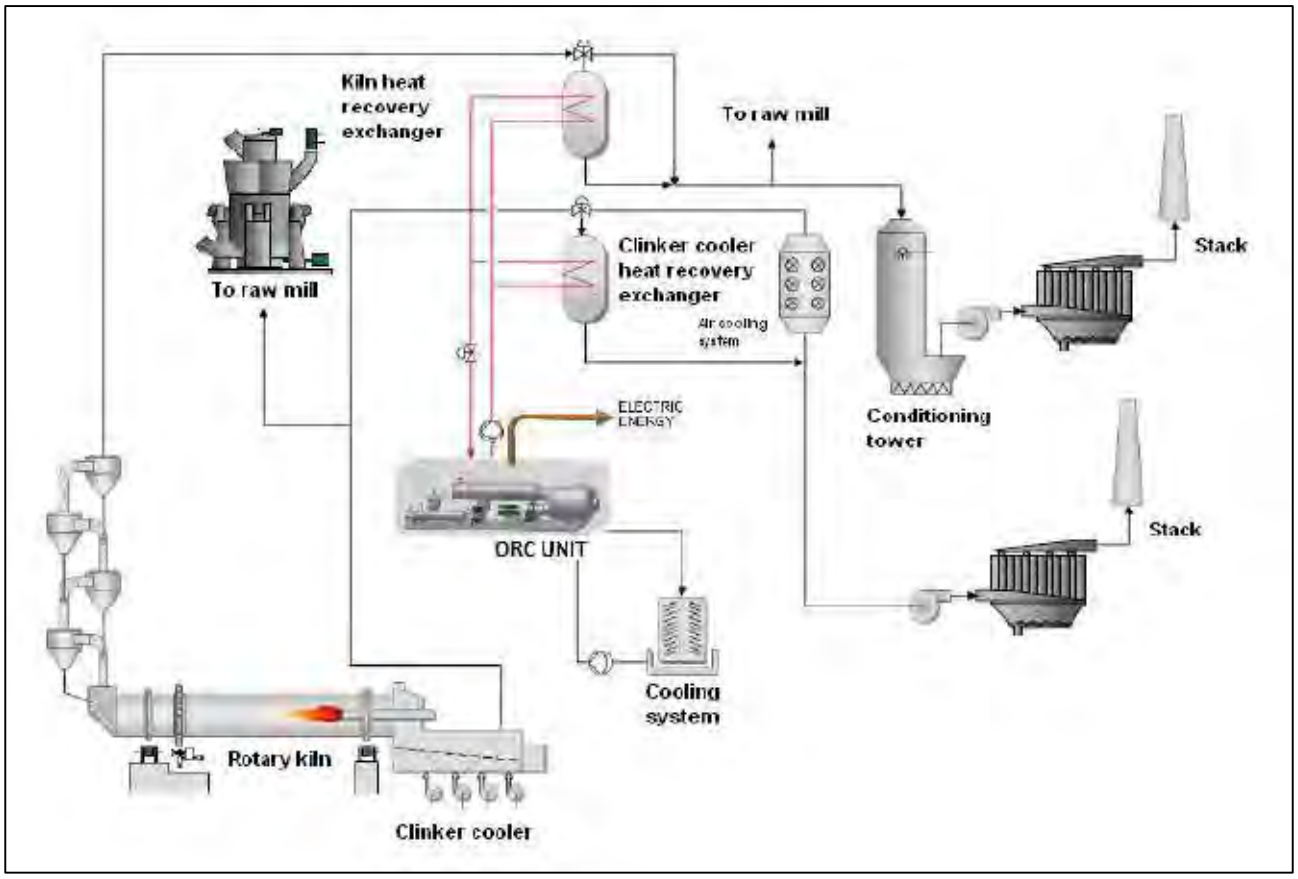

Figure 2.12 *Simplified scheme of ORC heat recovery system in a cement production process [8].*

The most important industrial processes suitable for the ORC heat recovery technology are the ones where energy consumptions has an important impact. Below is reported a list of potential applications:

- Cement industry: the cement production involves lime decarbonizing reactions, which being endothermic, requires great amounts of heat and high temperatures to take place. The unused heat supplied for these reactions can be found in the combustion gases, which via thermal oil recovery circuits, could be used as feeding sources of ORC. The mean production of a typical cement plant is in the range between 2000 and 8000 ton/day, with an energy consumption from 3.5 to 5 GJ/ton. As indication, the power that can be produced by an ORC het recovery system is in the range from 0.5 to 1MW/kton [8]. A schematic representation of this kind of plant is reported in Figure (2.12).
- Steel industry: in the steel production there are multiple waste heat sources where energy recovery with ORC is possible. They can be divided in relatively "clean" sources (fumes from rolling, pre-heating furnaces, forging pre-heating furnaces, thermal treatment) that are typically methane fuelled with a low dust content, and relatively "unclean" ones (fumes from blast furnaces, electric arc furnaces) [8].

- Glass industry: glass production involves the melting and the refining of raw materials, which take place at high temperatures. The unused heat supplied for glass production can be found in the combustion gases exiting the oven, and this flow can be used to feed the ORC heat recovery unit. It is not easy to define a general rule to guess the quantity of power producible from this kind of application, because glass production can show large variations in the typology of product, in the fuel employed and raw material size. Generally speaking, the exhaust gases temperatures are high (400-500°C), leading to high conversion efficiencies, up to 25%.

ORC can also be used in heat recovering from internal combustion engines. A typical engine in fact converts only about one third of the fuel energy into mechanical power, as a large amount of energy leaves the system through exhaust gases and through the radiator [1].

The first development of this idea followed the 70's energy crisis. Mack Trucks in 1976 designed and built a prototype of such system operating with exhaust gas of a 213kW truck engine, demonstrating the feasibility of the system. An improvement of 12.5% of the fuel consumption was reported [1].

Different architectures can be proposed to recover engine waste heat: the heat recovery system can be a direct evaporation system or a heat transfer loop system. In the first case, the evaporator of the ORC is directly connected to the exhaust gases. The advantage of such a configuration is the high temperature of the heat recovery, allowing higher cycle efficiency. In the second case, thermal oil is used to recover heat on the exhaust gases and is then directed to the evaporator. This second system acts as buffer and reduces the transient character of the ORC heat source, which simplifies its control [1]. In fact, the control of the system is particularly complex due to the transient regime of the heat source. However, optimizing the control is crucial to improve the performance of the system. It is generally necessary to control both the pump speed and the expander speed to maintain the required conditions (temperature, pressure) at the expander inlet [1].

2.4 Organic fluids

As the working fluid has largely influences the efficiency of the system, the size of the system components, the design of expansion devices, the system stability and environmental impacts, its selection plays a key role on ORC system performances.

The choice of the correct working fluid is a particularly complicated task, because the working conditions and the heat source have large variations in ORC (from 80°C geothermal low temperature to 500°C biomass applications). Moreover, in a defined operative temperature range, hundreds of

substances can be used as working fluids, including hydrocarbons, ethers, perfluorocarbons, clorofluorocarbons, alcohols, siloxanes etc. [2]

The main characteristics that are required in a working fluid are listed, concerning both physical and chemical features:

- Saturation vapour curve. This is one of the most crucial characteristic of the ORC's fluid, because it affects the cycle efficiency and the arrangement of associated equipments of the power generation system. Fluid can be categorized as "wet", "isentropic" or "dry", depending if the slope of the saturation vapour curve is respectively negative, vertical or positive. The three cases are showed in Figure (2.13). As typically the minimum dryness fraction at the outlet of the turbine has to be higher than 85% to avoid damages of turbine blades, dry and isentropic fluids are preferable. The use of a wet fluid instead requires a superheating section, which increases significantly the apparatus cost.

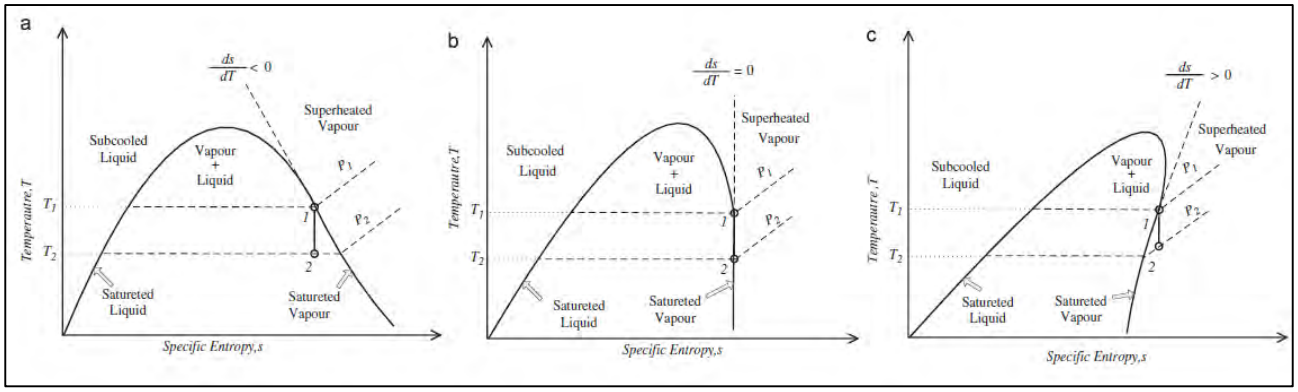

Figure 2.13 *T-s diagram for a wet (a), isentropic (b), dry (c) fluid [2].*

- Density, molecular mass. Fluids with higher molecular mass are preferable; for a certain condition defined by temperature and pressure a pure fluid that has this characteristic has higher density and lower specific volume. This leads to a reduction of the size of the components. Moreover, the expansion work tends to be in inverse relation to molecular weight, and this means that turbines for heavy fluids tend to have low peripheral speed and smaller number of stages [2]. On the other hand, this leads to large expansion ratios, causing problems with supersonic flows.
- Viscosity and conductivity. A low viscosity both in the liquid an in the vapour phases is required to maintain as low as possible friction losses. High conductivity moreover is an advantageous characteristic to obtain high heat transfer coefficient in the heat exchangers.
- Condensing gauge pressure. The condensing pressure is the lowest pressure achieved by the working fluid in an ORC. Its absolute value should possibly lay above the atmospheric

pressure in order to avoid air or water infiltrations. In this way special sealing for vacuum and degasser devices can be avoided and there is no threat of fluid deterioration caused by water and air contamination.

- Evaporating pressure. Usually the optimization process yields at determining the optimum evaporation pressure for each fluid. For a given condensing temperature, the evaporation pressure will be as high as possible to maximise the cycle efficiency, but low enough to keep the maximum cycle temperature far enough from the heat source temperature profile (through the pre-set pinch point constraints) and from the critical temperature. The example of Figure (2.14) shows the influence of evaporating pressure on the irreversibility of the heat transfer process; in (2.14b) the temperature profile of the working fluid better follows the temperature profile of the heat source, and this means that temperature difference between the two fluids in the heat exchangers is reduced, hence the irreversibility are reduced.

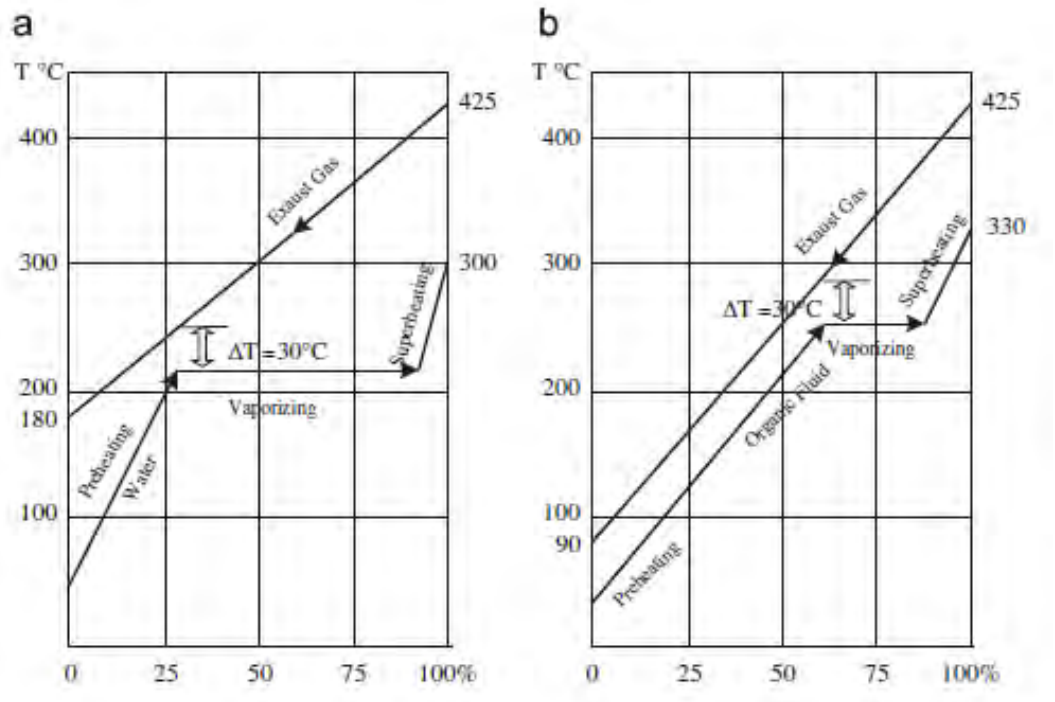

Figure 2.14 *Effects of the evaporating pressure on the heat exchange [2].*

- Boiling and freezing point. As the fluid should easy to handle at ambient environment, the boiling point temperature is expected to be in the range fro 0°C to 100°C. Moreover, the freezing point must be lower than the lowest temperature achieved by the cycle.
- Safety level. Safety includes two main parameters: the toxicity and the flammability. The ASHRAE Standard 34 classifies refrigerants in safety groups and can be used for the evaluation of a fluid. It contains a character (A: Lower Toxicity; B: Higher Toxicity) and a

number (1: No flame propagation; 2: Lower flammability; 3: Higher Flammability). For example,HCFC-123 is classified as B1, i.e. higher toxicity – no flame propagation [1].

- Ozone Depleting Potential (ODP): The ozone depleting potential is measured with comparison to the ODP of the R11, set to the unity. The ODP of current refrigerants is either null either very close to zero, since non-null ODP fluids are progressively being phased out by the Montreal Protocol (1987) [1].
- Greenhouse Warming Potential (GWP): GWP is measured with comparison to the GWP of CO2, set to the unity. Although some refrigerants can reach a GWP value as high as 1000, there is no legislation restricting the use of high GWP fluids.

From the structural point of view and type of atoms in the molecule, the ORC can be categorized under seven main classes, which are collected in Table (2.1).

Class	Characteristics
Hydrocarbons, including linear (n-butane, n-pentane), branched (Isobutane, Isopentane), and aromatic (Toulene, Benzene)	• Desirable thermodynamic properties; • Flammability issues;
Perfluorocarbons	• Extreme inert and stable; • Extreme molecular complexity; • Thermodynamically undesirable
Siloxanes	• Attractive for a mix of physical and thermal properties (low toxicity and flammability level; high molecular mass; prolonged use as a high temperature heat carrier); • They are often available as mixtures rather than as pure fluids; • Isobaric condensation and evaporation are not isothermal and exhibit a certain glide;
Partially flouro-substituted straight chain hydrocarbons	• There are several zero ODP fluids among them which are of considerable potential interest
Ethers and fluorinated ether	• Flammability and toxicity issues; • Thermodynamically undesirable;
Alcohols	• Flammability issues • Soluble in water • Thermodynamically undesirable
Inorganics	• Extensive and inexpensive; • Small environmental impact; • Some operation problems;

Table 2.1 *Main classes of fluids suitable for ORC [2].*

While fluid selection studies in the scientific literature cover a broad range of working fluids, only a few fluids are actually used in commercial ORC power plants. These fluids are the following, classified in terms of critical temperature [55]:

- HFC-134a: Used in geothermal power plants or in very low temperature waste heat recovery.
- HFC-245fa: Low temperature working fluid, mainly used in waste heat recovery.
- N-pentane: Used in the only commercial solar ORC power plant in Nevada, US. Other applications include waste heat recovery and medium temperature geothermy.
- Solkatherm: Waste heat recovery.
- OMTS: CHP power plants.
- Toluene: Waste heat recovery.

According to Wang et al. [9], the optimal selections of working fluids corresponding to the heat source temperature level are shown in Figure (2.15)

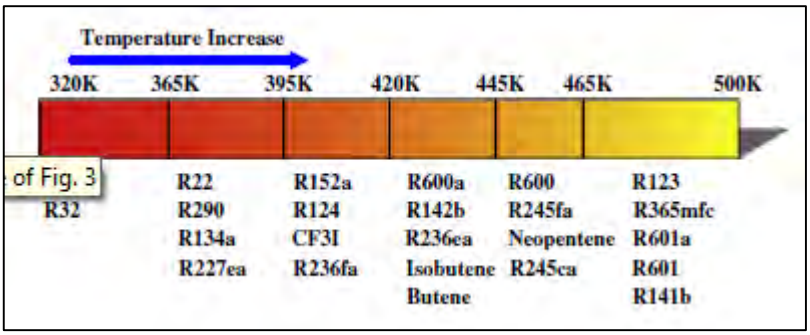

Figure 2.15 *Optimal selections of working fluids corresponding to the heat source temperature level [9].*

To conclude, there is not a working fluid suitable for any organic Rankine cycle system. At the same time, the working fluid selection should not only consider the thermodynamic performances and the system economy, but also consider other factors, such as the maximum and minimum bearable temperature and system pressure, expanders or turbines design and environmental and safety considerations.

Chapter 3

Radial turbines design

This chapter has the aim to introduce the theoretical background required for the design procedure of a radial expander, and more generally of a turbomachine. The first part concerns the classical similitude theory, which can be considered as the basis of the most of the design process usually proposed. Then other useful parameters are introduced, focusing the limits of the similitude theory, and pointing out the importance of the size of the expander and the fluid properties through the device.

3.1 Introduction

In order to state a convenient design process, the designer has to run firstly a meanline analysis and a correlated optimization.

These first steps play a key role in the whole turbine design procedure. In this particular case, the evaluation of achievable efficiency of Radial Inflow Turbines can also be seen as an important part in the design of the cycle configuration of an Organic Rankine Cycle [10].

In the one-dimensional optimization, several variables are chosen, both at the inlet and at discharge of the turbine, which are usually required by the application, such as pressure ratio, required power or mass flow rate. The principles of fluid and thermo dynamic used in the process simulation are able to give an estimation of the most important parameters involved (geometrical radii and blade angles, thermo dynamic and fluid dynamic quantities) [11].

In a subsequent step, they will be the input variables, in order to estimate the efficiency of the component and the main sources of power losses. Following this, the full blade geometry should be

defined in order to be able to make a detailed analysis of the flow in the blade passages, and a structural analysis of the rotor. In fact, once fully blade and rotor shapes are available, the designer can progress with a three-dimensional analysis of the flow through the blades, both with Euler codes (inviscid) or Navier-Stokes codes (viscous). At the same time, a similar study can be operated on the structure of the blades and of the rotor, with an evaluation of stresses in those parts, which are mostly exposed to fracture or damaging risk. These several steps could lead to a process drop back, in order to change some critical parameters and study their influence in the latter output [12].

The one-dimensional analysis is thus a key part of the design system; not only is used to initiate the design itself, but it will often be returned to several times during the process. This is required, to evaluate the effects of design changes, which are considered necessary in the light of later results, and to optimize further the design [11].

A poor application of the one-dimensional analysis can lead to time wasting in fluid dynamics and mechanical analysis, run in conditions not close to efficiency optimum. Anyway, is important to state that any model used in preliminary design is inevitably a very simplified representation of the real flow, especially for what concern the passage of the working fluid in the rotor, which has an extremely complex configuration, being unsteady, three-dimensional, viscous, supersonic or transonic[11].

3.2 Similitude theory

Classically, the preliminary theoretical bases to study turbomachines performances are related to similitude theory.

Formally, this permits to reduce several variables, representing a typical physical phenomenon, into a smaller number of non-dimensional groups [12]. The two main advantages of this approach are [13]:

- Possibility to predict the performance of a prototype device, basing on tests run with a scale model;
- Possibility to define the most advantageous kind of turbomachines, on the basis of the highest efficiency achieved for a certain enthalpy drop and mass flow rate;

The performance of a turbo-machine can be expressed utilising some control variables, some geometrical variables, and some fluid properties. In particular, as this Master Thesis refers mainly to radial turbines operating with compressible fluids, we will describe in this section the similitude theory related to this kind of devices. In this way, the typical variables are:

- Control variables: m (mass flow rate), ω (rotational speed);

- Geometrical properties: D, l_1, l_2,..., l_n, d_1, d_2,..., d_n;
- Fluid properties: μ (dynamic viscosity), ρ_{01} (density at the inlet of the machine), γ (specific heat ratio), a_{01} (total speed of sound at the inlet of the machine);

Thus ρ and a are values subjected to variations during the machine crossing, they are referred to a certain condition, in this case the inlet one [13]. The performance parameters, which are considered as dependent variables, are the total isentropic enthalpy drop ($\Delta h_{0,s}$), the efficiency η, and the power output (P). They can be then expressed as function of the independent variables as:

$$\Delta h_{0,s} = f_1\left(\mu, \omega, D, m, \rho_{01}, a_{01}, \gamma, \frac{l_1}{D}, \frac{l_2}{D}, \dots, \frac{l_n}{D}, \frac{d_1}{D}, \frac{d_2}{D}, \dots, \frac{d_n}{D}\right) \tag{3.1}$$

$$\eta = f_2\left(\mu, \omega, D, m, \rho_{01}, a_{01}, \gamma, \frac{l_1}{D}, \frac{l_2}{D}, \dots, \frac{l_n}{D}, \frac{d_1}{D}, \frac{d_2}{D}, \dots, \frac{d_n}{D}\right) \tag{3.2}$$

$$P = f_3\left(\mu, \omega, D, m, \rho_{01}, a_{01}, \gamma, \frac{l_1}{D}, \frac{l_2}{D}, \dots, \frac{l_n}{D}, \frac{d_1}{D}, \frac{d_2}{D}, \dots, \frac{d_n}{D}\right) \tag{3.3}$$

These equations can be then written in the implicit form:

$$\varphi_1\left(\Delta h_{0,s}, \mu, \omega, D, m, \rho_{01}, a_{01}, \gamma, \frac{l_1}{D}, \frac{l_2}{D}, \dots, \frac{l_n}{D}, \frac{d_1}{D}, \frac{d_2}{D}, \dots, \frac{d_n}{D}\right) = 0 \tag{3.4}$$

$$\varphi_2\left(\eta, \mu, \omega, D, m, \rho_{01}, a_{01}, \gamma, \frac{l_1}{D}, \frac{l_2}{D}, \dots, \frac{l_n}{D}, \frac{d_1}{D}, \frac{d_2}{D}, \dots, \frac{d_n}{D}\right) = 0 \tag{3.5}$$

$$\varphi_3\left(P, \mu, \omega, D, m, \rho_{01}, a_{01}, \gamma, \frac{l_1}{D}, \frac{l_2}{D}, \dots, \frac{l_n}{D}, \frac{d_1}{D}, \frac{d_2}{D}, \dots, \frac{d_n}{D}\right) = 0 \tag{3.6}$$

By the use of dimensional analysis, a group on n-variables can be here expressed as a function on (n-3) non-dimensional groups. They are obtained fixing three non-dependent variables; in this case ρ_{01}, ω, D are chosen for this purpose, so that the following non-dimensional groups are obtained (calculations are here omitted):

- Load coefficient:

$$\Psi = \frac{\Delta h_{0,s}}{\omega^2 D^2} \tag{3.7}$$

- Flow coefficient:

$$\Phi = \frac{\mathrm{m}}{\rho_{01}\omega D^3} \tag{3.8}$$

- Power coefficient:

$$\lambda_P = \frac{\mathrm{P}}{\rho_{01}\omega^3 D^5} \tag{3.9}$$

- Reynolds number:

$$Re_{01} = \frac{\rho_{01}\omega D^2}{\mu} \tag{3.10}$$

- Mach number:

$$Ma_{01} = \frac{\omega D}{a_{01}} \tag{3.11}$$

It should be underlined that the similitude theory involves a geometrical similitude. This means that the machines appertaining to the same family must have a constant ratio between relative dimensions [13].

This aspect, as will be shown in the following sections, is a characteristic that several authors do not properly take into account while they study the performance of radial turbines. Instead, this request is focal in the considerations about efficiency and operative conditions of the expanders.

Moreover, a fluid dynamic similitude is required, in the meaning that the flow must have similar triangular velocity in correspondent points. This implies a geometrical similitude of flow lines and a similar distribution of velocity vectors, perpendicular to the flow lines [13].

Several common applications of radial turbines require them to work with the exhaust gases of hydrocarbons combustion, but frequently scaling or verification testing is done using air for convenience. Fortunately, both exhaust gases of this type and air at the above ambient temperature are near-perfect in behaviour, and so the scaling rules can be applied with confidence providing it is recognized that the gases have different specific heat ratios γ and gas constants R *[11]*. Other applications such as process expanders work with a variety of organic and refrigerants fluids, often complex mixtures with many components, and with a behaviour which is far from ideal. These steam turbines constitute non-ideal cases, so that it would not be appropriate to apply the simple scaling rules to an air turbine to work with condensing steam, a refrigerant gas, or an organic fluid, for the results of the scaled machine would almost differ from the original design in ways which are very difficult to predict. A higher level of design, recognizing the quite different fluid properties, is required in cases like this [11].

3.3 Preliminary design of radial inflow turbines based on loading and flow coefficients

In radial turbines, there is a wide variation in blade speed due to radius change between the inlet and the exit section. Thus, unlike axial turbines where the blade speed is nearly constant through a blade row, the choice of blade speed used to define the coefficients is arbitrary. In this work, it has been chosen in accord to the definition expressed in Moustapha et al. "Axial and Radial Turbine" [11].
The inlet blade velocity was chosen as the reference velocity; in this way, we can express the loading coefficient as:

$$\psi = \frac{\Delta h_0}{U_4^2} = \frac{C_{u4}}{U_4} - \varepsilon \frac{C_{u6}}{U_4} \tag{3.12}$$

Where $\varepsilon = r_4/r_6$ is defined as the rotor radius ratio.
Sometimes the designer can plan to have a non-zero exit swirl, because this practice can be useful to rise the diffuser efficiency; in most of the cases anyway, is a common practice that the exit swirl is fairly small in order to maximize the specific work, as expressed in the following Euler work equation [11]:

$$W_x = U_4 C_{u4} - U_6 C_{u6} \tag{3.13}$$

As clearly shown by the equations, the maximum specific work is reached if $C_{\theta 6} = 0$.
In this case the loading coefficient can be expressed as:

$$\psi = \frac{C_{u4}}{U_4} \tag{3.14}$$

The flow coefficient is defined in the following way:

$$\Phi = \frac{C_{m6}}{U_4} \tag{3.15}$$

Figure (3.1) shows a statistic correlation between total-to-static efficiency and these design parameters [14]. From this graph, it could appear that the best design parameters could be easily chosen in the range of 0.2-0.3 for Φ, and 0.9-1.0 for Ψ. This statement is not completely true: many

designers reached high efficiency with quite different design parameters, because in many cases the application constrains the design; this is particularly apparent in automotive turbochargers, where size and rotating inertia are overwhelmingly important. In fact, with a higher than optimal flow coefficients increases the meridional velocity at exit (C_{m6}), for a given mass flow rate the exit area is reduced, and this implies a more compact stage [11].

Moreover, the statistics from which the graph is extrapolated concern turbines working with ideal gas (air, exhaust gases), so that could not be a priori generalized also for different fluids, as the ones analysed in this work.

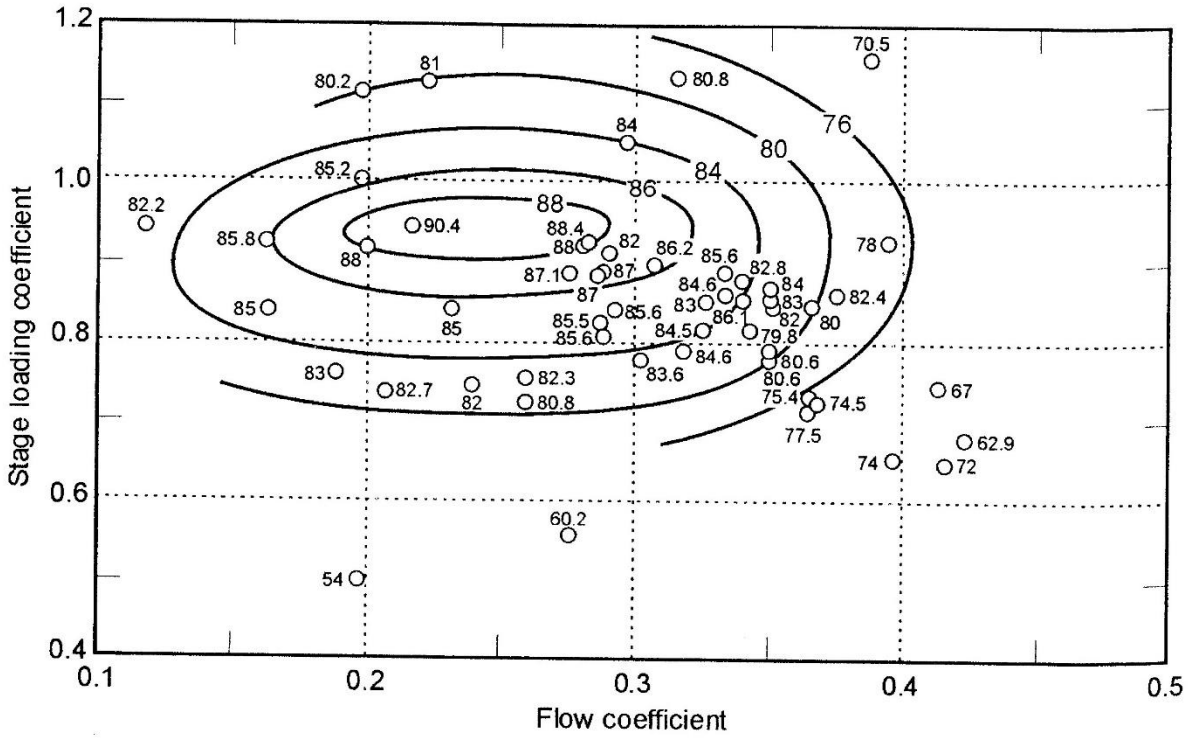

Figure 3.1 *Statistical correlation of total-to-static efficiency, as function of Φ and ψ[14]*

For example, in [15], a model run on RITAL software [16] has the aim to study different fluids related to optimised turbines. The starting point of the design are the conditions of inlet and outlet, but the parameters Φ and Ψ are chosen a priori, on the basis of the figure, which suggests that a turbine designed with Φ=0.215 and Ψ=0.918 could reach an efficiency around 90%. This approach can be a huge limitation of the analysis validity, because there is no way to prove that for different operating fluids this design condition could be the optimum one. In fact, the maximum efficiency reached by the different turbines is always lower than 80%.

For all these reasons, one of the aim of the model proposed was to find the highest efficiency configuration, starting the design with different values of Φ and Ψ.

3.4 Specific speed parameters

In order to select the correct type or form of machine to meet particular performance, the designer can refer to non-dimensional parameters. Baljè [17] makes extensive use of concepts of specific speed and specific diameters.

The specific speed is then defined as:

$$N_s = \frac{\omega\sqrt{V}}{\Delta h_0^{3/4}} \tag{3.16}$$

Specific speed is a non-dimensional parameter if ω is given in [rad/s] and Q and Δh_0 in consistent set of units such as [m^3/s] and [J/kg] respectively. This factor is function only of the operating conditions and contains no parameters directly related to geometry: it has not an obvious physical meaning, but it can be used to describe the general form or shape of a turbine [11].

Statistic studies based on a large number of turbine are shown in Figure (3.2)

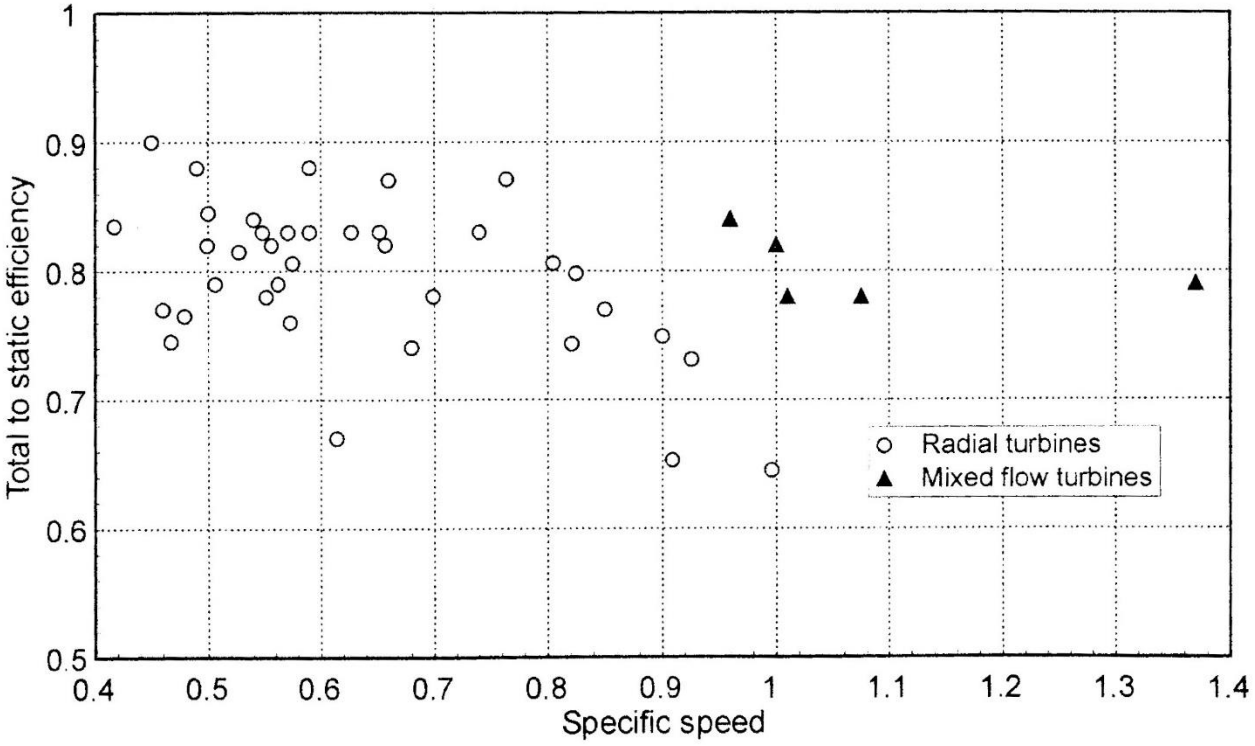

Figure 3.2 *Mesured efficiency as a function of specific speed for radial and mixed flow turbines [11].*

The peak of efficiency of radial turbines is around the values 0.4-0.8. However, in this range of *Ns* there is a gap of 15-20% between the best and the worst turbines efficiency. It means that the use of an appropriate specific speed does not automatically lead to a high efficiency design [11].
In the work presented, the specific speed is not considered an input parameter, but is anyway a good indicator of the quality of the design procedure, if it is included in its ideal range.
Another non-dimensional parameter strictly correlated to specific speed, that also includes the typical dimension of the turbomachine is the specific diameter [12]:

$$D_s = \frac{D\Delta h_0^{1/4}}{\sqrt{V}} \tag{3.17}$$

Where *D* expressed in [m] is a representative diameter, in our case the inlet one D_4.
In literature several studies that correlates *Ns* and *Ds* were presented: in particular is worthy to present the "*Ns-Ds* Chart", in which are represented the best efficiency point reached for each couple of parameters, producing the so called "Cordier Line", reported in Figure (3.3) [12]. This chart represents the state of the art of designs available at the date of their construction, so that as turbomachine performance improves, it is necessary to keep this chart up to date [12].

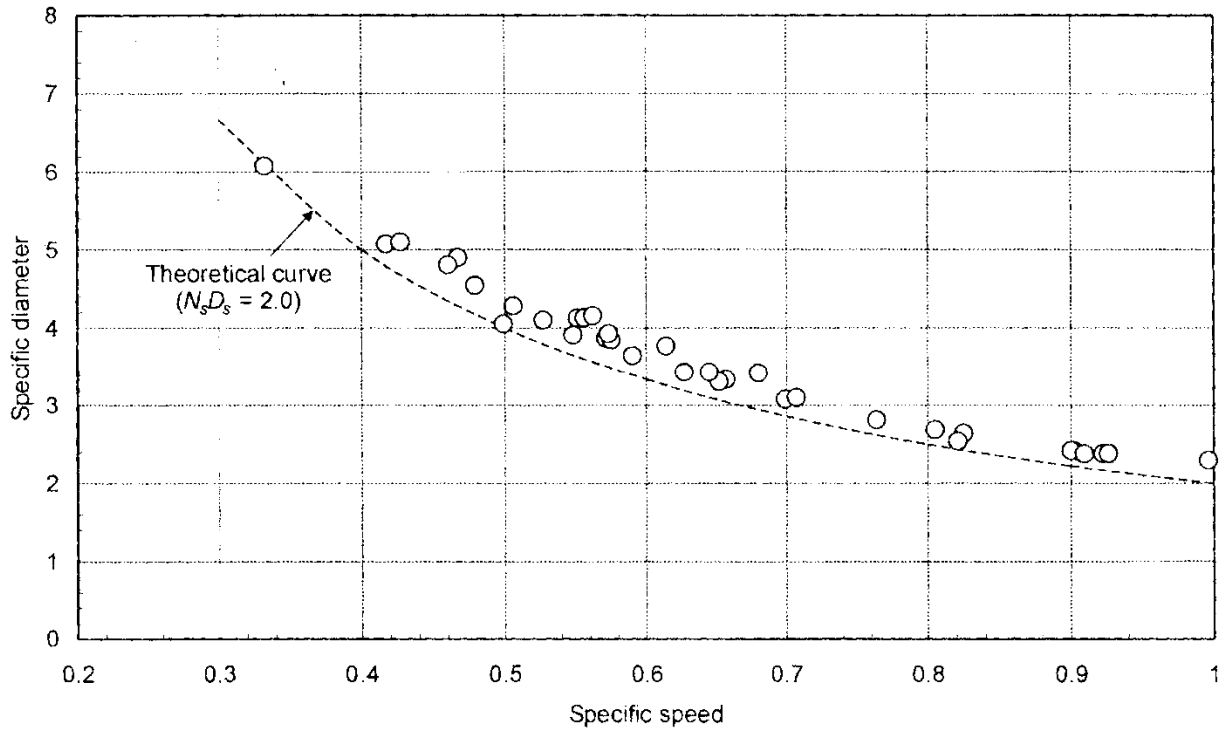

Figure 3.3 *Correlated specific speed and specific diameter for radial inflow turbines, "Cordier line" [11].*

3.5 Link between flow-load coefficients and specific speed coefficient

Some authors obtained the specific speed and the specific diameter parameters showed in the previous Equation (3.16) and (3.17) by the combination of flow and load coefficients (as in the case of Whitfield and Baines in [12]). The definition of Φ and Ψ can be considered completely arbitrary, so that each author can suggest his own way.

Following the definition given in [12], we can express as:

$$\Psi_{W-B} = \frac{\Delta h_0}{U_4^2/2} \tag{3.18}$$

$$\Phi_{W-B} = \frac{V}{U_4 d_4^2}\frac{4}{\pi} \tag{3.19}$$

Their combination will produce:

$$\frac{\Phi_{W-B}^{0.5}}{\Psi_{W-B}^{0.75}} = \frac{\omega\sqrt{V}}{(2\Delta h_0)^{0.75}\sqrt{\pi}} \tag{3.20}$$

Moreover, this lead to the specific speed expressed in the previous paragraph:

$$N_s = \frac{\omega\sqrt{V}}{\Delta h_0^{3/4}} = \frac{\Phi_{W-B}^{0.5}}{\Psi_{W-B}^{0.75}}\sqrt{\pi}2^{0.75} \tag{3.21}$$

This equation represent the fact that *Ns* is a dependent variable of the flow and load coefficients as defined in [12]. Thus, if in the design procedure two of them are chosen, also the third will be fixed. For this reason, the performance characteristic of Figure (3.1) could be re-plotted in terms of different non-dimensional groups. In this work, however, the flow and load coefficients are expressed in the form suggested by Moustapha et al. in [11]. The reason will be showed in latter chapters, but can be indicated in a simpler approach required by the preliminary design of the main geometry of the rotor. The combination of Φ and Ψ as expressed in (3.20) is now:

$$\frac{\Phi^{0.5}}{\Psi^{0.75}} = \frac{\left(\frac{2E\ V_4}{\pi\lambda d_4^3\omega}\right)^{0.5}}{\left(\frac{\Delta h_0}{\omega^2 d_4^2}\right)^{0.75}} = \frac{\omega\sqrt{E\ V}}{2(\Delta h_0)^{0.75}\sqrt{\lambda\pi}} \tag{3.22}$$

Where $E=C_{m4}/\ C_{m6}$ is the meridional velocity ratio, and $\lambda=b_4/d_4$ is the inlet blade height to inlet diameter ratio.

Using this combination, we can obtain the non-dimensional typical number:

$$N_t = \frac{\omega}{\Delta h_0^{3/4}} \sqrt{\frac{E\ V}{\lambda}} = \frac{\Phi^{0.5}}{\Psi^{0.75}} \sqrt{\pi} 2 \tag{3.23}$$

Differently from before, the typical number is clearly also dependent on geometrical parameters of the rotor. In addition, the meridional velocity ratio is a parameter that takes role in the definition of the typical number. Actually in many project cases, and also in this work, E is a constant; in particular it is fixed in the way that the meridional velocity would be constant between the inlet and the outlet: thus it is set as $E=1$. Hence, the typical number will result:

$$N_t = \frac{\omega}{\Delta h_0^{3/4}} \sqrt{\frac{V}{\lambda}} = \frac{\Phi^{0.5}}{\Psi^{0.75}} \sqrt{\pi} 2 \tag{3.24}$$

In comparison with Ns, Nt presents one more variable. This means that in analysis where Δh_0, Q and ω are fixed, the Ns will be surely a constant, but Nt will be a variable linked to λ variations.

3.6 Size parameter

The size parameter is a dimensional factor introduced by Macchi in [18], expressed in the following form:

$$VH = \frac{\sqrt{V}}{\Delta h_{is}^{0.25}} \tag{3.25}$$

If Q is expressed in [m^3/s] and Δh_{is} in [J/kg], VH presents the dimension of a length [m]. It has a really strength physic significance, because it is directly correlated to the machine dimensions. As reported in [19] turbines with the same VH have the same actual dimension. This parameter is related in several papers to the decay or increase of efficiency related to the size of a turbine.

It is almost clear from experience and manufacturers data, that a machine of large size is able to reach higher efficiency than a machine of smaller size [19]. As far as geometrical similarity is concerned,

turbines of different size characterized by same non-dimensional parameters (for instance *Ns, Ds, Re*) should show the same maximum efficiency. But in a design process many dimensional constrains are introduced, so that small turbines will behave differently from large ones, because of different thickness, surface roughness, clearance and other geometrical parameters [19].

3.7 Volumetric flow rate variation

Another parameter that will be used in order to analyse the turbines performance is the volume flow rate variation, expressed in the following form:

$$VR = \frac{V_6}{V_1} \tag{3.26}$$

Where 1 refers to the turbine inlet condition and 6 to the rotor outlet.
Many publications used to analyse the performance in correlation with the pressure ratio:

$$r_p = \frac{p_6}{p_1} \tag{3.27}$$

Again, according to the similarity rules, results obtained for turbines characterized by same non-dimensional parameters should be the same. If it is provided that Reynolds number are neglected, the thermodynamic behaviour of fluid is the same, the geometric similarity is completely preserved [19].

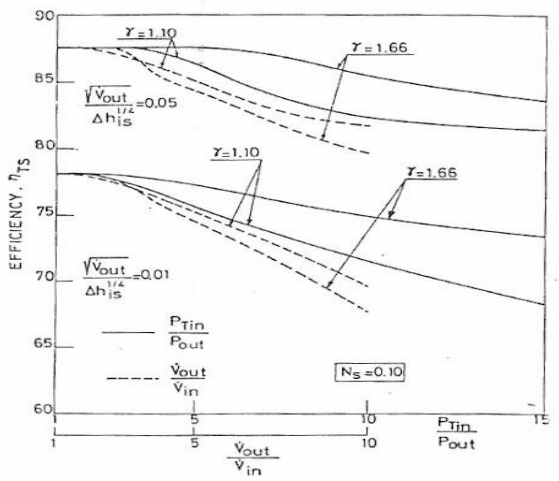

Figure 3.4 *The influence of pressure expansion ratio and volumetric flow rate variation on the efficiency definition of a radial turbine. Here are considered two fluids characterized by a different specific heat ratio γ [11].*

In our analysis we can consider that the effects of Reynolds number vanish because it is assumed larger than the limiting Reynolds number (turbulent flow). In this way the thermodynamic properties of the working fluid affect the turbine design in two main ways:

- The variation of specific volume influences the turbine geometry;
- Different Mach number will give different losses coefficients, so that fluids with different specific heat ratio γ and same r_p, will lead to different geometry and efficiency

Figure (3.4) shows different turbines optimized for very different fluids, one with a complex molecule ($\gamma=1.10$) and one monoatomic ($\gamma=1.66$): for low-pressure ratio, the effects are negligible, but for higher-pressure ratios, important efficiency differences appear for the two fluids. The efficiency decrease is larger for the complex molecule fluid, which experiences larger volume variations. Nevertheless, if the performance of the turbines is compared at equal *VR*, the efficiency gap becomes much lower, and is mostly due of the different Mach numbers.

For this result, this model will use *VR* as a parameter of study of the turbine performance.

Chapter 4

Expanders' literature review

This chapter has the aim to analyse the previous studies about expanders for organic Rankine cycle applications. The first part introduces all the utilised types of expanders, which are suitable for this purpose, and in particular volumetric ones and turbomachines (axial and radial). Then, as this Master Thesis is mainly about the performance prediction of radial turbines, different design procedures are studied, focusing advantages and limits. Moreover, the last section points out the importance that a correct efficiency prediction of the expander gains in the optimization of the whole thermodynamic cycle.

4.1 Introduction

The expander can be considered as the most important component of an electric generation plant utilizing an Organic Rankine Cycle technology. The other main components of this kind of plant are, in the basic configuration, a heater, a pump and a condenser. The configurations have been widely analysed in §2.2.

It has the aim to convert kinetic energy of a moving fluid into mechanical power by the impulse or reaction of the fluid with a series of buckets, paddles, or blades. A shaft connected to the component it will then transfer the energy to an electrical generator, which has the capacity to convert the mechanical energy into electrical one.

By this simple explanation of the electrical generation process, it is understandable the focal point that the expander occupies in a cycle design. If we focus the attention on price evaluation, it is possible to note that this component has the highest influence on the definition of investment cost. In [1]

Quoilin developed a thermo-economical optimization for a waste heat recovery Organic Rankine Cycle, calculating the cost of several components related with the evaporation temperature of the cycle. It can be seen in Figure 4.1 that for low evaporation temperature T_{ev} the cost of the expander can reach a relative weight on the total cost of the plant of more than 50%, and decreasing when the T_{ev} gets increased [1].

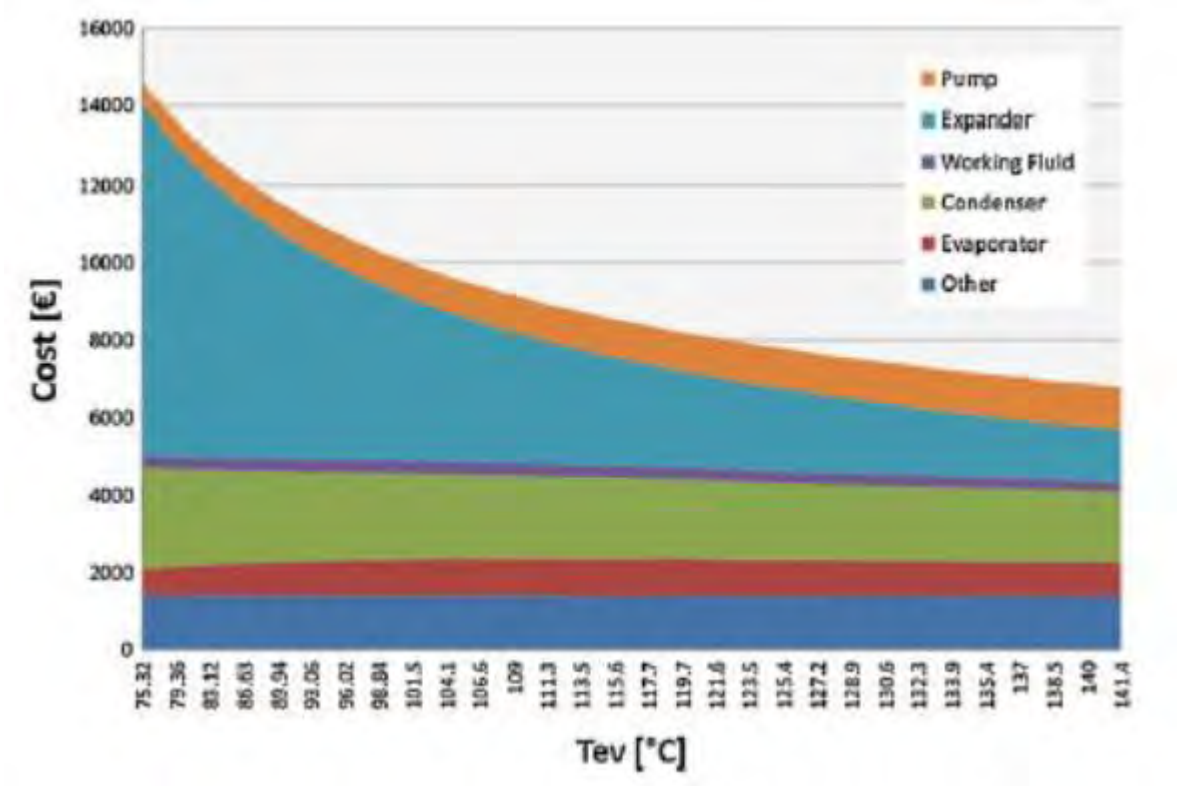

Figure 4.1 *Study of the costs of several components of an ORC, as a function of the evaporation temperature of the cycle. Fluid R-245fa [1].*

While other components of the ORC plant show a barely constant cost of investment, expander and pump are characterized by an opposite price behaviour. Actually, if we consider a cycle layout without super-hating, the more T_{ev} is high and the more p_{ev} is high. This clearly leads to the need of a higher performance pump that is able to reach higher evaporation pressure. At the same time in this condition where also the power output is considered as a constant, a higher pressure ratio allows to design the cycle with a lower mass flow rate. This means that smaller dimensions will characterize the expander, and the dimensions are directly linked with the cost of the component [1].

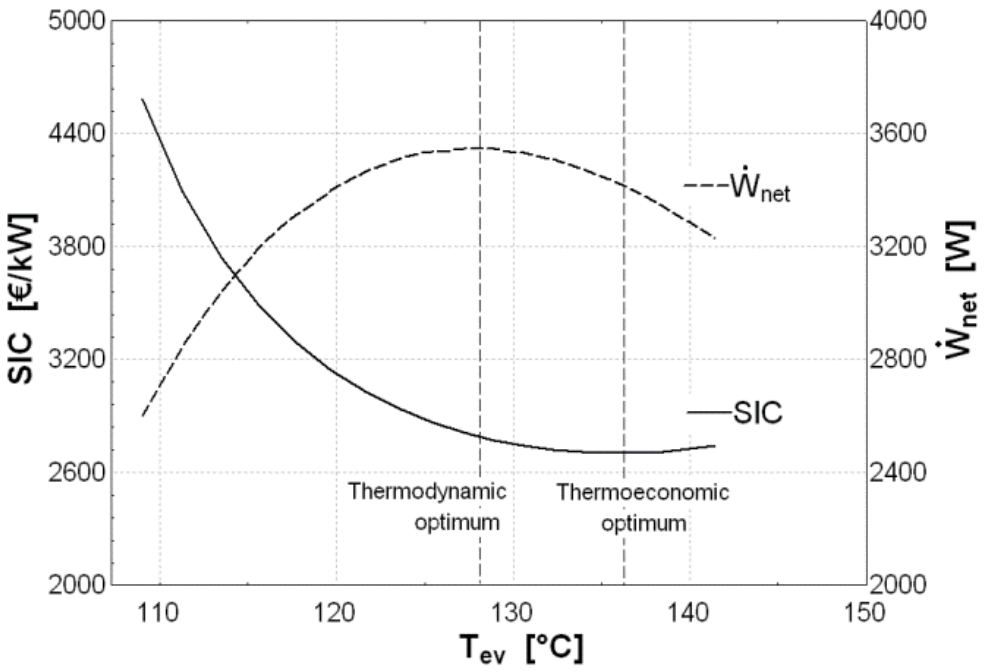

Figure 4.2 *Specific Investment Cost (SVI) and Power output (W_{net}) as functions of the cycle evaporation temperature. Note that thermodynamic and thermo-economic optimum conditions do not take place for the same T_{ev} [1].*

As reported in [1], it is important to state that the thermodynamic and thermo-economic optimum do not take place in the same condition. In Fig (n) the Specific Investment Cost (*SIC*) and the net power output are shown (W_{net}): a minimum value for the SIC is observed around 136°C for the particular case of working fluid R-245fa, but this minimum does not coincide with maximum output power obtained at 128°C. This observation could be extended to other fluids [1].

The importance of the expander in the cycle design definition does not clearly concern only the component cost. Its choice, project and operative condition are a focal point that the designer must always keep in his mind in order to achieve the best layout of the whole energy plant. This means that the definition of both, expander and cycle characteristic, cannot be considered as standalone features of a project, because the behaviour and constrains imposed by the first have a strong influence on the second and vice versa.

In addition, the matching with working fluid plays a fundamental role in the definition of performance, since the isentropic efficiency depends on thermodynamic and fluid conditions during its expansion through the component. The choice of a working fluid takes with it several constrictions not always related to operative conditions or thermodynamic considerations. Many of them actually are characterized by environmental risk as greenhouse effect, flammability or toxicity [2]; these characteristics can influence the designer to choices that can appear non-optimal from a thermodynamic point of view. Also the price of the fluid is an important feature that can impose

constrains, especially in those application where plant and operative costs gain a primary consideration, such as heat recovery systems [1].

The first part of this chapter wants primarily point out the different kind of expander, which are mostly utilized in ORC applications.

4.2 Volumetric expanders

The volumetric expander are positive displacement, whose principal feature is to have a fixed volumetric ratio [2]. This is physically compulsory, because they are characterized by a fixed build-in volume, where is supposed to happen the fluid expansion in order to extract mechanical work. This feature involves usually two main kind of losses, occurring when the actual specific volume ratio is not equal to the nominal machine volume ratio: under-expansion and over-expansion. These effects reduce strongly the efficiency of the expansion process, so that volumetric expanders are less adapt than turbomachines in plants where a high expansion ratio is required [2].

4.2.1 Scroll expanders

The scroll expanders are characterized by the most complicated geometry, required by the fluid through-flow. The fluid flows in the suction chamber, which is in communication with the suction pipe; when the suction chamber get closed and not anymore in communication with the inlet section, the expansion process begins. By generating a momentum on the walls of the chamber, the fluid expands until the volume is opened, generating a movement of the orbital scroll respect to the fixed one. At this moment the discharge process starts, and the fluid flows in direction of outlet section [1]. Thus, the cycle involves three different processes: suction, expansion and discharge, as showed in Figure 4.3.

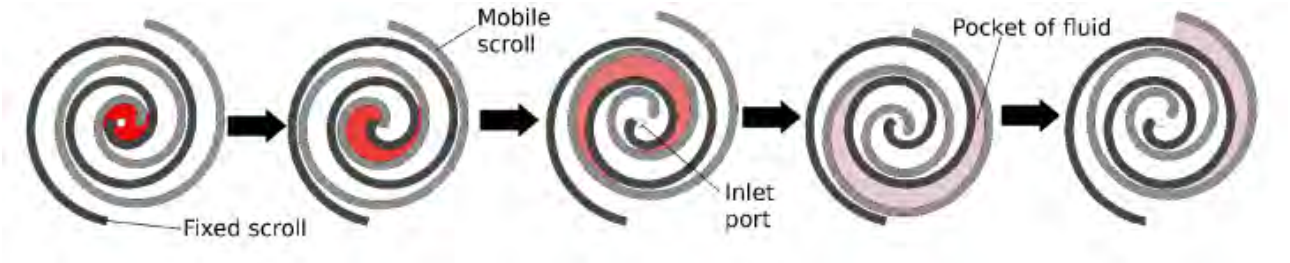

Figure 4.3 *Phases of the expansion in a scroll expander: from the suction (left), through the proper expansion, until the discharge (right) [1].*

The scroll expanders are generally categorized in two family, depending on the mechanism that maintains the orbiting scroll in contact with the fixed scroll [2]:

- Compliant scroll expanders: in this kind of scroll expanders, only the centrifugal effect of the orbiting scroll wrap is used to maintain the contact between both wrap sidewalls as they slide against each other, separated only by a thin oil film. In this way, they require lubrication to operate efficiently without causing significant wear. They also require inlet and outlet valves in order to isolate the expansion volume [1].
- Cinematically constrained scroll expanders: here the linking mechanism between orbiting and fixed scrolls permits a relative movement of the first respect the second. They can operate without lubrication, and the manufacturing tolerances are critical in the minimization of the gap between the two scroll wrap sidewalls. An advantage of this kind of scroll expanders is that they do not require inlet and exhaust valves, so that noise is reduced and the durability of the device is increased [1].

In table (n) are collected data of some prototype scroll expander researches, as reported in [2], in order to point out some of the main feature of existing devices.

Researchers	**Working fluid**	**Isentropic efficiency [%]**	**Power [kW]**	**Rotate speed [rpm]**	**Pressure ratio**
Zanelli and Favrat	R134a	63-65	1-3.5	2400-3600	2.4-4.0
Mathias et al.	R123	67; 81; 83	1.2; 1.38; 1.75	3670	8.8; 5.5; 3.1
Peterson et al.	R123	45-50	0.14-0.24	600-1400	3.28-3.87
Wang et al.	R134a	70-77	0.5-0.8	1015-3670	2.65-4.84
Saitoh et al.	R113	65	0.46	4800	-
Kim et al.	Water	33.8	11-12	1000-1400	10.54-11.5
Manolakos et al.	R134a	10-65	0.35-2	300-390	-
Lemort et al.	R123	42.5-67	0.4-1.8	1771-2660	2.75-5.4
Lemort et al.	R245fa	45-71	0.2-2	-	2-5.7
Guangbin et al,	Air	-	0.4-1.1	1740-2340	3.66

Table 4.1 *Main characteristics of prototype scroll expanders collected by [2].*

4.2.2 Screw expanders

These devices require a relatively high level of technology in their production. They mainly consist in a fixed shaped chasing and a helically toothed gear, which has the role of the rotor. The fluid flows from the suction inlet through the gap existing between the rotors, generating an angular momentum [1]. As in all the positive displacement devices, the seal is a critical aspect that has a strong influence

on machine performance because of increasing in leakage losses. At the same time, a direct contact between the lobes has to be prevented in order to avoid noises and fretting. Thus, lubrication is required, and in particular two methods have been developed, depending on different applications [2]:

- Oil injected type: this kind of screw expander is cheaper in manufacture, simpler in mechanical design, and can achieve high efficiency. As disadvantage cannot permit a complete separation between lubricant and working fluid [2];
- Oil free type: this device separates any oil from working fluid, preventing any contact of it with lubricated part of the rotors outside the working chamber. This entail internal seals against bearings and chamber walls, and all these additional requirements are related to a more expensive manufacture [2];

Because of tight sealing requirements, screw expanders tend to work better with wet fluids; a dry fluid system would require seals that highly increase the cost of the machine.
A schematic representation of a screw expander is reported in Figure 4.4.

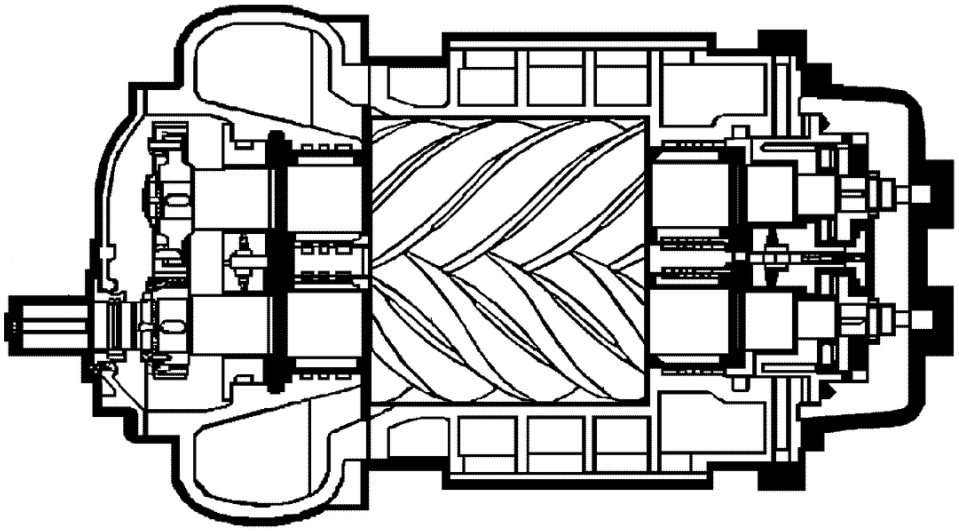

Figure 4.4 *A 2-D section of a screw expander. The screws and the expansion area are visible.*

In Table 4.2 are collected data from some prototype screw expander researches, as reported in [2], in order to point out some of the main features of existing devices.

Researchers	Working fluid	Isentropic efficiency [%]	Power [kW]	Rotate speed [rpm]	Pressure ratio
Wang et al.	Air	26-40	0.5-3	400-2900	-
Smith et al.	R113	48-76	6-15.5	1300-3600	2.11

Table 4.2 *Main characteristics of prototype screw expanders collected by [2].*

4.2.3 Reciprocating piston expanders

The thermodynamic cycle of these expanders is well known and widely used in many technical applications. It consists mainly of four different phases [2], whose ideal cycle is represented in Figure 4.5:

- Intake (1-2): the inlet valve is opened and the high pressure fluid is admitted inside the cylinder, moving the piston from the upper dead centre to the bottom dead centre. At a certain angle, the so-called "cut off", the intake valve is closed;
- Expansion (2-3): after the "cut off" the chamber is supposed to be completely isolated, so that an isentropic expansion could take place;
- Discharge (3-5): after reaching the bottom dead centre, the exhaust valve is then opened and the fluid discharged, at a pressure that should be higher than the one existing in the outlet pipe, in order of not incurring in pumping phenomena. The piston now is moving towards the upper dead centre.
- Admission (5-1): once that the piston has reached the upper dead centre, the exhaust valve is closed and the intake one is opened, permitting to the pressurized fluid to fulfil the cylinder.

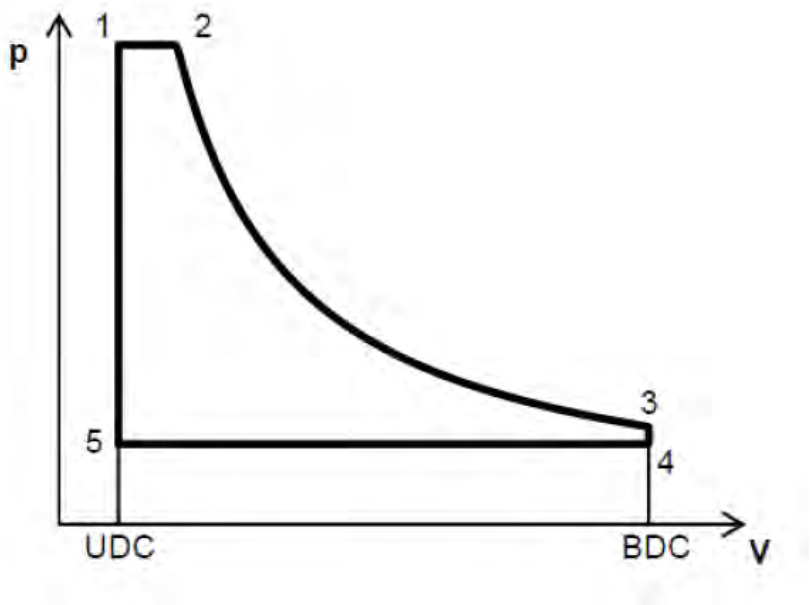

Figure 4.5 *Ideal cycle of a reciprocating expander in a p-V diagram.*

Even this simple analysis of the thermodynamic cycle allows to understand that reciprocating pistons expanders are a quite complex device, in particular in terms of time of opening and closing valves [2]. They are also characterized by high friction losses because of the large interacting surfaces. Phenomena related to torque pulsation appears necessarily due of inherent discontinuity associated to finite numbers of pistons. Also the lubrication is necessary, but

involves some difficulties, because the oil should be mixed with the working fluid, decreasing the efficiency.

All these feature do not make of these device the first choice for ORC application, but several studies show that, when the expansion ratio is high, reciprocating piston expanders can achieve higher efficiency than scroll expanders.

In Table 4.3 are collected data of some prototype piston expander researches, as reported in[2], in order to point out some of the main features of existing devices.

Researchers	Working fluid	Isentropic efficiency [%]	Power [kW]	Rotate speed [rpm]	Pressure ratio
Baek et al.	CO_2	10.5	24.35	114	2.1
Zhang et al.	CO_2	43-48	0.025-0.032	2200-3000	21.54-24.17

Table 4.3 *Main characteristics of prototype reciprocating piston expanders collected by [2].*

4.3 Turbomachines

Nowadays, the most used technology utilised in energy production field concerns turbo-expanders. Turbines for ORC do not present basically large differences, if compared to water steam ones. Anyway, different applications and working fluids imply special features [21]:

- The low sound speed of organic fluids with higher molar mass suggest not to have supersonic condition, in order to avoid additional shock losses;
- At fixed temperature difference between inlet and outlet, ORC expansion process is characterized by a low enthalpy drop and a higher expansion ratio, and this fact have large influence on losses definition;
- Due to higher density than water, turbines designed for ORC applications can be characterized by overall smaller dimensions in flow passages [2];
- The positive slope of saturated vapour curve of organic fluids permits to avoid any problem related to wet condition of fluid at the exhaust section, because the vapour is still superheated;

Currently, turbines can be classified in radial and axial, depending on the flow passage geometry.

Even if next sections will concern only the design and the mean-line analysis of radial inflow turbine, an introduction of both technologies is here reported.

4.3.1 Axial turbines

The flow through the turbine is supposed to be mainly mono-dimensional, as the fluid enters and leave the device in axial direction. They are commonly used in systems with high flow rates and low-pressure ratios, and it is common to have multi stage configurations in order to afford higher pressure drops.

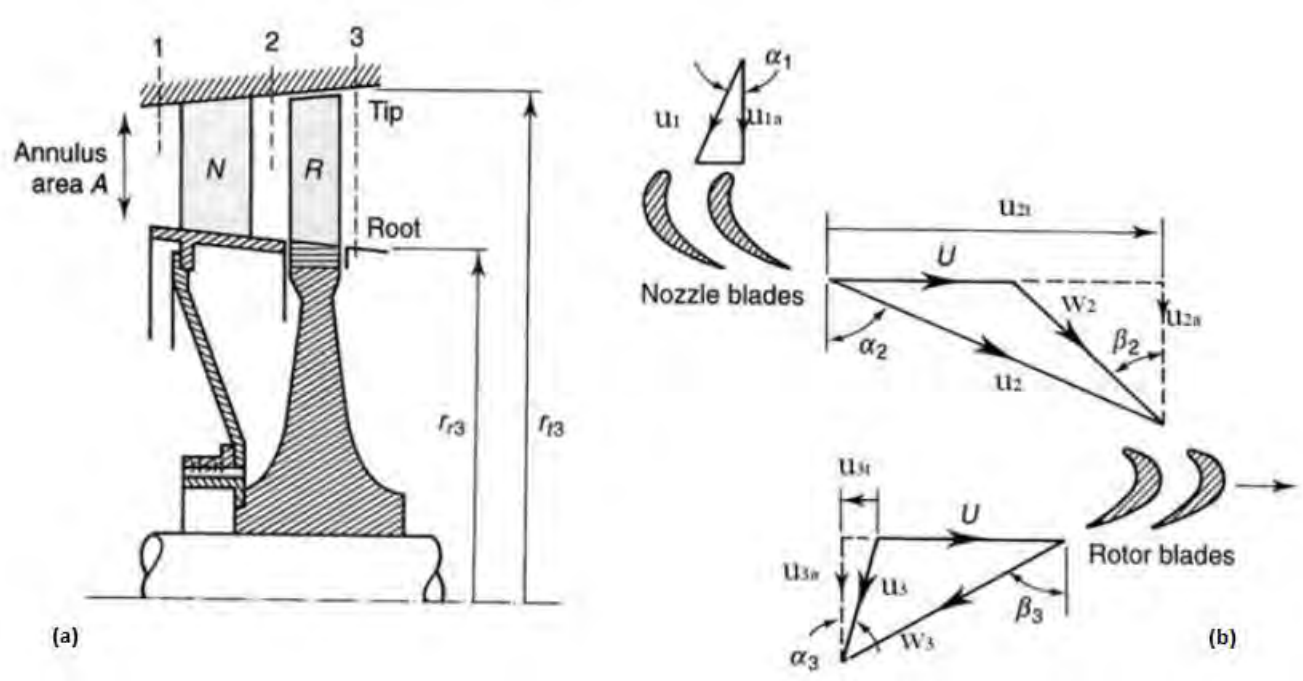

Figure 4.6 *In (a) is showed a cross section of a stage of a axial expander; typical velocity triangles of nozzle inlet inlet (top), rotor inlet (middle) and rotor outlet (bottom) are showed in (b).*

In particular in ORC applications, less stages are required than classical steam one, because of the already mentioned lower enthalpy-drop. They can be categorized in two main families based on the degree of reaction R [11]:

$$R = \frac{h_2 - h_3}{h_1 - h_3} \tag{4.1}$$

Where the subscripts 1, 2, 3 refers respectively to stator inlet, rotor inlet and rotor outlet.
In this way, the category are:

- Impulse turbines: $(R = 0)$ the working fluid is completely expanded in the stator, where is accelerated to a high absolute velocity; the velocity triangles between rotor inlet and outlet are the same [22].

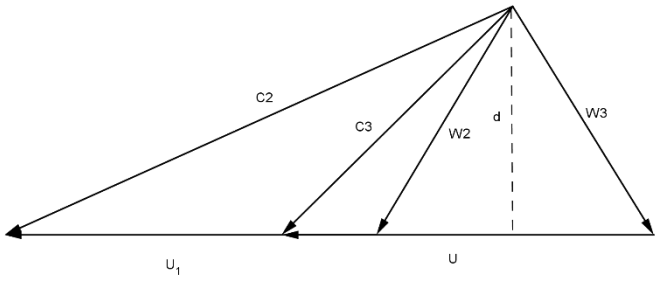

Figure 4.7 Velocity triangles of an impulse axial turbine.

- Reaction turbines: $(R > 0)$: the expansion of the fluid takes place both in stator and rotor passage, and the flow passages change continuously section to allow the expansion in the device [22].

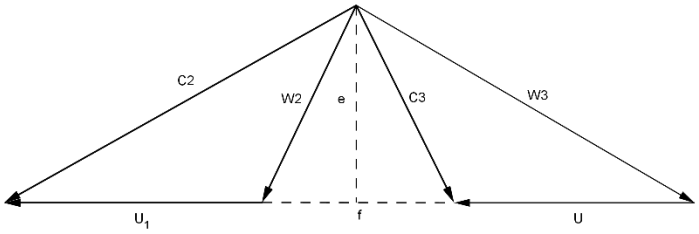

Figure 4.8 *Velocity triangles of a reaction axial turbine (Λ=0.5).*

4.3.2 Radial turbines

In radial turbines, the flow is strongly three-dimensional and definitely harder to analyse than in axial ones. In radial in-flow turbines, which are surely the most used in industrial and energy application, the pressurized fluid enters the machine in a radial direction, streaming through a peripheral volute and a stage of radial nozzle vanes. Then it goes into the rotor, where is deflected, so that the outlet section is axial or mixed axial and radial.

These turbomachines are suggested in application where a low flow rate and high pressure drop are required: compared to axial ones, radial stage are suitable to elaborate higher pressure ratio, but the multi-staging technology is easier made between axial stages [12]. For these reasons, radial ones are suggested for application from a few kilowatts up to a few Megawatts, while in larger scale plants (from 5 MW and over) the choice of axial devices should be carefully considered.

Referring in particular to small size turbomachines, radial turbines have been preferred to axial ones, because in this power range the blades have to be made very small and numerous, so that the wetted

area and hence the friction losses increase. Most significantly, the running clearance required between blade tips and shroud becomes a significant fraction of blade height so that tip leakage losses can become quite severe [12]. Moreover, the manufacturing cost is less expensive for radial ones, also because they could be derived from standard production, being less sensitive to blade profile. The blades are attached to the hub, so that the rotor dynamic stability of the system is improved by a higher stiffness [2].

Although in-flow configuration is surely the most common, or maybe the only one commercially produced, some authors suggested also an out-flow configuration. This is the case of [23], where Pini et al. proposed a design procedure to model and give a performance estimation of a radial centrifugal turbine.

This configuration is surely more common for centrifugal compressors, as suggested by Euler work equation for turbomachinery:

$$W_{Eu} = \frac{C_2^2 - C_3^2}{2} + \frac{U_2^2 - U_3^2}{2} - \frac{W_2^2 - W_3^2}{2} \tag{4.2}$$

Where subscripts 2 and 3 represent respectively rotor inlet and outlet.

Indeed, in a centrifugal flow, $U_3 > U_2$ and so the tem relative to the blade speeds:

$$\frac{U_2^2 - U_3^2}{2} < 0 \tag{4.3}$$

This means a reduction of the specific work, due to centrifugal force.

On the other hand, they pointed out some advantage, as:

- The passage area naturally increase along the expansion process, fitting with the huge increase of specific volume [23];
- The turbines appear more compact than equivalent axial turbine, and lower Mach number and higher efficiency and flexibility characterize them [23].

Starting by these considerations, they propose a mono-dimensional design procedure based on loss correlation, followed by a CFD simulation for the blade definition. In Table (4.4) the main features of a design exercise are reported:

The CFD simulation operated on the geometry generated by the mean-line design confirm the goodness of the mono-dimensional analysis, calculating an efficiency of 88.8% [23]. In Figure (4.9) is showed the Mach number trend, where is possible to note that the maximum value achieved is just a little in the supersonic range (Ma=1.1).

Configuration	Multistage centrifugal
Number of stage	6
Fluid	Siloxane MDM
Power output [MW]	1.3
p_{in} [bar]	10
T_{in} [°C]	270
Rotational speed [rpm]	3000
Exit radius [m]	0.7
Efficiency	0.89

Table 4.4 *Main characteristics of an out-flow radial turbine designed in [23].*

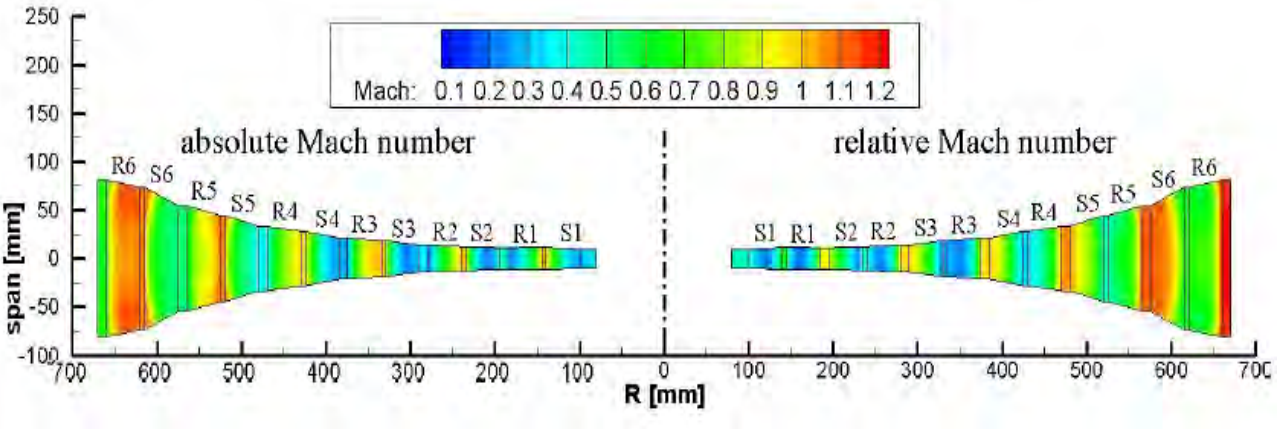

Figure 4.9 *Mach trends (absolute and relative) of the flow passage in the designed out-flow turbine, as a function of radius and cross section. The higher Mach numbers are reached in the outlet section, at the external radii of the expander [23].*

4.4 Review of radial inflow turbines design

The design of radial inflow turbine for ORC is a topic that in the last year has been taking more and more place, though during the 80's performance prediction of this kind of technology was deeply analysed.

In that period in fact, the energetic scenario showed the first changes: oil cost crisis due to Middle East conflicts suggested to improve the effort to produce electricity in different ways. One of them was, as said, the use of ORC linked to heat sources at lower temperature than traditional plants: geothermal heat, solar irradiation and industrial waste heat typical of some kind of production [24].

Then, after some years when this technology was in a certain way forgotten, ORCs and their studies became again a largely discussed topic among scientific community, for the suitability of being used,

coupled to renewable heat sources. In addition to the ones already cited, they can include boilers fuelled with biomass: the maximum temperature that this technology can achieve is largely inferior to the one reached by fossil fuel boiler, so that the choice of organic fluids as working fluids can involve several advantages than water steam one.
For the reasons just explained, also scientific studies about expanders specific for ORC are concentrated in two separate periods, the 80's and the recent years.

4.4.1 A specific design for turbines working with "heavy fluids"

Several researches and professors from "Politecnico di Milano" developed the most important studies about turbines for ORC in the 80's.
The first ORCs were utilising turbines already developed for classical fluid applications as steam and air. In [18] Macchi pointed out the problem of proposing a different way to design turbomachines operating with unconventional fluids. One of their principal characteristic was to have low speed of sound compared to water steam, and to work in very different stress conditions of power and temperature range. Indeed fluid properties play such an important role on turbine design, that the optimization of an organic fluid turbine stage is likely to yield solutions, which could appear quite unusual for a steam or gas turbine designer [18].
Macchi underlined also the importance of fixing good boundary conditions for design procedure, because, while for conventional turbines is possible to refer to simple rules based on previous similar machines experience, a more rigorous approach should be followed for turbines operating with non-conventional fluids. This appears of high importance when the procedure is implemented in a computer code, which should permit a simultaneous optimization for all variables affecting turbine performance [18].
The characteristic that mainly distinguish a steam and an organic fluid turbine can be summarized as:

- Enthalpy drop: typical values for heavy fluids are 10-100 kJ/kg, due to their high molecular weight; the most important consequence of it, as said before, is the possibility to design single-stage high-velocity devices [18].
- Volume flow rate: is a characteristic largely dependent on cycle features, but generally this value is lower than the one of a steam cycle, for the same power output. The combination of small enthalpy drop and low volume flow rate yields to a volume flow rates ratio that is larger than those which are usually adopted in gas and steam turbines [18].
- Mach numbers: they are surely high because of the low sound speed of the fluid and the high inlet/outlet volume flow ratios [18].

The theoretical procedure proposed wants to achieve the optimization of the expander efficiency. The efficiency is here defined neither as the total-to-total one nor as the total-to-static one; a hypothesis on the exit kinetic energy was made. Thus:

$$\eta = \frac{U_2 C_{u2} - U_3 C_{u3}}{\Delta h_{ts} - \phi_e \frac{C_{m3}^2}{2}} \tag{4.4}$$

Where $C_{m3}^2/2$ represents the kinetic energy at the rotor outlet section, and ϕ_e the fraction of kinetic energy recovered. The proposed study [18] does not include the presence of a model of an exhaust diffuser.

Following works developed the idea proposed by Macchi. We will focus in particular on the ones related to radial inflow turbines, but the same principles were used in [19] and in [21]. Especially in [20], Perdichizzi settled a design criterion for the mean-line project of axial turbines: even if our stadium will concern only radial turbines, the analysis of this paper can be considered surely preparatory, as it shows general principles suitable to design turbomachines supposed to work with organic fluids.

The first project phase can be summarized in four main points [20]:

- Choice of velocity triangles at the mean section;
- Choice of the rotational speed, as the specific speed;
- Selection of the geometry;
- Losses evaluation and performance prediction;

These points can be separately solved, following criteria proposed by several authors, but in this way it appears barely non-possible to reach a true stage optimization. In fact, the interaction of all the variables affecting the turbomachine efficiency is not fully understood. Indeed, it is preferable to arrange a method, which is able to achieve a global optimization taking into account simultaneously all the different design points [20].

Analysing previous methods proposed by several influential authors, Perdichizzi pointed out the limits that those methods were showing; as said these consideration can fit with the design procedure of all turbo-expanders, both radial and axial. In particular, the design procedures proposed by Smith corrected by Craig-Cox in [25], and by Baljè-Binsley in [26] were characterized by some missing aspects:

- Lack of generality, which does not permit the correct application for unconventional fluids (Smith, Craig-Cox);
- Overlook about compressibility and size effects (Baljè-Binsley);

For these reasons, he proposed a procedure based on the study of a large stage database (350 stages), in order to comprehend a wide field of applications. Moreover, the missing aspects of previous models were fixed, and in this way, the main features of the new one proposed can be summarized as [20]:

- The geometrical, non-dimensional and performance parameters are simultaneously optimized;
- All the loss sources are taken into account;
- Compressibility is explicitly considered as a variable that affects the performance;
- The method is fluid independent, so that it could be applied to different working fluids;
- Turbomachine size is considered, through the use of the dimensional value "size parameter", $VH = VH = \sqrt{Q_3}/\Delta h_{is}^{0.25}$;

The function to maximise is clearly the efficiency, following the definition proposed by Macchi in Equation. (4.4).

The use of the Size Parameter *VH* sets an important step forward in relation with the classical similitude theory for turbomachines, where non-dimensional parameters as specific speed and specific diameter are considered as enough to describe an entire family of expanders, characterized by the same values. The limits related to this approach have already been explained in §3.7 and §3.7. The primary result of the study is summarized in Figure (4.10) and (4.11).

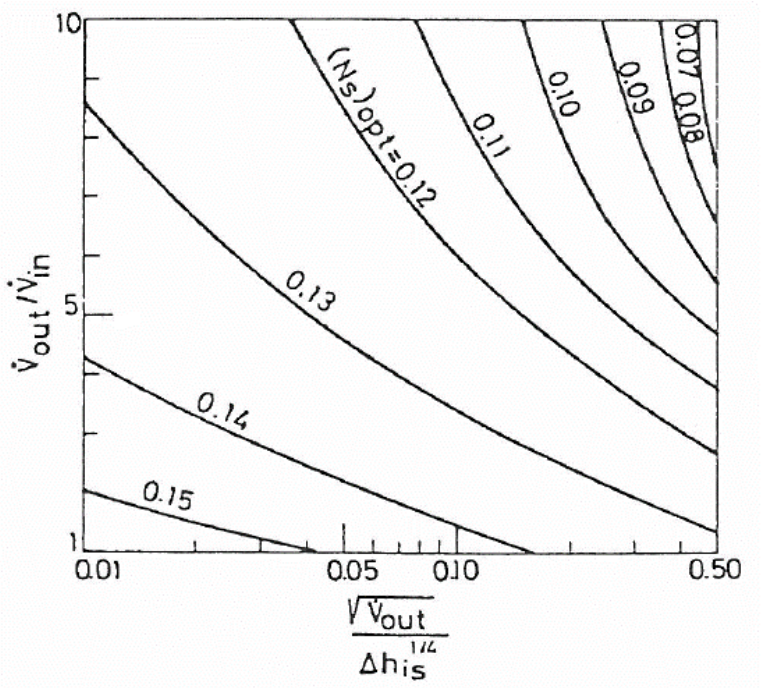

Figure 4.10 *Optimal specific speed for an axial stage, as function of size parameter and volume expansion ratio. Here Ns is calculated as* $Ns = N\sqrt{V_{out}}/\Delta h_{is}^{0.75}$ *[20].*

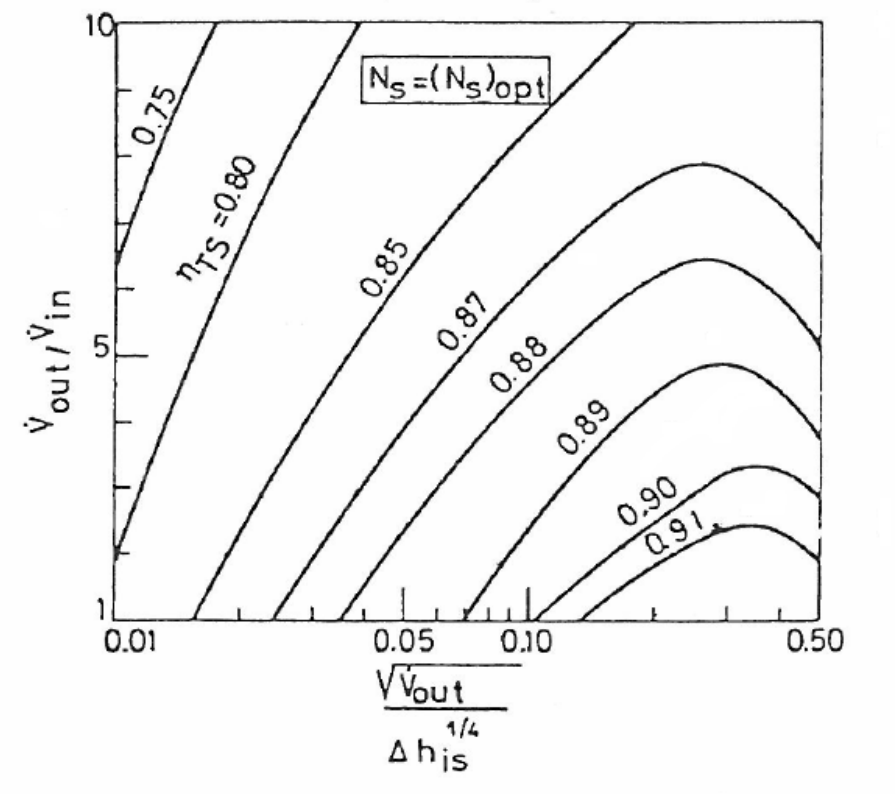

Figure 4.11 *Maximum achievable efficiency for an axial stage, at optimum specific speed condition [20].*

The specific speed *Ns* is a parameter that can be optimized if any constrain on rotation speed is set. The graph of Figure (4.10) shows the optimal values calculated for each couple of *VH* and *VR*; in the optimal condition of specific speed, the graph of Figure (4.11) shows the maximum achievable efficiency that the axial stage can achieve. As can be seen large efficiency penalties occurs at higher volume expansion ratio, characterizing the effect of compressibility and the higher Mach number achieved. Large efficiency penalties occur also when the size parameter *VH* is small, because of the reduced dimensions of the device, which comport the typical increase of some loss sources [20].

The analysis propose also a large variety of typical values (geometry, reaction degree, load coefficient, velocity triangle) that, through simulations, were optimized in a wide range of *VH* and *VR*. In this section, we are not going to analyse all of them because it does not strictly concern the aim of this Master Thesis. It is important, anyway, to underline that this procedure permits to realize a satisfactory one-dimensional project of axial turbine for unconventional fluids applications.

A similar approach to the one just explained was followed in [27] by Pedichizzi and Lozza. Here, a theoretical investigation of radial inflow expanders was developed for different design conditions. The scheme of the device was implemented in a computer code, following components models and losses correlations proposed by several authors.

The principles applied were the same as those explained for axial turbine: the importance of going forward compared to the classical similarity theory, taking into account the fluid compressibility and

the size of the expanders. The procedure optimize also in a simultaneous way the velocity triangles, geometrical values, speed of revolution and calculates the total-to-static efficiency for several design input. The fluid dynamic analysis is one-dimensional in the stator and rotor inlet, while a radial equilibrium equation is solved at the rotor exit. In Table (4.5) are summarized the loss models used in this work.

The function to be optimized is again the efficiency. In this work, it is defined in a slightly different way than the one of Equation 4.4, because of the presence of average values at the rotor exit. Furthermore, the presence of losses that subtract net power is taken into account, even if they are not supposed to change the thermodynamic values at the outlet conditions (leakage and disk friction losses):

$$\eta = \frac{U_2 C_{u2} - \overline{U_3 C_{u3}} - L_{df} - L_{cl}}{\Delta h_{ts} - \phi_e \frac{C_{m3}^2}{2}} \tag{4.5}$$

LOSS SOURCES - COMPONENTS	CONSIDERED MODELS
Scroll losses	The friction coefficient is calculated as a function of Re and surface roughness
Stator losses	Craig-Cox correlation (1971) calculated for the equivalent axial cascade by conformal transformations of the actual radial cascade
Vaneless losses	Kahlil-Tabakoff correlation (1976)
Rotor losses	Glassmann correlation (1976) based on experimental analysis carried out by NASA, which is considered as the most complete and representative of the experimental data
Leakage losses	Glassmann correlation (1976)
Friction losses	Glassmann correlation (1976)
Leaving kinetic energy	Following the definition of ϕ_e , is taken into account the eventually presence of an exhaust diffuser, integrating the radial distribution at the outlet

Table 4.5 *Index of the loss source considered in [27], and models utilized for their evalution.*

The paper presents a comparison between the code suggested geometry and literature test cases, showing a good agreement. In particular, fig (n) reports the optimisation of two proposed radial inflow turbines, where is particularly valuable the loss division study.

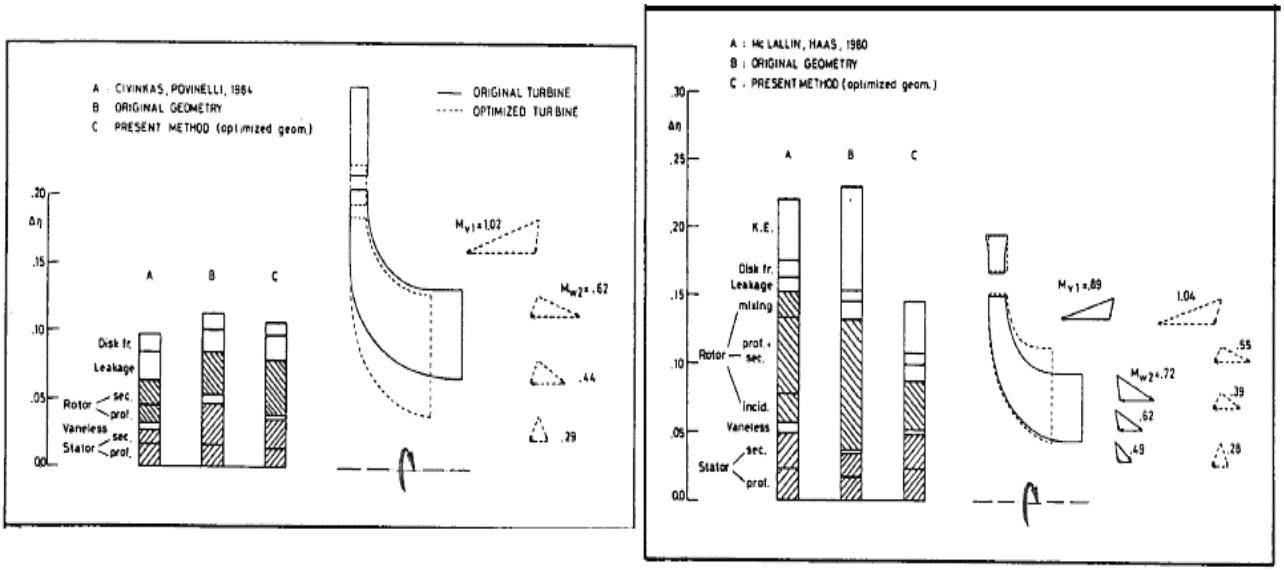

Figure 4.12 *Efficiency penalties, meridional geometries and velocity triangles for the test cases of Civinkas and Povinelli [28] and McLallin and Haas [29] reported in [27].*

As for the axial turbine, a study at optimum specific speed is carried out, in order to predict the maximum achievable efficiency for several sizes (represented again by size parameter *VH*) and volume expansion ratio (*VR*). The graph in Figure (4.13) shows the relation between efficiency and the couple (*VH,VR*), while Figure (4.14) between optimum *Ns* and (*VH,VR*).

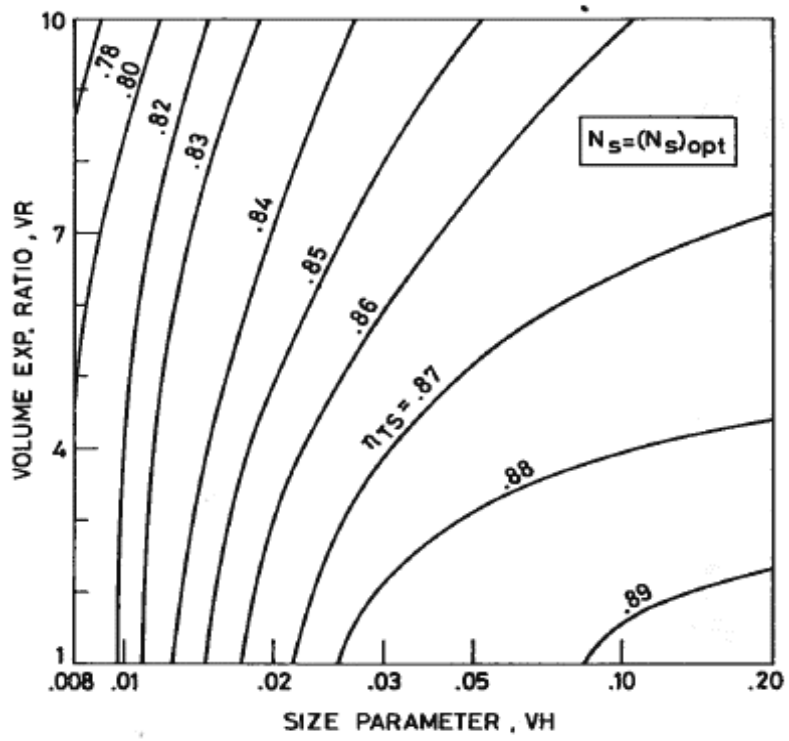

Figure 4.13 *Maximum achievable efficiency for a radial stage, at optimum specific speed condition [27].*

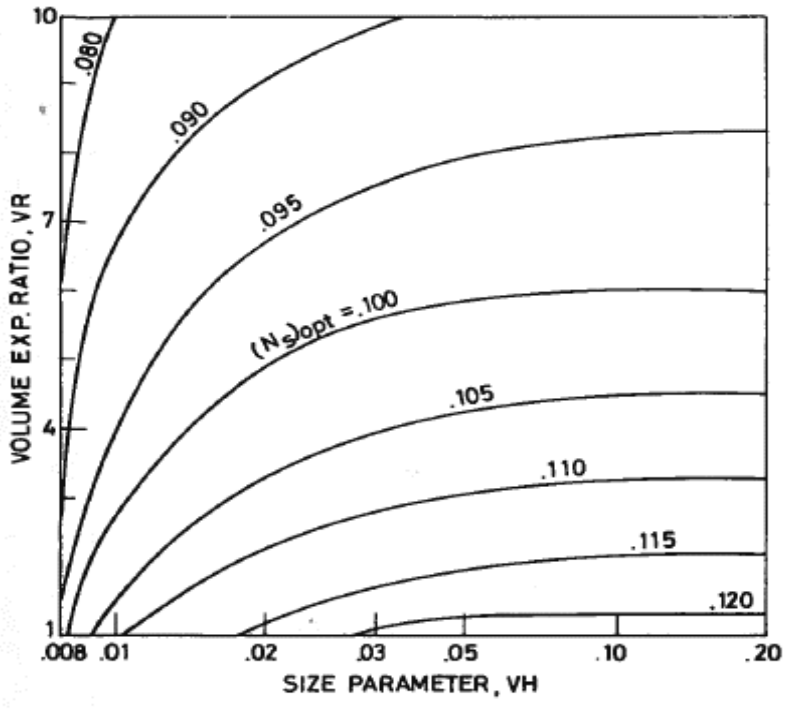

Figure 4.14 *Optimal specific speed for a radial stage, as function of size parameter and volume expansion ratio. Here Ns is calculated as Ns=NV(V_out)/〖Δh〗_is^0.75 [27].*

Significant efficiency penalties occur at large *VR*: this is mainly due to very small blade height of the stator and rotor inlet because of the low volume flow rate, compared to the one at the rotor exit. Nevertheless, compressibility does not produce dramatic effects, as in the case of axial turbines, as shown in fig (4.11). Two main effects can explain the reasons [27]:

- It is much more easier to dimension the exit areas large enough to limit kinetic energy losses;
- A substantial part of the useful work is due to centripetal effect $\Delta U^2/2$, so that the Mach numbers are generally lower;

Larger efficiency penalties instead take place due to reduction of size parameter, in particular because of the increasing trend of stator and leakage losses, because of trailing edge and surface roughness.

The study proposed by Perdichizzi and Lozza in [27] is furthermore important, because it shows the behaviour of a well-designed radial inflow turbine, when several constrains could make it work in non-ideal condition for what concern the specific speed. In Figure (4.15a) the trend of the efficiency is shown for fixed condition of *VH* and *VR*, calculated for a range of *Ns*. Small penalties seem to take place for incompressible flows (*VR=1.1*) in a relatively wide range of *Ns*, while for larger *VR* the efficiency rapidly drops.

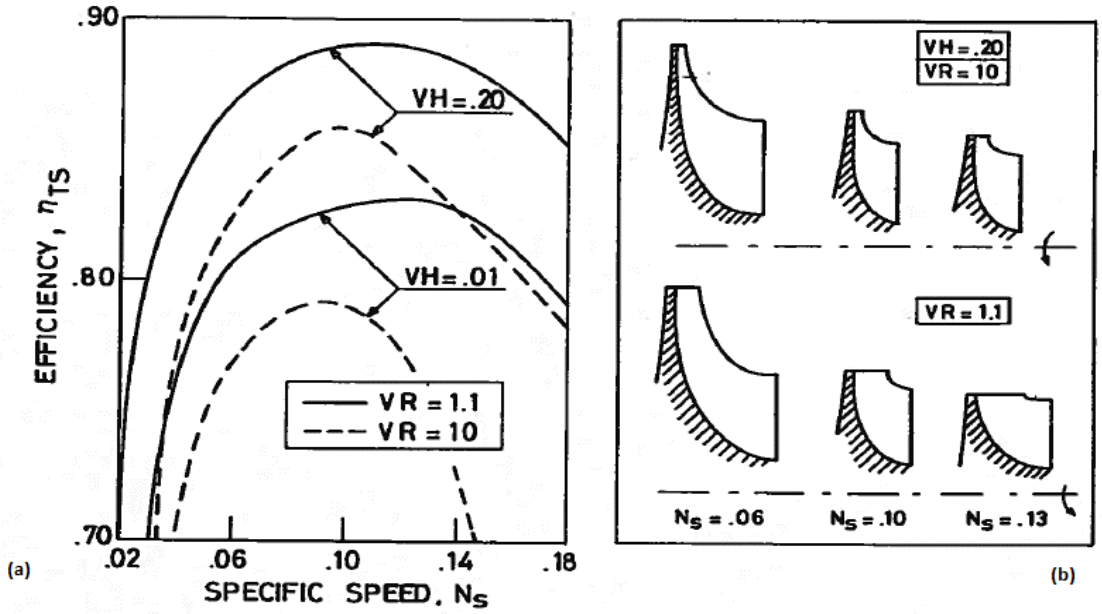

Figure 4.15 *Efficiency prediction for specific speeds different from optimum (a), and corresponding meridional geometries (b) [27].*

The figure (4.15b) instead shows the changing in rotor geometry due to the effects of input parameter: it is possible to appreciate the difference in inlet-outlet areas for different values of compressibility, and the different shroud curvature, which is a parameter that strongly affects the flow in rotor passage [27].

Fig (4.16) shows the losses division for each source, occurring at different specific speeds.

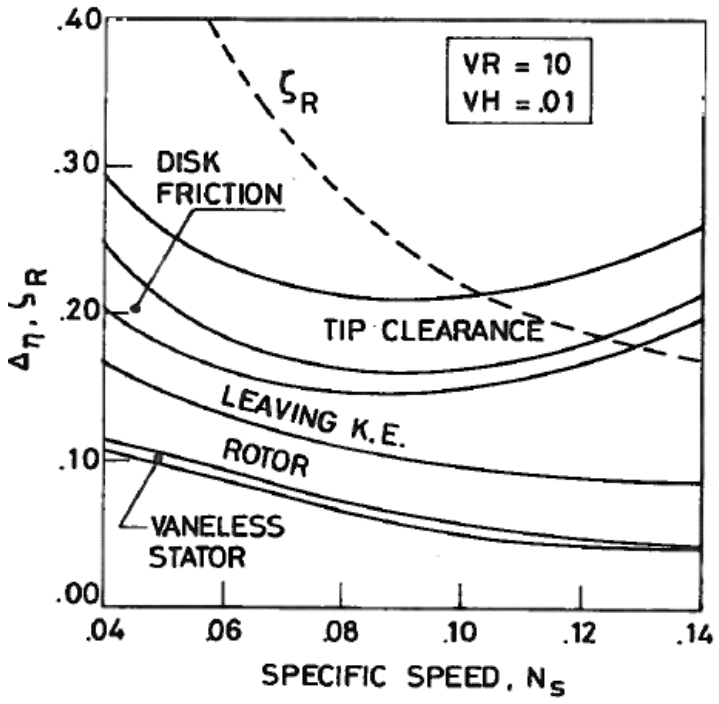

Figure 4.16 *Efficiency penalties and rotor loss coefficients as a function of the specific speed [27].*

4.4.2 Recent years' turbine design and efficiency prediction

As said in previous sections, recent years have seen a large increase of interest concentrated in radial inflow turbines and ORCs in general [15].

The selection of best design options for turbo expanders appears even nowadays a difficult task, especially for those unconventional applications at low temperature typical of geothermal and solar thermal energy conversions.

Not only the design of the radial inflow turbine, but also its interaction with several working fluids, have been a widely analysed topic, in order to define optimal operating conditions.

[30] has considered as a reliable preliminary design procedure for radial expander, which takes into account their different behaviour related to the use of several working fluids [2]. Indeed, the paper presents a design procedure whose main innovation is to consider the expansion of real fluids, while in the past mostly they were analysed basing on ideal gas equations. As said in previous sections, the operating field of organic fluids in this kind of Rankine cycles is surely far away from ideal gas conditions, and compressibility factor plays a key role sometimes not sufficiently considered [30].

Following these ideas, [30] reports some optimized configuration for a 50kW expander with inlet temperature of 147°C, achieved using EES (Engineer Equation Software [31]) where losses relations were implemented. The most important features are collected in the Table (4.6); the underline indexes are referred to the ones used in this Master Thesis.

Moreover, Figure (4.17) reports the optimized condition on *T-s* and *h-s* diagram obtained for the fluid R-245fa, analysed also in this Thesis. The obtained optimum cannot totally be compared with the best-design solutions that we achieved (see also §6.2), because the input data are slightly different: for instance, in [30] Fiaschi et al. fixed the inlet temperature and the power output, while we fixed size parameter and volume expansion ratio.

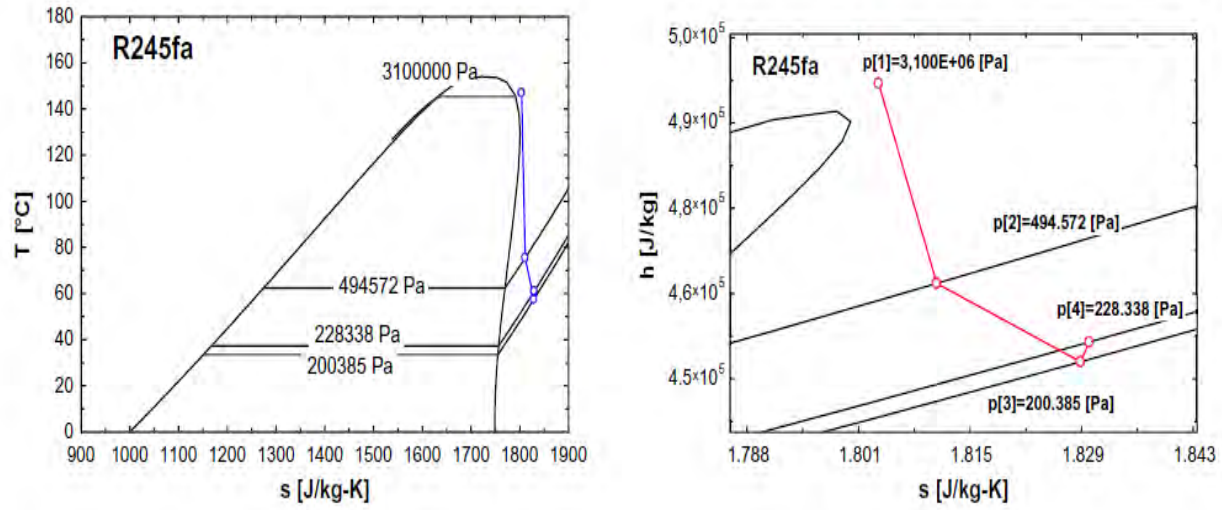

Figure 4.17 *Thermodynamic diagrams T-s and h-s with expansion lines [30].*

It is also important to note that for this fluid, in optimised condition the condenser pressure is above the atmospheric one, and this aspect is suggested to simplify the cycle layout, because the problem of non-condensable gas infiltrations is avoided [30].

Characteristic	R-134a	Cyclo-Hexane	N-Pentane	R-245fa	R-1234yf	R-236fa
Ψ	1.52	1.70	1.7	1.55	2.4	1.65
Φ	0.21	0.17	0.23	0.20	0.35	0.23
R	0.24	0.24	0.26	0.28	0.13	0.25
p_1 [bar]	38	5	10	31	31	30
d_3 [m]	0.048	0.138	0.0769	0.062	0.057	0.057
Δh_0 [kJ/kg]	28.36	91.20	74.77	37.26	21.68	27.29
Ns	0.496	0.603	0.615	0.584	0.465	0.590
η_{ts}	0.83	0.73	0.69	0.76	0.54	0.71
η_{tt}	0.85	0.80	0.78	0.82	0.69	0.78

Table 4.6 *Main characteristics of optimized radial inflow turbines, working with different organic fluids [30].*

The design procedure leads clearly to different expanders layouts, related to different fluids characteristics. With the exception of Cyclo-Hexane, the rotor inlet diameters are in the range from 50mm to 80mm. The specific numbers for all the cases is the typical one suggested by classical radial turbomachines theory (*Ns=0.3-0.8* [12]). It appears instead important to underline, the strong difference occurring between the load and flow parameters that are statistically suggested by Chen and Baines, as reported in Figure (3.1), and the ones that are here calculated. The analysis of Fiaschi's work recommend in this way, that a true optimization of turbine geometry for non-conventional fluids must comprehend a wide simulation of several flow and load conditions.

This important aspect pointed out in this analysis can be seen as the as the limit of studies carried out by several authors [10]. The study presented by Sauret and Rowlands in [15], for instance, has the aim to provide a preliminary design for expander operating in sub-critical and trans-critical ORCs. Moreover, the approach presented wants to focus on the non-constant efficiency that expanders can achieve in different fluid conditions, as their best performances do not normally match with the optimum cycle layout. In this way, for fixed cycle constrains, several preliminary analysis of radial expanders were obtained, characterized by different features depending on the selected fluid [15].

The simulations were realised, using the commercial software RITAL [16], in which the design procedure and loss correlation suggested by Mustapha et al. in [11] are implemented.

The results of this study arrange a ranking of expander based on power output and dimensions, as expressed by the Performance Factor:

$$PF = \frac{P}{(2r_{in})^2} \tag{4.6}$$

The index assumes that obtaining a greater power output from a smaller turbine is more attractive from a material, manufacturing and economic perspective than less power from a larger one [15].
The ranking obtained for fixed cycle conditions is reported in Table (4.7), while a comparison between the obtained relative dimension is represented in Figure. (4.18).

Ranking	Fluid	Performance factor [kW/m^2]
1	R-143a	17.2
2	R-134a	15.2
3	R-236fa	8.0
4	R-245fa	4.6
5	n-Pentane	3.0

Table 4.7 *Rankine of obtained turbines working with different fluids, based on performance factor [15].*

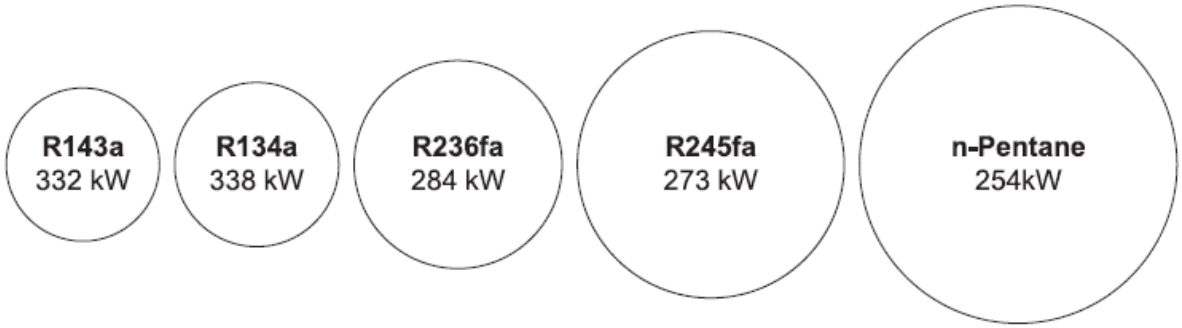

Figure 4.18 *Relative inlet rotor diameters and net cycle power output calculated from preliminary mean-line turbine sizing [15].*

Although this analysis could lead to important suggestions for a designer who is approaching the project or the study of the ORC's expander, is important to underline the limits that affects this results. The mean-line performance evaluation in fact, considers for each case fixed values of flow and load parameters. In particular, they are selected following the suggestion of Chen and Baines diagram of figure (3.1), with:

- $\phi = 0.215$
- $\psi = 0.918$

These values were statistically obtained by radial turbine stages working with ideal gases (air, steam, CO_2). As Fiaschi's paper showed, for high-density fluid the behaviour can be deeply different, so that an optimisation process can suggest slightly altered values for the best-design conditions.

For this reason, a change on input flow and load coefficients can lead to currently unknown variations on performance of the analysed turbines. This means that the study [15] carried out by Sauret and Rowlands could be not in an optimal-design context, so that the ranking evaluation could imply a different solution.

In recent years, many other applicative researches were carried out, about the design of radial inflow turbines for several ORC plants.

In [32], a review of the main features of a turbo-expander was carried out, considering two kind of fluid: Isobutane in ORC and a mixture of water and ammonia in Kalina cycle, which is nowadays utilised in geothermal binary plants. A design procedure is achieved considering the optimum specific speed suggested by Baljè in [17], as reported in Figure (4.19).

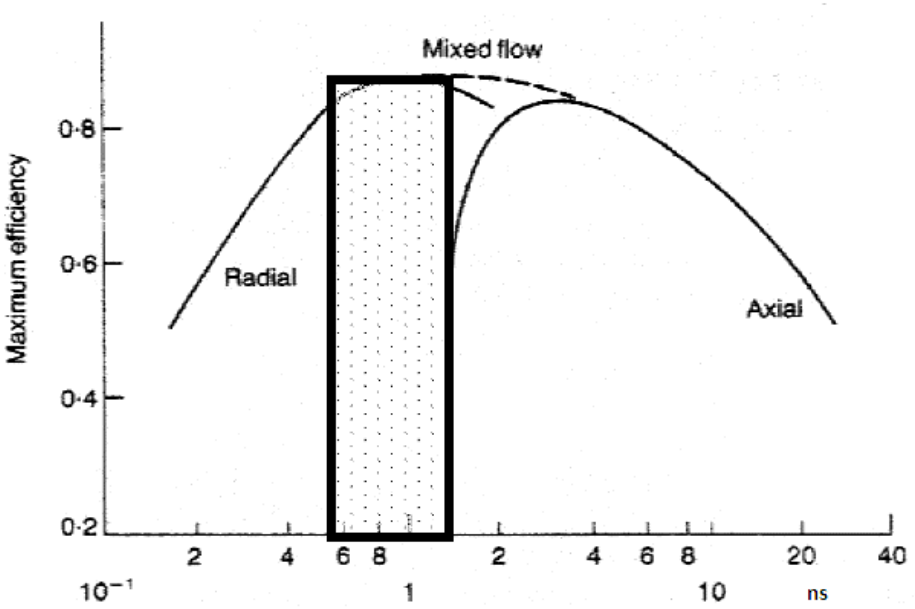

Figure 4.19 *Efficiency as a function of specific speed. Here ns is a dimensional parameter calculated with: ns=0.014358*N*√(V_out)/〖Δh〗_is^0.75*

The project is developed with a value of Ns included in the highlighted area of the graph. Again, this project does not take care of an optimization of non-dimensional project input, but are assumed directly values taken by literature. As shown in previous section, Perdichizzi and Lozza in [27] explained how the value of optimum specific speed changes in relation with the size of the expander and the fluid compressibility.

Anyway, as numerical data are not declared in this paper, it results not possible to give an evaluation of the gap between the achieved and the expected efficiency.

A similar remark can be made for [33]. Here an expander for an ORC coupled to a geothermal heat source is fully designed, both with a mean-line preliminary study and with a three-dimensional analysis. The main declared features of the device are collected in Table (4.8) and the designed nozzle vanes and rotor are showed in Figure (4.20).

Characteristics	Value
Working fluid	n-Butane
Number of stages	1
Number of blades	26
N [rpm]	6000
P [kW]	143
m [kg/s]	2.49
p_1 [bar]	21.8
T_1 [°C]	120
p_6 [bar]	4.5
D_4 [mm]	500
Declared turbine efficiency	79.43

Table 4.8 *Main features of the ORC analysed in [33]*

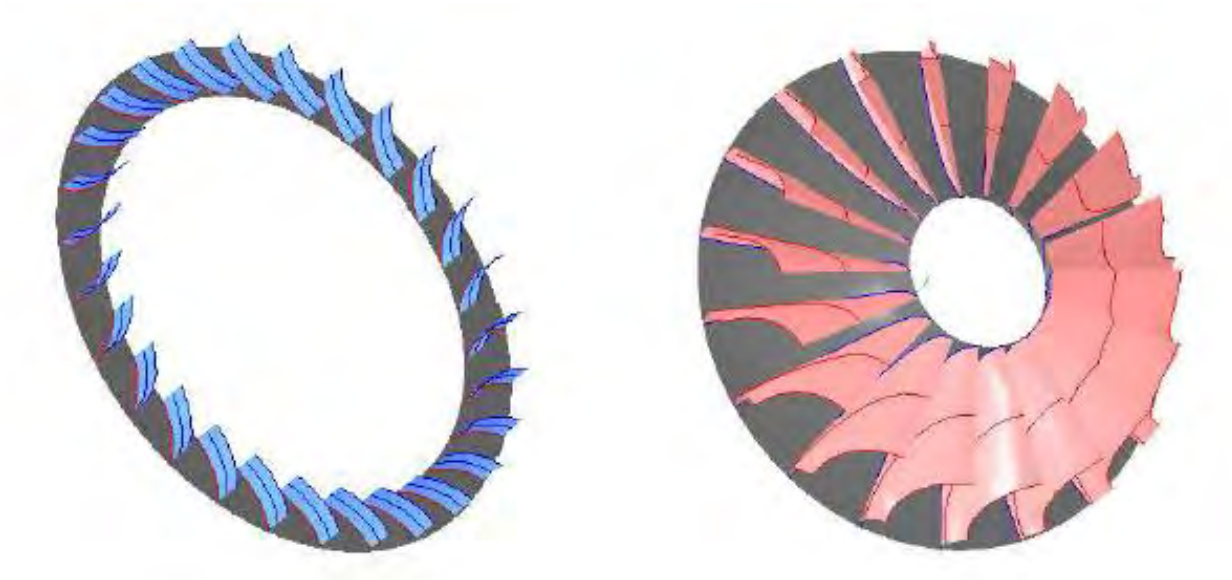

Figure 4.20 *3D design of nozzle vanes and rotor in [33].*

The preliminary design is based on the selection of an optimal specific speed as suggested by Aungier in [34], which is showed in fig (4.21).

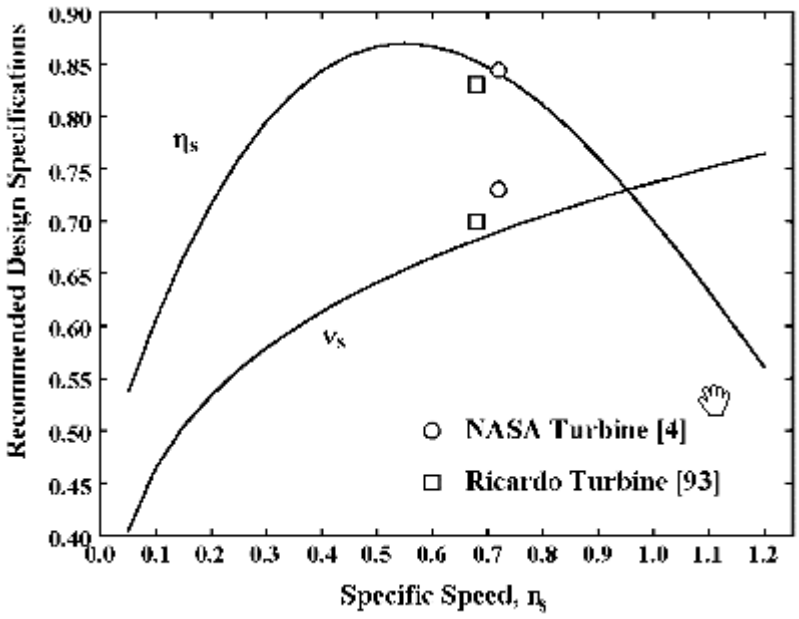

Figure 4.21 *Efficiency as a function of specific speed, [34].*

The figure shows that the maximum achievable efficiency for this kind of turbine at optimal-Ns should be approximately 85%, but actually the achieved one is only 79.43% [33]. This confirm the thesis that the project of an expander can be considered complete when an investigation about non-dimensional optimal parameters is carried out.

In [35] the operative project of a whole ORC plant is reported, where also the turbine is designed on purpose. The size of the cycle is quite small, because the mean power output is around 30kW; for what concern the radial turbine, in this case it is stated that three-dimensional design of the expander was conducted by considering the geometrical similarity of existing model turbine and the preliminary model results. This means that it is obtained by scaling down an already existing three-dimensional geometry, considering then the mean output required by cycle design. As it is reported, the model turbine has a different power output, 190kW, but most of all it was not properly projected for organic fluid applications, but for air [35]. Even if this procedure can lead to a considerable advantage in project time, reducing considerably the initial phase, we can consider that the expander design is not carried out in its optimal condition. This procedure in fact provide just a derived geometry that does not take care of size of the required device and of the different working fluid utilised.

In the following Table (4.9) are collected experimental studies, in which radial turbines are tested in ORCs. They will not be detailed analysed because any design procedure of the expander is reported. In fact, in the majority of the cases, commercial micro-turbines from other applications were employed.

Researchers	Working fluids	Isentropic efficiency	Power output [kW]	Rotational speed [rpm]	Pressure ratio
Yamamoto et al.	R-123	0.48	0.15	17000	-
Nguyen et al.	n-pentane	0.498	1.44	65000	3.45
Yagoub et al.	HFE-301	0.85	1.50	60000	1.1
Yagoub et al.	n-pentane	0.40	1.50	60000	1.3
Inoue et al.	TFE	0.70-0.85	5-10	15000-30000	4.8
Pei et al.	R-123	0.65	1.36	24000	5.2
Li et al.	R-123	0.68	2.40	40000	6.3

Table 4.9 *Main characteristics of radial turbines utilized in ORCs [2].*

In Figure (4.22) is showed the optimal field of application in terms of temperature of evaporation and temperature of condensation for radial turbines, for several organic fluids applications.

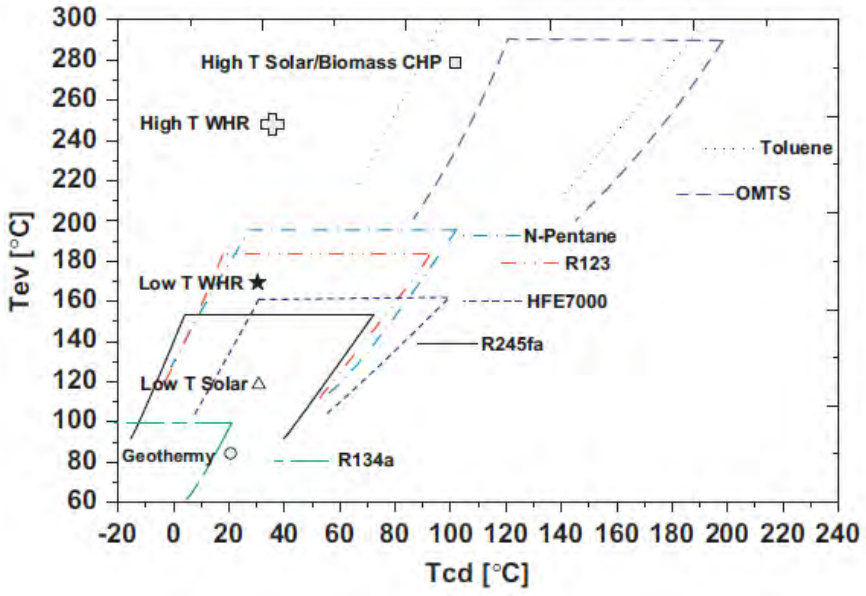

Figure 4.22 *Ideal fields of applications of several organic fluids, coupled with radial turbines in ORCs. [1]*

4.5 Optimization of ORCs taking into account real turbine efficiency

Several studies about ORCs in the literature are focused on the research of the optimal cycle parameters and working fluids that maximise the net power output. However, only few of them are evaluating the real turbine efficiency. In fact the thermodynamic optimization is performed, assuming a fixed and somewhat arbitrary efficiency value [10]. The aim of the majority of these studies is usually to find best cycle configuration or best fluid selection, that permits to optimise a certain objective function.

Some example of this approach are showed in [36], [37], and [38], which stress the importance of selecting working fluids or mixtures yielding high thermal efficiency and low values of $\dot{Q_{in}}$ and $\dot{Q_{in}}/\dot{Q_{out}}$.

However, all of these studies calculate the selected performances parameters only giving some qualitative information about the operative conditions of the turbine.

In [39], a study related to the maximisation of the net power output is presented.. A mathematical model of the turbine is created and implemented into a code, which simulates the ORC. Though here the efficiency of the expander is not considered as a fixed parameter, it is evaluated as a function only of the actual rotating speed, following the formula suggested by Zhang and Cai in [40].

$$\frac{\eta_{exp}}{\eta_{exp,des}} = \left[1 - t\left(1 - \frac{N_{exp}}{N_{exp,des}}\right)^2\right] \cdot \left(\frac{N_{exp}/N_{exp,des}}{\frac{\dot{m_{rid}}}{\dot{m_{rid,des}}}}\right) \cdot \left(2 - \frac{N_{exp}/N_{exp,des}}{\dot{m_{rid}}/\dot{m_{rid,des}}}\right) \tag{4.7}$$

Where N_{exp} and $N_{exp,des}$ are the actual and design rotating speeds, and $\dot{m_{rid}}$ and $m_{rid,des}$ are the actual and design reduced flow rates.

Even this approach cannot be considered satisfactory, because some important characteristics that have a strong influence on the expander efficiency are not considered, as the size and the expansion ratio.

A new design optimization procedure is, instead, introduced in [10], by Lazzaretto and Manente. The paper focuses the importance and the weight that the expander has on the whole cycle design definition, embedding directly the evaluation of its isentropic efficiency in the thermodynamic cycle optimization [10].

This approach utilises the correlations to calculate the efficiency suggested by Macchi Perdichizzi, in [19], basing on the map showed in Figures (4.10) and (4.11) for axial stages. As already analysed in §4.4.1, this map relates the isentropic efficiency with size parameter *VH* and volume expansion ratio *VR*. Lazzaretto and Manente assume to operate at the optimal specific speed, by properly selecting the rotational speed, fitting the relation (4.8) by a fourth order polynomial:

$$\eta_{is} = f(VR; VH) \tag{4.8}$$

The configuration of cycle considered is non-regenerative, and the heat source is a geothermal flow, characterized by a mass flow rate of 100 kg/s and an inlet temperature of 150°C. The simulation have been run in Aspen Plus environment [41] considering four working fluids: Isobutane, R-245fa, R-236fa, R236ea [10].

The net power output was maximised by varying the cycle maximum temperature. The net power output is obtained by subtracting the power generated by the turbine and the one absorbed by the pump [10]. Figure (4.23) shows the variation of the power output for the four considered fluids, taking into account a fixed value of isentropic efficiency $\eta_{is} = 0.87$.

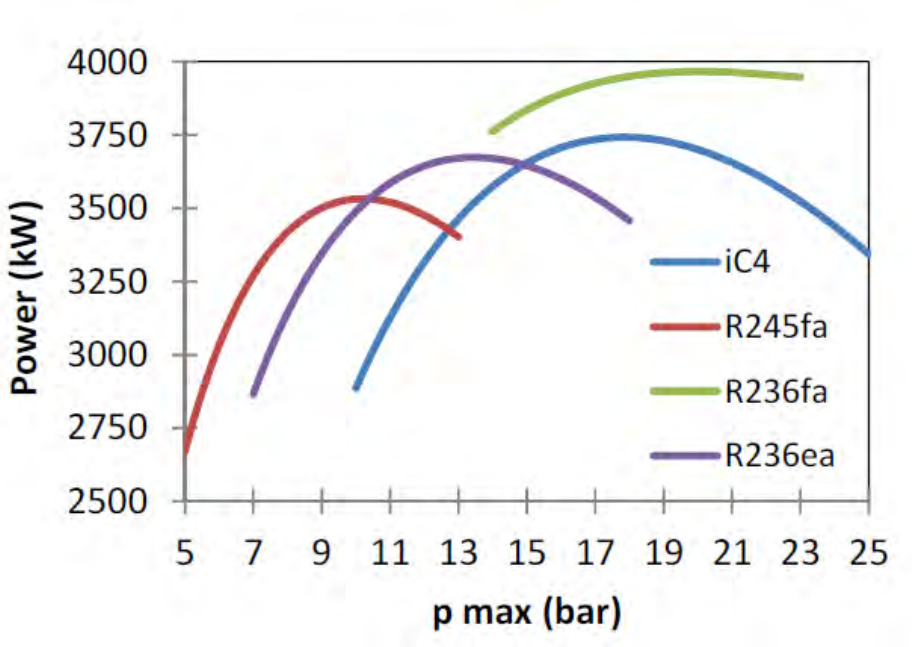

Figure 4.23 *Variation of net power output as a function of maximum cycle pressure [10]*

Considering then the cycle parameters associated to the optimal cycles, the efficiency of the expander was calculated basing on the relation proposed in relation (4.8). In this way, the effect of different *VH* and *VR* is taken into account, so that the obtained values of efficiency are collected in table (N):

	Isobutane	**R-245fa**	**R-236fa**	**R-236ea**
VR	4.357	5.071	7.007	5.206
VH	0.1821	0.2750	0.2340	0.2584
η_{is}	0.8948	0.8803	0.8710	0.8803

Figure 4.24 *Values of VH and VR calculated for different cycle configurations. Knowing these values, is possible to calculate ηis by relation (4.8).*

The variation of turbine isentropic efficiency with cycle parameters modifies the optimal configuration, in which η_{is} is fixed. Figure (n) shows the variation of net power output and turbine isentropic efficiency with the cycle maximum pressure, for the four considered fluids.

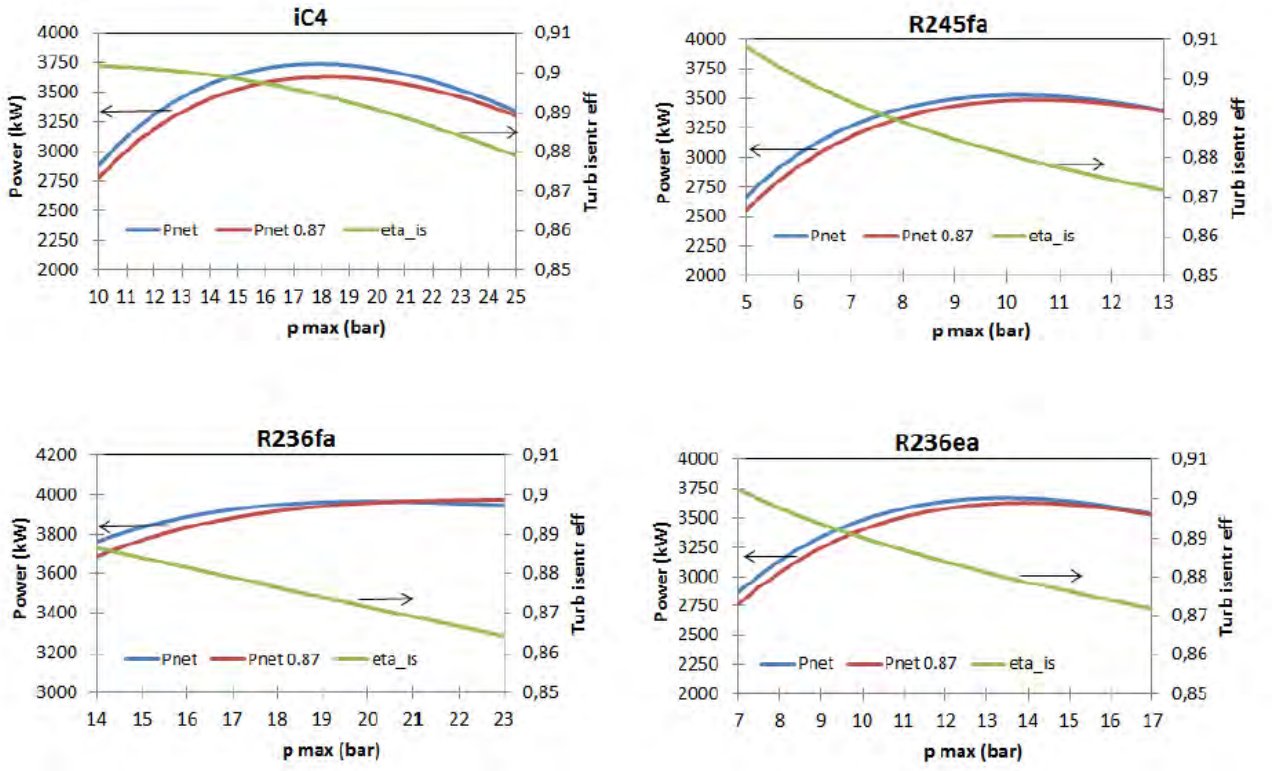

Figure 4.25 *Variation of net power output and turbine isentropic efficiency for Isobutane, R-245fa, R-236fa, R-236ea. Red line refers to a fixed ηis =0.87.*

The overall effect is to move the optimal cycle high pressure to slightly lower values compared to the fixed efficiency analysis.

This optimization procedure is general and could be applied not only to single stage axial flow turbines, but also to radial turbines if reliable efficiency correlation maps are available (as the ones showed in section §4.4.1 and by this Master thesis).

Chapter 5

Operative design procedure

The chapter will focus the operative design procedure proposed and implemented in a code, in order to design radial inflow turbines. The first part is introductive, but necessary to fix the tools and the constrains of the analysis. Then the structure of the code will be carefully analysed, separating an initial part where the geometry of the expander is created basing on theoretical models, and a second part where this geometry is studied in order to give an estimation of the achievable performances. In this second part, loss models utilised will be explained and examined. All the sections will be enriched by parts of the proposed code.

5.1 Thermodynamic properties and working fluid

The design procedure wants to have a truly general purpose, in order to be useful for wide-ranging applications.

The software code utilised for the purpose is Matlab [42], which is mathematically useful in order to implement optimization cycle. The only limit of Matlab software is that there are not any thermodynamic tools already implemented. Because of this, in past several analysis related to ORC were run with calculations referred to ideal gas, even if thermodynamic properties of organic fluids are far away to be idealised as perfect gasses [18]: this is clearly a strong limitation of a design procedure. The issue has been solved by implementation of a routine ("function" in Matlab language) able to calculate thermodynamic properties of a wide variety of fluids: the routine recall for its aim

the software Refprop-Nist [43]. This point is extremely important, because it permits to the model to refer always to real gas thermodynamic properties.

The thermodynamic routine is called in the code "refpropm"; it has a simple syntax as shown in the following example (5.1):

```
T1=200;  %[K]
p1=1000; %[kPa]
enthalpy = refpropm('H','T',T1,'P',p1,'water'); %[J/kg]
```

Code section 5.1 *Syntax required to recall a thermodynamic property from the subroutine "refpropm".*

The calling input in the example (5.1) are:

1. The required thermodynamic property ('H' means enthalpy);
2. The first input thermodynamic property, with its value ('T', 'T1');
3. The second input thermodynamic property, with is value ('P', 'p1');
4. The fluid (or the mixture) for which is necessary run the calculation ('water')

Utilising this procedure, all the required properties can be calculated starting from a couple of values already known. The main input-output properties are: temperature, pressure, density, enthalpy, entropy, internal energy, quality, speed of sound, c_p, c_v, ratio of specific heats γ, cinematic and dynamic viscosity, compressibility factor (and many others, that will not be used in this Master Thesis, but that are available in the subroutine) [43].

The design procedure is run utilising a typical organic fluid: R-245fa or *penthafluorepropane*. The choice of this fluid is related to its increasing interest in energy production studies. Several authors and studies as [24], [17], [18] utilized this fluid for their analysis, because it suitable for cycle operation conditions. One of its positive aspect, is to provide an appropriate condensation pressure, creating overpressure in the condenser at standard condensation temperature (circa 25-35°C). This means that a cycle operating with this fluid does not need any degasser for non-condensable gasses inasmuch as, the pressure into the condenser is higher than the atmospheric pressure. Furthermore, it does not damage the ozone layer, so that it is not subject to green-house emission regulations, it is not flammable, not toxic, and has a satisfactory thermal stability [24]. Moreover, the positive slope (see Figure (5.1)) of the curve of saturated vapours, avoids the problem of having a wet fluid at the turbine outlet section. A superheated vapour is here preferred, in order to escape damage problems caused by liquid drops hitting turbine blades.

In Table (5.1) are reported some of the main properties of R-245fa.

Molecular name	Molecular weight	Critical pressure	Critical Temperature	Boiling point
$CF_3CH_2CHF_2$	134 g/mol	3640 kPa	427.2 K	288.4K (at 100kPa)

Table 5.1 *Properties of R-245fa.*

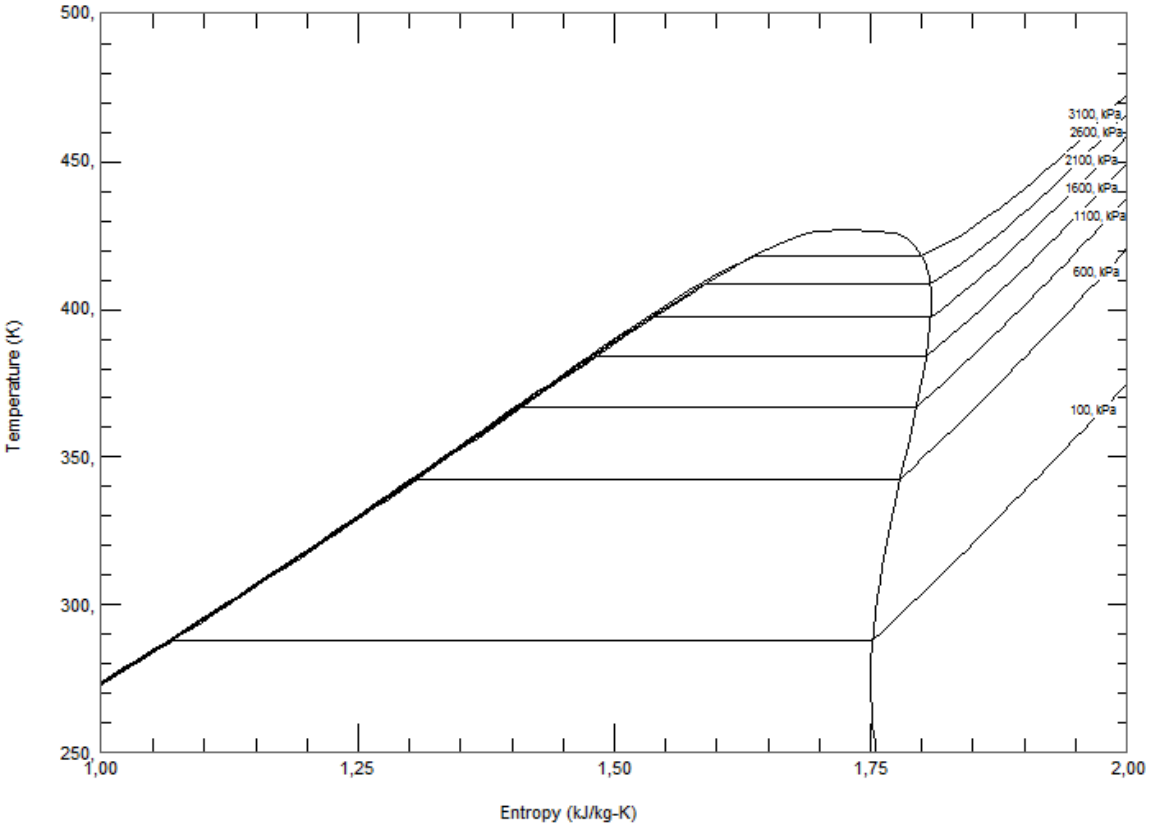

Figure 5.1 *T-s diagram of R-245fa.*

5.2 Code structure

The code structure can be mainly split in two different parts, in which the second is a consequence of the first and cannot be seen as a standalone code. Also the first one, anyway, requires iteration on some parameters involved in the second part:

- Preliminary geometry design (PGD); in this first part the main geometry dimensions and velocity triangles related to the rotor and the stator are generated. The model used is quite similar to the one suggested by Moustapha in [11].
- Performance prediction (PP); the second part will analyse, following several losses models and correlations, the efficiency that the geometry already produced in the first can achieve. Moreover, in this part are generated also the geometrical parameters of other components

linked to the stage, as volute, inlet vanes and diffusor. These components clearly affects the achievable efficiency and the turbine functioning in several ways.

To run the code starting from different input parameters allows to appreciate their incidence on the achievable performance changes. This can be clearly considered one of the most important goals of this work, because it can provide important informations for a further design strategy, not only for the expander but also for the cycle parameters.

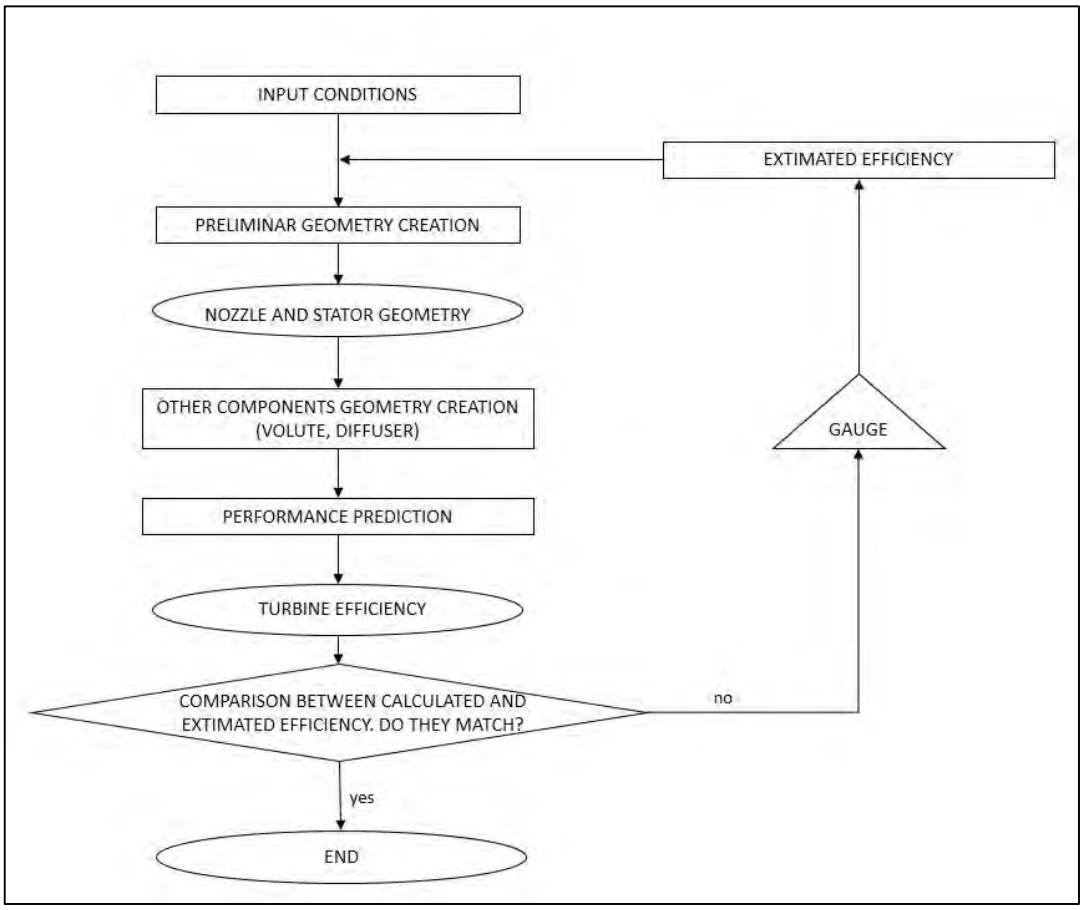

Figure 5.2 *Schematic representation of the code architecture.*

5.3 Preliminary geometry design

The design routine starts fixing several input parameters, and calculating the thermodynamic properties of characteristic points related to inlet and outlet fluid conditions.
In this way, we can here clarify the main inputs:

- Size parameter *VH*; the analysed range is from 0.008m to 0.3m, which are approximately correlated to produced power from 60kW until 500kW ;
- Volumetric flow rate variation *VR*; the analysed range goes to VR_{min}=2.80 to VR_{max}=8.20; to be exact this parameter is set by choosing the inlet condition (T_{01} and p_{01}) and the outlet pressure (p_{06}).

  The value of p_{01} is chosen by the designer in a useful range, which means that it should be a value suitable for a cycle system utilisation. From that, the saturation conditions characterized by a unitary quality are known. It would be better, and it is a common design practice, to set an overheating of 5-10°C, in order to have an overheated fluid entering the turbine. In this way the possibilities to have liquid phase at the inlet conditions are avoided.

  The pressure p_{06} is fixed, valuating a typical operative temperature in the condenser; this could be in the range of 25-45°C.

  VR fixes also an important parameter, as to say the isentropic enthalpy drop Δh_{0s} between inlet and outlet, which is a very important design value that has a large influence on the subsequent steps.
- Flow coefficient Φ, whose analysed range goes from Φ_{min}=0.15 to Φ_{max}=0.4;
- Load coefficient Ψ, whose analysed range goes from Ψ_{min}=0.7 to Ψ_{max}=1.4;
- Speed of rotation *N*; the range of this input must be changed in different simulations, in order to maintain the specific speed in the ideal range (between 0.4 and 0.8, according to [12]). In particular, maintaining other input as constant (so Δh_{0s}=constant), if *VH* decreases, the mass flow rate will decrease, so also *Q*. In order to maintain *Ns* in the ideal range, *N* must be increased (see relation (5.1)).

$$VH = \frac{\sqrt{V}}{\Delta h_{is}^{0.25}} \downarrow \rightarrow Q \downarrow \quad if\ N_s = \frac{\omega\sqrt{V}}{\Delta h_0^{3/4}} = cost. \rightarrow \ \omega \uparrow \tag{5.1}$$

Other geometrical parameters, that are considered as fixed will be discussed in the following sections. We can here consider that having VH and VR as input parameters, means that also the mass flow rate is fixed:

$$m = \rho_{06s}\sqrt{VH \cdot \Delta h_{0s}} \tag{5.2}$$

In Code section (5.2) is reported an example of this first part. It is important to note, that here are reported some of the typical values, which have been use in one of the simulations.

```
p01=1000;          %kPa
[T01sat, h01sat, s01sat]=refpropm('THS','P',p01,'Q',1,'r245fa'); %K          J/kg
J/(kg*K)
surr=7;            %°C   hypothesis of overheating
T01=T01sat+surr;
[h01, s01, rho01]=refpropm('HSD','T',T01,'P',p01,'r245fa');       %K          J/kg
J/(kg*K)
T06sat=30+273.15; %K
[p06]=refpropm('P','T',T06sat,'Q',1,'r245fa'); %kPa
[h06ss, rho06ss]=refpropm('HD','P',p06,'S',s01,'r245fa');  %J/kg kg/m^3
Dh_is=(h01-h06ss);      %J/kg

VR=rho01/rho06ss;
rpm=[17000];
VH=0.008;    %m

phi=.2;
psi=0.9;

m=sqrt(VH*Dh_is^.25)*rho06ss; %kg/s
```

Code section 5.2 *Example of the calculation of the initial thermodynamic parameters. In particular, are here reported some inputs as inlet and outlet pressure, overheating, VH, Φ and ψ.*

The next step is to give an estimation of the total-to-total efficiency η_{tt}. It should be clear that, thus the evaluation of the efficiency is the main aim of the whole model, this parameter have to be considered not as fix but as the base of iteration. Indeed, at the end of the code calculation, η_{tt} have to be re-compute using losses models and correlation implemented in the second part (PP). Anyway, is here necessary to give a first attempt value, that will generate a specific geometry: the efficiency of this geometry will be later evaluated and a new value of η_{tt} will be both the result of the performance evaluation, and the value utilized in the second attempt iteration.

From the definition of total-to-total efficiency, now is possible to calculate the enthalpy of the point 06:

$$h_{06} = h_{01} - \eta_{tt}(h_{01} - h_{06s}) \tag{5.3}$$

$$\Delta h_0 = h_{01} - h_{06} \tag{5.4}$$

And the power output *P* as:

$$P = m\Delta h_0 \tag{5.4}$$

It is now necessary to calculate the rotor tip blade speed U_4. In some particular applications U_4 could be an input datum, because, for instance, of high temperature gasses or stress consideration. In our case however, the inlet temperature is always set under 120°C, so we can consider our applications far away from this kind of technical problems. In this way, the rotor tip blade velocity is, from definition of load coefficient Equation (3.14):

$$U_4 = \sqrt{\frac{\Delta h_0}{\Psi}} \tag{5.5}$$

The rotor exit swirl at design condition is set to be zero. Indeed, high levels of tangential velocity at the outlet section cannot effectively be diffused, giving a rise of kinetic energy losses. The Euler turbomachinery equation can be now written as:

$$C_{u4} = \Psi U_4 \tag{5.6}$$

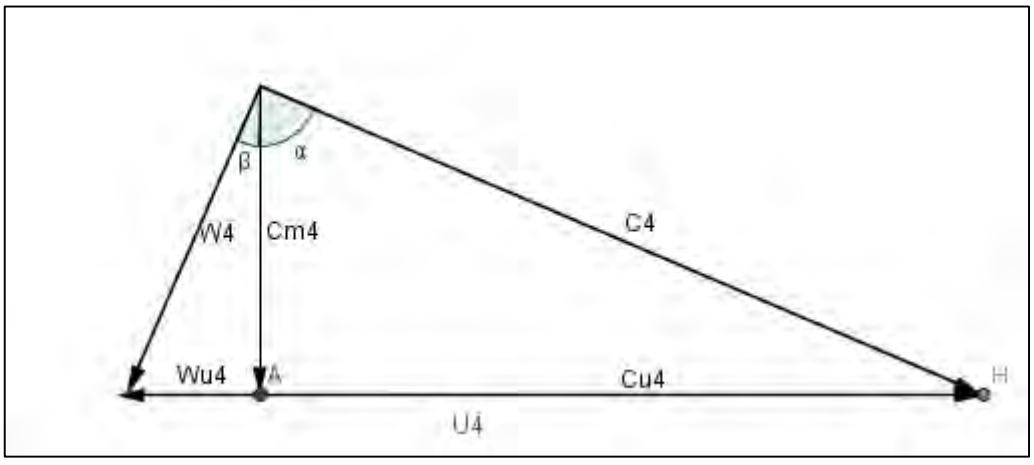

Figure 5.3 *Velocity triangle at the rotor inlet*

In this way, the velocity triangle at the rotor inlet (state 4) can be completely defined by the relations:

$$C_{m4} = E\Phi U_4 \tag{5.7}$$

Where E is the meridional velocity ratio. E has influence on the definition of the geometrical aspect of inlet and outlet blade height. In this project, as said before, it has been considered constant as $E=1$; this means that also the flow coefficient is a constant at inlet and outlet ($C_{m4} = C_{m6}$).
Hence, the absolute velocity:

$$C_4 = \sqrt{C_{m4}^2 + C_{u4}^2} \tag{5.8}$$

$$\alpha_4 = tan^{-1}\left(\frac{C_{u4}}{C_{m4}}\right) \tag{5.9}$$

$$\beta_4 = tan^{-1}\left(\frac{C_{u4} - U_4}{C_{m4}}\right) \tag{5.10}$$

The rotor tip radius is:

$$r_4 = \frac{U_4}{\omega} \tag{5.11}$$

If we fix the inlet blade geometry is completely radial, so the blade angle will be $\beta_{4b}=0°$. This choice is up to the designer, and has been preferred to other technical solution because is particularly suggested in applications, which demand a high level of rotor stress. This could be the case of a heavy-duty application for electricity generation.
The incidence angle is now:

$$i = \beta_4 - \beta_{4b} \tag{5.12}$$

The incidence angle is an inlet characteristic that should be carefully investigated during the design procedure: several studies show that the best efficiency occurs not at zero incidence, but when its value is slightly negative [12]. This is because the blade loading produces a large static pressure gradient across each passage, which tends to move the flow from the pressure to the suction surface against the direction of rotation [12], as showed in Figures (5.4). Indeed, Rodgers in [44] quotes angles of -20°, Rohlik in [45] indicates values as high as -40°, instead studies by Yeo and Baines in [46] assess -25°. Anyway, an empirical procedure to calculate the ideal i will be presented in §5.4.2, in order to evaluate the incidence losses.

If the designer is free to set the inlet blade angle β_{4b}, this can be set in order to achieve the ideal condition.

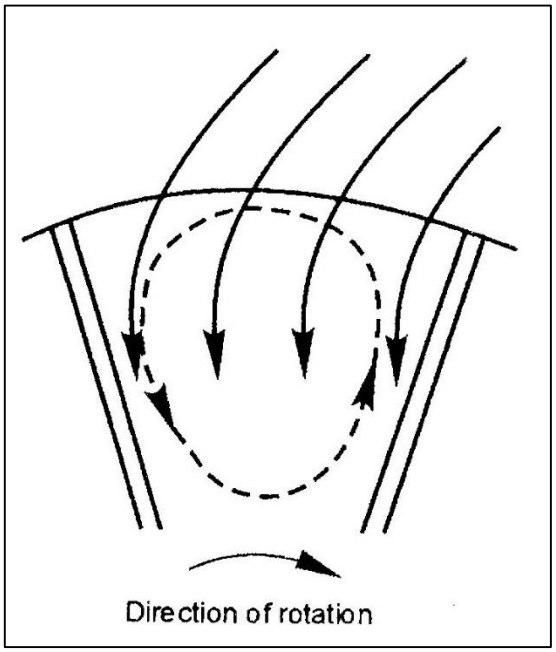

Figure 5.4 *Recirculation in the inlet region of a radial turbine rotor passage [11].*

The part of the Matlab code related to inlet velocity triangles is reported in Code section (5.3):

```
E=1; %rotor meridional velocity ratio;
U4=(Dh_tt/psi(k))^.5;   %m/s
Cu4=psi(k)*U4;          %m/s
r4=U4/omega;            %m
Cm4=E*phi(h)*U4;        %m/s
C4=(Cm4^2+Cu4^2)^.5;    %m/s
alfa4=atand(Cu4/Cm4);   %°
beta4=atand((Cu4-U4)/Cm4);    %°
W4=Cm4/cosd(beta4);     %m/s
beta4b=0;               %radial inlet blade
i=beta4-beta4b;
```

Code section 5.3 *Evaluation of the magnitudes of inlet velocity triangles vectors.*

The thermodynamic properties of the working fluid at state 4 are now calculated.

Considering with good approximation an adiabatic stator, it is possible to evaluate the enthalpy as a constant between the stator inlet and the rotor inlet ($h_{01} = h_{04}$); from this it follows the static enthalpy as:

$$h_4 = h_{04} - \frac{C_4^2}{2} \tag{5.13}$$

Referring to the definition of nozzle loss coefficient in terms of static enthalpy ε_h, given by Benson in [47]:

$$\varepsilon_h = \frac{h_4 - h_{4s}}{h_{04} - h_4} = \frac{h_4 - h_{4s}}{\frac{C_4^2}{2}} \tag{5.14}$$

Is possible to calculate the enthalpy of the state 4s. This is clearly worthy, because this state is situated on the isentropic line staring from the station 01, so that two input are known in order to calculate pressure of the point 4s, which is isobaric with 4.

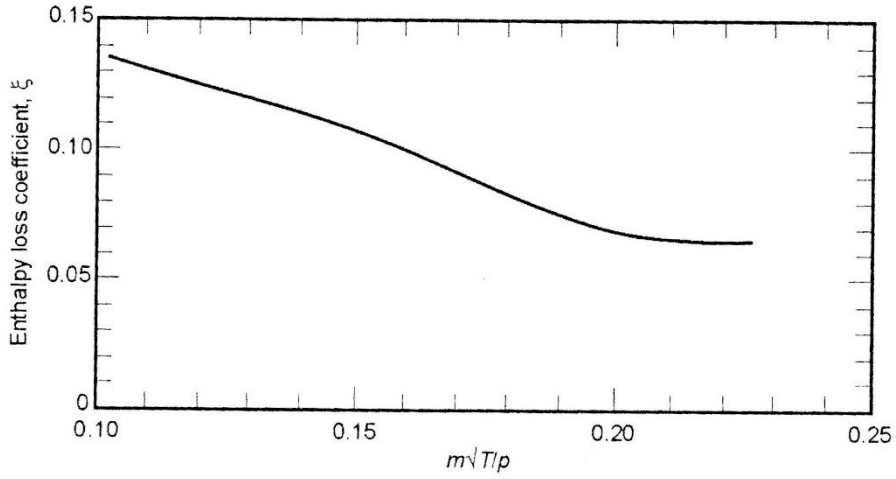

Figure 5.5 *Nozzle loss coefficient [47].*

The calculation of the parameter ε_h is done referring to the Figure (5.5) reported in [22]. The graph has been implemented as a Matlab function called "`stator_losses_benson`", whose input is the non-dimensional flow rate $\left(m_{rd} = \left(m\sqrt{T_{01}}\right)/p_{01}\right)$.
The enthalpy of point 4s is then:

$$h_{4s} = h_4 - \varepsilon_h \frac{C_4^2}{2} \tag{5.15}$$

By Refprop subroutines we have:

$$\{h_{4s}, s_{4s} = s_{01}\} \xrightarrow{Refprop} \{p_{4s}\} \tag{5.16}$$

$$\{p_4 = p_{4s}, h_4\} \xrightarrow{Refprop} \{T_4, \rho_4, s_4, a_4\} \tag{5.17}$$

$$\{h_{04}, s_{04} = s_4\} \xrightarrow{Refprop} \{T_{04}, p_{04}\} \tag{5.18}$$

In addition, the Mach number at inlet is now known:

$$Ma_4 = \frac{C_4}{a_4}; \tag{5.20}$$

The inlet rotor area and the blade height, from continuity equation are:

$$A_4 = \frac{m}{\rho_4 C_{m4}}; \quad b_4 = \frac{A_4}{2\pi r_4} \tag{5.21}$$

```
h04=h01; %adiabatic stator
h4=h04-.5*C4^2;
eps_h=stator_losses_benson(m_rid); %stator enthalpy losses from Benson (1970)
h4s=h4-.5*eps_h*C4^2;
p4s=refpropm('P','H',h4s,'S',s01,'r245fa'); p4=p4s;
[T4, s4, rho4, a4]=refpropm('TS','P',p4,'H',h4,'r245fa'); s04=s4;
[T04, p04]=refpropm('TP','H',h04,'S',s04,'r245fa');
Ma4=C4/a4;
Ma_rel4=W4/a4;
A4=m/(rho4*Cm4);  %m^2
b4=A4/(2*pi*r4);  %m
```

Code section 5.4 *Stator model and thermodynamic evaluation of state 4.*

For what concern the outlet velocity triangle, we consider as design principle to have a completely axial flow, without swirl. Indeed:

$$C_6 = C_{m6} = \Phi U_6 \tag{5.22}$$

The static enthalpy at station 6 is:

$$h_6 = h_{06} - \frac{C_6^2}{2} \tag{5.23}$$

$$\{s_6 = s_{06}, h_6\} \xrightarrow{Refprop} \{T_{6,}, \rho_6, s_6, a_6\} \tag{5.24}$$

From the continuity equation, the outlet area is:

$$A_6 = \frac{m}{\rho_6 C_{m6}} \tag{5.25}$$

With a known outlet area value, the code has to relate this to hub and tip radii at this point. Usually the hub radius is limited by crowded of the blades or shaft sizes, so is set as a ratio of the rotor inlet radius; a value suggested by literature in [11], as minimum attainable is $\frac{r_{6h}}{r_4} = 0.3$.

The outlet blade height is defined as:

$$b_6 = r_{6s} - r_{6h} \tag{5.26}$$

```
Cm6=phi(h)*U4;     %m/s
C6=Cm6;            %m/s
h6=h06-.5*C6^2;    s6=s06;
[T6, p6, rho6, a6]=refpropm('TPDA','H',h6,'S',s6,'r245fa');
A6=m/(rho6*Cm6);   %m^2
b4=A4/(2*pi*r4);   %m
r6h=.3*r4;         %m
r6s=sqrt(A6/pi+r6h^2);  %m
b6=r6s-r6h;        %m
r6_RMS=sqrt(r6h*r6s);   %m
```

Code section 5.5 *Outlet velocity triangles and geometry.*

It is at this step also possible to define completely the velocity triangles at the state 6, as all the main related variables are known; in particular, the radius change of this section implies the variation of the blade velocity from the hub, increasing until the shroud. This creates different velocity triangles in different sections, so that it is worthy to calculate the corresponding ones at r_{6h}, r_{6s}, r_{6rms} (root mean square radius).

$$U_{6h} = \omega r_{6h} \;\; ; \;\; U_{6s} = \omega r_{6s} \;\; ; \;\; U_{6rms} = \omega r_{6rms} \tag{5.27}$$

$$W_{6h} = \sqrt{C_{m6}^2 + U_{6h}^2} \;\; ; \;\; W_{6s} = \sqrt{C_{m6}^2 + U_{6s}^2} \;\; ; \;\; W_{6rms} = \sqrt{C_{m6}^2 + U_{6rms}^2} \tag{5.28}$$

Thus, considering a completely axial flow, the exit blade angle is:

$$\beta_{6h} = tan^{-1}\left(\frac{-U_{6h}}{C_{m6}}\right) \quad ; \quad \beta_{6s} = tan^{-1}\left(\frac{-U_{6s}}{C_{m6}}\right) \quad ; \quad \beta_{6rms} = tan^{-1}\left(\frac{-U_{6rms}}{C_{m6}}\right) \tag{5.29}$$

The design procedure in Whithfield and Baines [12] suggest to have an exit flow angle $\beta_{6b}=65°$ when the outlet flow is completely axial.

These equations allows the designer to estimate a first attempt geometry, which can be subsequently tested in order to estimate its performance and the achievable efficiency. Changing one of the input will clearly affect the defined geometry, so that is possible to study several possibilities and design parameters.

In a second step these geometrical parameters can be optimized, accounting the fact that many assumptions were initially made [11]. Anyway, the experience from literature suggest that these conditions should not be too far from the optimal one.

Some important parameters should be checked: in a previous section, we reported some indications suggested by literature for what concern the incidence angle, but also the inlet and exit blade tip radii must be compared. This parameter is directly linked to the curvature of the rotor shroud contour in the meridional plane. In particular is often suggested that light curvature can lead to higher efficiency; a typical value suggested is $r_{6s}/r_4=0.7$ [11].

In the following graph of Figure (are reported some values obtained for different optimised configuration, as function of *VH* and *VR*; for exception of VH=0.008, is shown a decreasing trend with VH: this means that larger turbine can effort slightly higher curvature maintaining a high efficiency without penalties.

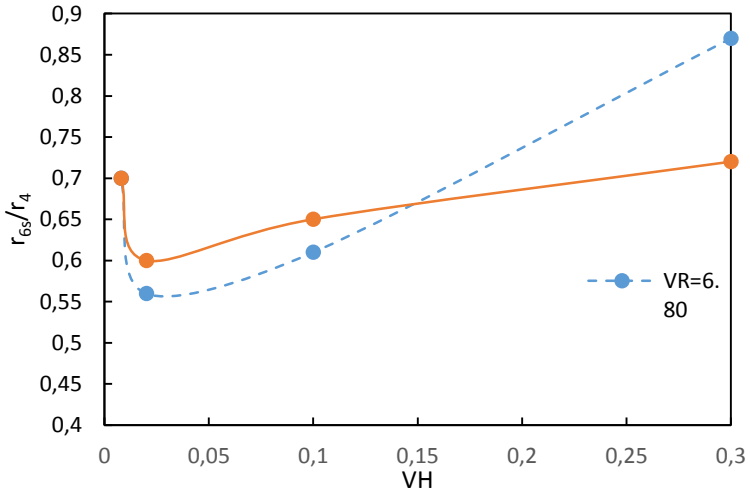

Figure 5.6 *Inlet to outlet shroud radii ratio, as a function of VH and VR. This parameter is an important geometric aspect, which has influence on the curvature of the shroud section of the expander*

This range of value is also supported by the graph from Rodgers and Geiser in [48], which represent the relative maximum achievable efficiency, as a function of r_4/r_{6rms} and solidity ($s = Z_b/2r_4$). Here the maximum efficiency are achieved in the range of inlet to outlet shroud radii ratio between 0.55 and 0.67; it is important to note that the reference is not the shroud radius but the root mean square one.

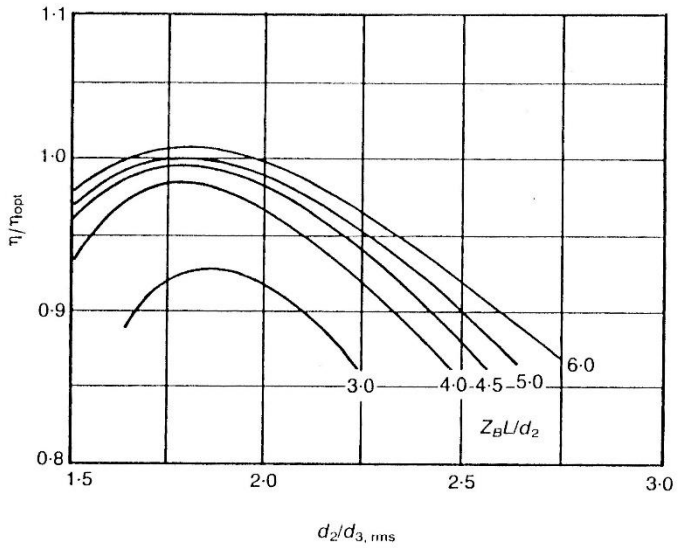

Figure 5.7 *Effect of rotor diameter ratio and blade solidity on radial turbine efficiency [48]*

To run this first part of the code is useful in order to produce indications and terms of comparison with the final results of the whole code, that will take into account both the generated geometry and the losses correlation by several components.

In the code section (5.6), are collected some outputs generated by the preliminary geometry design, for a specific input condition: this a good is way for the designer to check the outputs of the PGD, in particular for the most sensible parameters.

Moreover is possible to create figures as the one of (5.8), in order to control the thermodynamic states of the main sections of the expander. From it, the designer can also easily get a fast idea of the degree of reaction, which is calculated by the following relation:

$$R = \frac{\Delta h_{rot}}{\Delta h_{stage}} = \frac{h_4 - h_6}{h_1 - h_6} \tag{5.30}$$

This parameter is extensively used in axial and radial turbine design, because it represent the amount of static enthalpy exchanged by the rotor, with respect to that in the stage. Even if is a non-dimensional parameter, it cannot be directly correlated to flow and load coefficients. Although in many

publications it is considered as an input parameter, in this code it is just an output of the design procedure, but still be an important value that has to be investigated.

```
     PRELIMINARY GEOMETRY OUTPUT

 Design Parameters
[kW]     P= 1000.0000
[kPa]    p01= 1500.0000
[K] T01= 401.0013
[kPa]    p06= 211.7154
[rpm]    rpm= 9000.0000
[m]    VH=0.5
       VR=7.28

 Input parameters
psi= 0.9180
phi= 0.2150
eta_tt= 0.8000
Cm4/Cm6= 1.0000
r6h/r4= 0.3000

 Calculated general parameters
[kg/s]  m= 31.1754

[j/kg]  Dh_tt= 32076.5927
Ns= 0.6900
R= 0.5277

 Rotor inlet (4)
[m/s]    U4= 186.9273
[m/s]    C4= 176.2427
[m/s]    W4= 43.0132
 [K] T4= 375.3250
 [kPa]   p4= 657.2094
[m^2]   A4= 0.0245
[m] r4= 0.1983
[m] b4= 0.0197
[°] alfa4= 76.8186
[°] beta4= -20.8766
[°] angolo di incidenza con beta_b4=0
i= -20.8766

Ma4= 1.2328
Ma_rel4= 0.3009

 Rotor outlet RMS (6)
 [m/s]   U6_RMS= 94.7509
[m/s]   C6= 40.1894
[m/s]   W6_RMS= 102.9219
[K] T6= 351.0299
[kPa]   p6= 203.6897
[m^2]   A6= 0.0795
[m] r6_RMS= 0.1005
[m] r6h= 0.0595
[m] r6s= 0.1699
[m] b6= 0.1104
[°] beta6_RMS= -67.0154
Ma6= 0.2726
Ma6__RMS_rel= 0.6982
```

Code section 5.6 *Typical output values of the preliminary geometry design.*

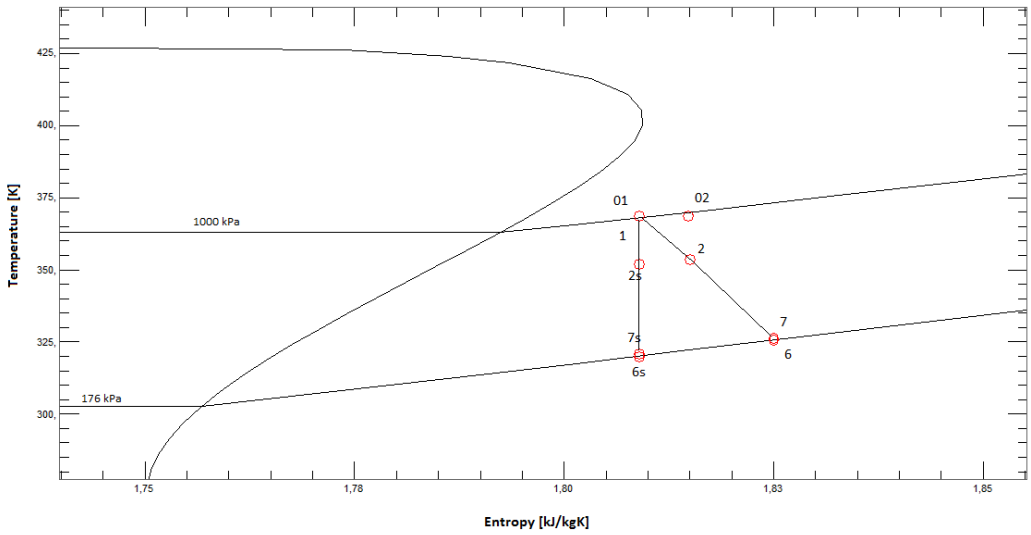

Figure 5.8 *Example of expansion on T-s diagram.*

5.4 Performance prediction

The first part of the code was explained, and principally we can state that its main aim is to create an expander geometry. In particular, the main information are linked to the velocity triangles at the inlet and the outlet of the rotor.

This allows the designer to add other components into the analysis, as the volute, the inlet nozzle and the exhaust diffuser, in order to have a full idea of the performance that the whole stage can achieve.

The code follows now the flow of the operative fluid through the different devices of the stage. For each, several assumption will be made, according to literature sources, in particular to [11] and [12], which are the most used theoretical basis to create the model.

5.4.1 Volute

The purpose of the volute is the correct distribution of the flow to the stator, from the periphery of the component to the central part [12]. Ideally, the flow entering each vane of the stator should have the same mass flow rate and a uniform static pressure. In this way, every rotor blade should process the right amount of fluid in the condition of load for which it was designed.

Indeed, these conditions are hard to get, given the complexity of the flow. The flow enter the volute in a tangential direction to the rotor, and here it is turned with a large swirl component of velocity, in order to enter in the periphery of the stator. Moreover, the part of the flow which cannot enter, should

re-enter in the main stream, mixing at the tongue of the volute. For this reason, there is just a little agreement among designers about the best volute geometry [11].

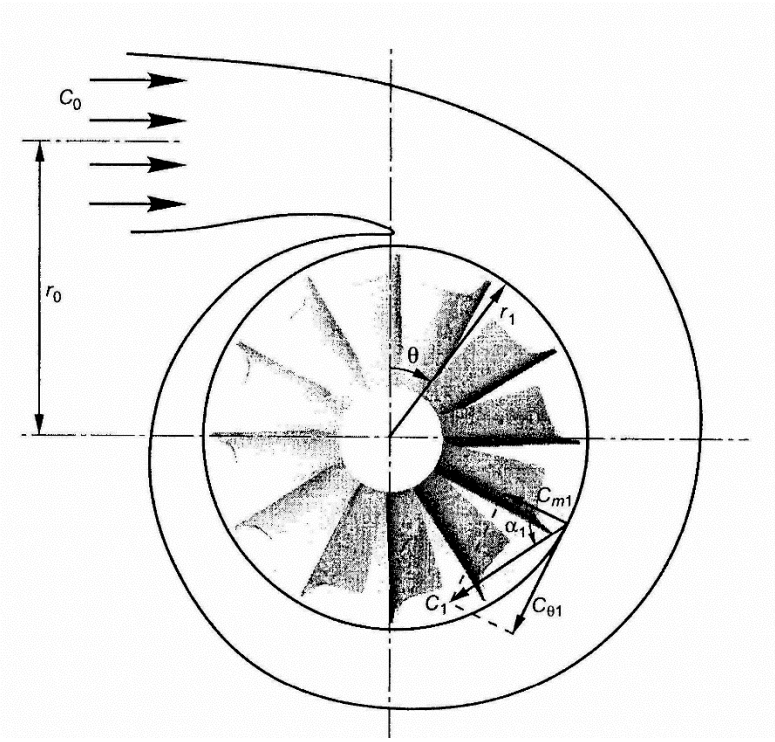

Figure 5.9 *Scematic representation of the volute*

Barnard and Benson in [50] measured up to 1.5% variation in turbine total to total efficiency drop, due to different stage profile and cross section. Chapple et al.reported in [50] the measurement of circumferential static pressure variation in both the volute exit and the rotor exit planes, which confirm the propagation of non-uniformities in the flow through the rotor. This unsteady flow can lead to non-designed condition, but also it can promote undesirable rotor blade vibration.

Anyway, the code proposed to study the flow through the volute is simple, taking into account an ideal condition. Its main aim is to fix the velocity condition entering into the stator. For this reason, the geometrical radii aspects were fixed by the designer as constant. In particular they are:

- $r_1/r_4 = 1.3$
- $r_0/r_1 = 2$

In this way is possible to estimate the velocity components at the inlet of the stator basing on free-vortex equation:

$$rC_u = constant \tag{5.31}$$

The velocity at the inlet of the volute is defined, using the continuity equation, as:

$$C_o = \frac{m}{\rho_1 A_0} \tag{5.32}$$

where A_0 represent the inlet volute area. The tangential and meridional components of the velocity entering the nozzle (point 1) are calculated using the relations:

$$C_{u1} = C_0 \frac{r_0}{r_1} \quad ; \quad C_{m1} = C_0 \frac{A_0}{A_1} \tag{5.33}$$

At this step is necessary to introduce an iterative process, in order to calculate the characteristic of the thermodynamic state 1.In fact, the density of this state is required in equation (5.32). In the following sections, many iterative procedure will be implemented in the code, using "while cycle", a Matlab function that fits in the best way an iterative calculation.

In the "while cycle" the code repeats a statement an indefinite number of times, until an expression is satisfied. This means that, in our case, the designer can choose as expression to be satisfied the accuracy of a particular thermodynamic property, so that the code will repeat the calculation until two subsequent iterations will give results included in the accuracy range.

The choice of the accuracy range is clearly up to the designer, and can affect both the reliability of the outputs (in a little percentage) and the code time execution: the more the range is narrow and the more iteration are required, requesting time, but giving more exact results. Only the experience of the designer is able to suggest a good compromise.

In the application we choose to iterate basing the "while cycle" on the density at static state 1. The first attempt value fix it equal to the one of the total state 01, so $\rho_1' = \rho_{01}$.

From it, using Equations (5.31) and (5.32), the absolute velocity C_1 is known.

Thus:

$$h_1 = h_{01} - \frac{C_1^2}{2} \tag{5.33}$$

From the real fluid properties of Refrprop:

$$\{h_1 , s_1 = s_{01}\} \xrightarrow{Refprop} \{\rho_1''\} \tag{5.34}$$

In this way, the code has two values of density to compare; in this case the acceptable range was set as $\Delta\rho = 0.1\ [kg/m^3]$. Considering the calculated values of ρ_1, the error introduced by this iterative process is around 0.2-0.5% of the density.

```
r1=1.3*r4;  %[m]
b1=b4;      %[m]
A1=2*pi*r1*b1;    %[m^2]
r0=2*r1;    %[m]
A0=pi*(r0-r1)^2;  %[m^2]

rho1_prec=1000;   %first attempt value
rho1=rho01;       %first attempt value
   while (abs(rho1-rho1_prec))>.1
            C0=m/(rho1*Av);   %[m/s]
            Cu1=Cv*rv/r1;     %[m/s]
            Cm1=Av/A1*Cv;     %[m/s]
            C1=sqrt(Cu1^2+Cm1^2);   %[m/s]
            h1=h01-.5*C1^2;         %[kJ/kg]
            s1=s01;                 %[kJ/kgK]
            [p1, rho1_prec_c]=refpropm('PD','H',h1,'S',s01,'r245fa');
            rho1_c=sqrt(rho1*rho1_prec);
   end
```

Code section 5.7 *Model of the volute, with "while cycle" to calculate the state 1.*

At the convergence of the iteration process, the static state 1 is thermodynamically completely known, as well as the absolute module of and the angle α_1 from Equation (5.35):

$$\alpha_1 = tan^{-1}\left(\frac{\rho_1(A_1/r_1)}{\rho_0(A_0/r_0)}\right) \tag{5.35}$$

In order to define the cross section, considering density variation relatively small, the following relation can be used:

$$\frac{A_\theta}{r_\theta} = \frac{m}{\rho_1 C_0 r_0}\left(1 - \frac{\theta}{2\pi}\right) \tag{5.36}$$

Where r_θ is the radius of the centroid of the section related to azimuth angle θ [rad].

The angle of flow at which the fluid approaches the rotor has a large influence on the swallowing capacity of the turbine, in particular in the case of nozzleless turbine [12].

5.4.2 Nozzle

The nozzle consist of an annular ring of vanes, which set the angle of approach of the working fluid to the rotor. It receive the flux from the volute, which has already given a swirl velocity component, whose approach angle is expressed by the value of α_1 in Equation (5.35). The main aim of the couple volute-nozzle is to accelerate the working fluid and give to it and ideal incidence angle while leaving the nozzle annulus, as required by the rotor inlet in the preliminary geometrical design [11]. The vanes will therefore need a little camber, or possibly not at all. In this work indeed was decided to design the blade as completely straight, without camber geometry. A straight vane set at some angle to the radial direction will actually turn the flow in the tangent direction as it moves inwards, and that is to say that it is aerodynamically loaded.

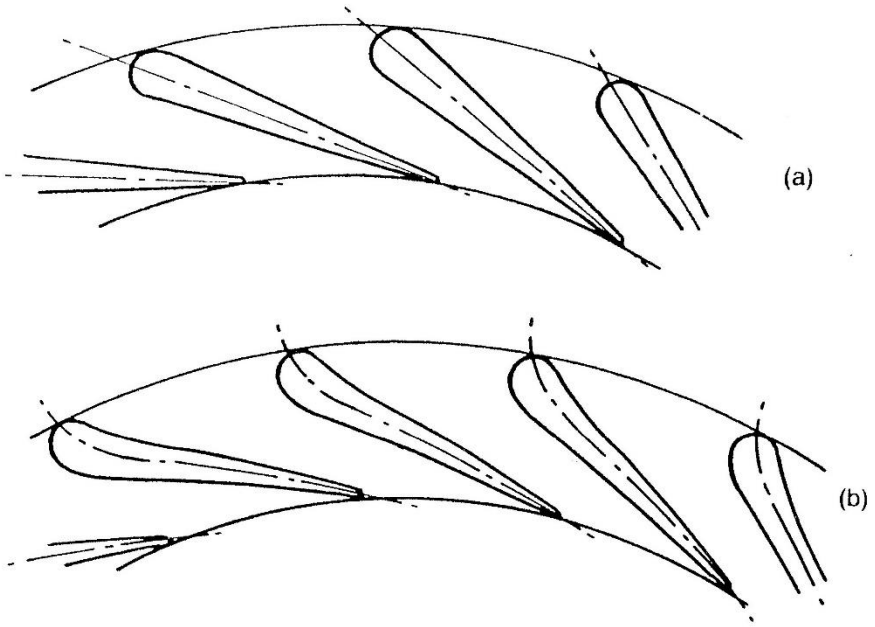

Figure 5.10 *Uncambered (a) and cambered (b) radial turbine nozzle guide vanes [11].*

The profile considered for inlet vanes is simple, consisting of a straight taper from the leading edge to the trailing edge circle; this is often quite adequate, so that an airfoil vane section is here not required. It must also be state that the aerodynamic load on each nozzle vane is a direct function of the number of vanes. If they are too few, the load will be excessive and this will lead to a large

reduction in vane surface velocities due to separations. Jansen in [51] suggested a minimum number of vanes, by studying a simple pattern, as shown in figure (5.11). Here the minimum number of vanes has been related to the inlet-outlet nozzle angles or the radii ratio. In our case the radius ratio was fixed as 1.3, and the inlet angle in the best configurations is always in the range of 70-80°. In this way, the graph would suggest a minimum number of blade between 12 and 20. In order to avoid any problem related to separation flux in the nozzle the number of blade was fixed as Z_B=25.

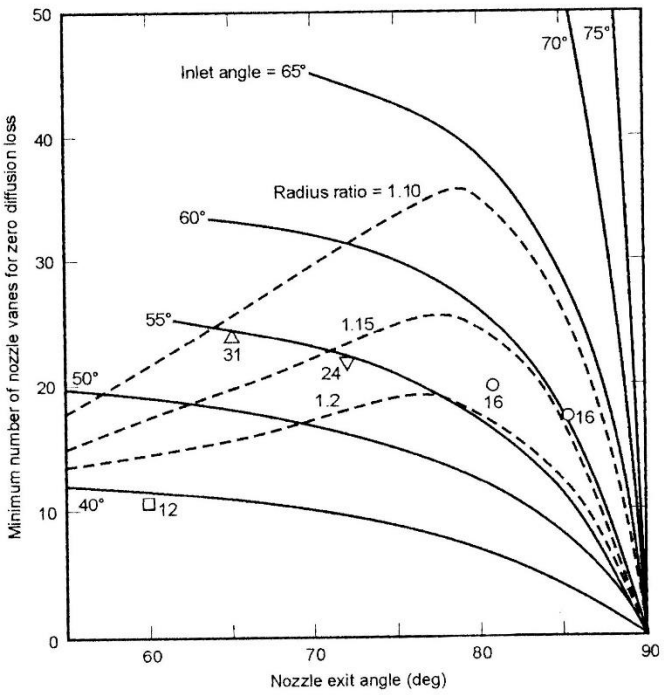

Figure 5.11 *Correlation of minimum nozzle vane number with vane inlet and exit angle and vane inlet/exit radius ratio [51].*

As the characteristics of the velocity triangles at the inlet of the rotor has been generated in the preliminary geometry design, this part of the code has the aim to design a satisfactory nozzle geometry. At this point, the flow leaving the nozzle does not follow exactly the vanes direction, but turns by an amount of deviation [11]. This phenomenon can be explained by the combination of two main effects: firstly, a sudden expansion occurring as a result of finite trailing edge thickness with its related blockage; this sudden expansion decrease the radial component of velocity, so that the flow overturns. Secondly, an underturning occurs because of the non-perfect guidance of the flow by the vanes, particularly in the uncovered region of the suction surface from the throat to the trailing edge, and usually this is the predominant effect [11].

The loss occurred in the nozzle can be expressed either in the terms of total pressure drop (5.37), or static enthalpy loss coefficient (5.38):

$$K_p = \frac{p_{01} - p_{02}}{p_{02} - p_2} \tag{5.37}$$

$$\varepsilon_h = \frac{h_2 - h_{2s}}{h_{02} - h_2} = \frac{h_2 - h_{2s}}{\frac{C_2^2}{2}} \tag{5.38}$$

In this work, ε_h was estimated following the Benson's loss correlation of Figure (5.5), as also explained in §5.3. Benson obtained values of enthalpy loss between 0.05 and 0.15, as a dependent variable of the non-dimensional flow rate.

The relation used to give a first estimation of the geometrical characteristic is known as "cosine rule", expressed in the form [11]:

$$\alpha_2 = cos^{-1}\left(\frac{o}{s}\right) \tag{5.39}$$

Where *o* is the throat opening and *s* the vane space.

Hiett and Johnston in [52] found out that the cosine rule overpredicts the deviation at low exit nozzle vane angles, but as confronting with Figure (5.12), in the range of α_4 considered in this study (70-80°) the fitting is acceptable.

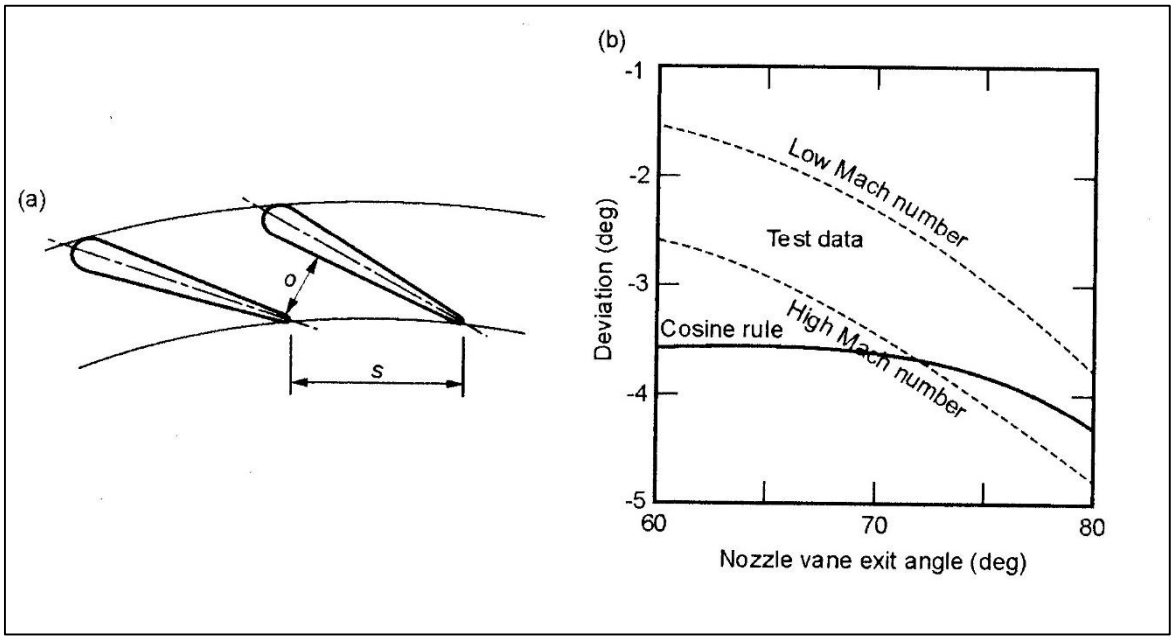

Figure 5.12 *Nozzle vane section (a). Comparison and measured deviation [52].*

In the code is imposed that $\alpha_4 = \alpha_2$. The opening vane spacing is calculated by:

$$s = \frac{2\pi r_2}{Z_S} \tag{5.40}$$

Thus:

$$o = s\cos(\alpha_4) \tag{5.41}$$

An iterative procedure was then implemented, in order to define the thickness of the nozzle blade. The thickness of them is important to achieve the desired velocity triangles. To do this, a Matlab "while cycle" was utilised, with an acceptable range of $\Delta th_s = 0.1mm$.
Setting a first attempt of blade thickness value th_s', the area occupied by the nozzle blade in the radial direction will be:

$$A_{nozzle\ blade} = th_s b_2 Z_B \tag{5.42}$$

Where b_2 is the nozzle width, considered the same of b_4. Hence, the throat area:

$$A_{th} = o b_2 Z_s - A_{nozzle\ blade} \tag{5.43}$$

At this point, it is necessary to calculate the thermodynamic state of the static point 2. To do this is used a second "while cycle", similar to the one utilised to calculate the point 1, with the iteration based on the density ρ_2. Actually, the absolute velocity at the nozzle outlet, considered as orthogonal at the throat area, is expressed by:

$$C_2 = \frac{m}{A_{th}\rho_2(1 - bk)} \tag{5.44}$$

Where *bk* represents the blockage factor that takes into account the growth of the boundary layer at the throat section, as represented in Figure (5.13). This parameter depends on many characteristic of the flow in the throat area, such as Reynolds and Mach number, but according to [53], this value can be considered as 1% of the whole area in case of considered turbulent flow.

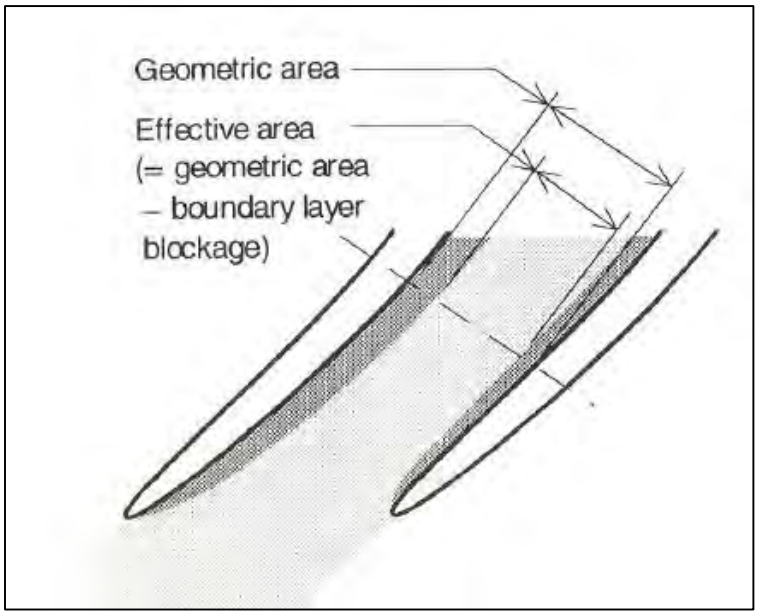

Figure 5.13 *Growth of boundary layer at the nozzle throat section [47].*

The enthalpy at the point 2s, for an isentropic flux, is then:

$$h_{2s} = h_{02} - \frac{C_2^2}{2} \tag{5.45}$$

Using the definition of the enthalpy loss coefficient, given in Equation (5.38):

$$h_2 = h_{2s} + \varepsilon_h \frac{C_2^2}{2} \tag{5.46}$$

Considering then that the point 2 and 2s are isobaric, p_2 can be calculated using Refprop:

$$\{s_{2s} = s_{01}, h_{2s}\} \xrightarrow{Refprop} \{p_{2s} = p_2\} \tag{5.47}$$

In this way, the state 2 is completely known, as far as two thermodynamic properties are known. The second attempt value of the density can be calculated and confronted with the first attempt one:

$$\{p_2, h_2\} \xrightarrow{Refprop} \{\rho_2''\} \tag{5.48}$$

The convergence of this second loop will give the thermodynamic state at point 2. The convergence of the first iteration process is still at this point not complete.

An interspace between rotor and stator is advantageously leaved, because this permits the mixing of the wakes generated in the nozzle passage. It is also important since it reduces the mechanical coupling between the two, which can cause resonance and lead to premature failure [11].
Anyway, the losses that happen in this region are in this model not considered because of the little dimension of this area (is fixed an interspace of 1.5mm). Is also to say that other studies as [54] did not consider them, because in design condition the losses occurring here can be ignored.
In this way, the velocity vector at the outlet of the nozzle can be considered equal to the one entering the rotor($C_2 = C_4$), and the same for the thermodynamic properties.
As said before, from the preliminary geometry procedure, an ideal velocity triangle at point 4 is already known: the aim of the loop procedure is then to calculate the thickness of the blade, which is suitable to achieve this condition. To do this. the velocity triangle depending on the first attempt thickness is calculated using the following equations:

$$C_{m4} = C_4 cos(\alpha_4) \;\; ; \;\; C_{u4} = C_{m4} tan(\alpha_4) \;\; ; \;\; W_{u4} = (C_{u4} - U_4) \tag{5.49}$$

And in this way the relative angle β_4:

$$\beta_4 = tan^{-1}\left(\frac{W_{u4}}{C_{m4}}\right) \tag{5.50}$$

This angle is now confronted with the ideal one, which is an output of the geometry generation. This permits to achieve a second attempt value for the blade thickness, in the following way:

$$\mathrm{th}_s'' = \mathrm{th}_s' \frac{|\beta_4 - \beta_{4,\mathrm{des}}|}{\beta_{4,\mathrm{des}}} \tag{5.51}$$

Δth_s is set at 0.1mm. The convergence of this cycle will have as output the complete definition of the state at the outlet of the nozzle, considered as constant at the inlet of the rotor.
The losses accounted to the nozzle vanes are defined by:

$$\Delta h_s = h_{2s} - h_2 \tag{5.52}$$

The part of the code which defines this component is reported in the Code section ().

```
int=0.0015;
r2=r4+int;
s=2*pi*r2/Zs;
o=s*cosd(alfa4);
A2=2*pi*(r4+0.0015)*b4;
b2=b4;
h02=h01;

th_s_prec=100;    %first attempt values
th_s=0.001;       %first attempt values
while abs(s_pale-s_pale_prec)>0.0001
      A_nozzle_blade=th_s*b2*Zs;
      A2_th=o*b2*Zs- A_nozzle_blade;
      eps_h=stator_losses_benson(m_rid); %nozzle enthalpic loss coefficient, from
      function "stator_loss_benson", which takes into account the Benson's
      correlation (1970)
      bk=0.01; % blokage factor

      rho2_prec=1000;
      rho2=rho01;
    while abs(rho2_prec-rho2)>.1
        C2=m/(A2_th*rho2*(1-bk)) ;%[m/s]
        h2s=h02-(C2^2)/2;
        h2=h2s+eps_h*(C2^2)/2;
        p2s=refpropm('P','H',h2s,'S',s01,'r245fa');
        p2=p2s;
        rho2_prec_c=refpropm('D','H',h2,'P',p2,'r245fa');
        rho2_c=(rho2+rho2_prec)/2;
    end

rho2=sqrt(rho2_prec_c*rho2_prec);
[T2, s2, Q2, a2]=refpropm('TSQA','H',h2,'P',p2,'r245fa');
[T02, p02, rho02, Q02, a02]=refpropm('TPDQA','H',h02,'S',s02,'r245fa');
[T2s, rho2s, s2s]= refpropm('TDS','H',h2s,'P',p2s,'r245fa');
Ma2=C2/a2;
Dh_stat=h2-h2s;   %[kJ/kg]    stator losses

    %%%%%ROTOR NOZZLE INTERSPACE
p4=p2;      rho4=rho2;  h4=h2;      C4=C2;

    %%%%%ROTOR INLET
Cm4=C4*cosd(alfa4);
Cu4=Cm4*tand(alfa4);
C4=Cm4/cosd(alfa4);
U4=r4*omega;
Wu4=Cu4-U4;
beta4=atand(Wu4/Cm4);
W4=Cm4/cosd(beta4);

th_s_prec=th_s*(abs(beta4-beta4_des))/abs(beta4_des);
th_s=(th_s+th_s_prec)/2;
end
```

Code section 5.8 *Model of the nozzle vanes.*

5.5 Rotor

The rotor can be considered the most important and most complex component of a radial inflow turbine. The part that has the purpose of subtracting the energy from the flux and transferring it to the rotating shaft.

Typically, in a radial inflow turbine, the flow is here turned by 90° from radial inlet to axial outlet, producing strong hub-to-shroud flow profile due to curvature effects. For this reason for many years the design techniques were mostly empirical, based on trial-and-error and accumulated experience of the designer [11]. In the modern development, two main aspects permitted a technological progress in understanding completely the complex flow pattern: modern measurement techniques, such as non-invasive laser velocimeter and their visualisation, and the development of three-dimensional software models, able to solve complex viscous equation modelling the component and the flow through it [11].

A mono-dimensional approach, as used in this work, tends to simplify this complex fluid dynamic problem, dividing the rotor in two main sections: in the inlet region the flow is mainly considered as meridional coming in a radial direction from the nozzle vanes, in the exducer region instead is considered, and designed, mainly axial. In this way, also the turning of the fluid is largely simplified.

5.5.1 Inlet region and incidence losses

Many years of studies concerning the inlet region of the rotor agreed that the best incidence angle was included in the range of -20° to -40°, for radial inlet blade angles.

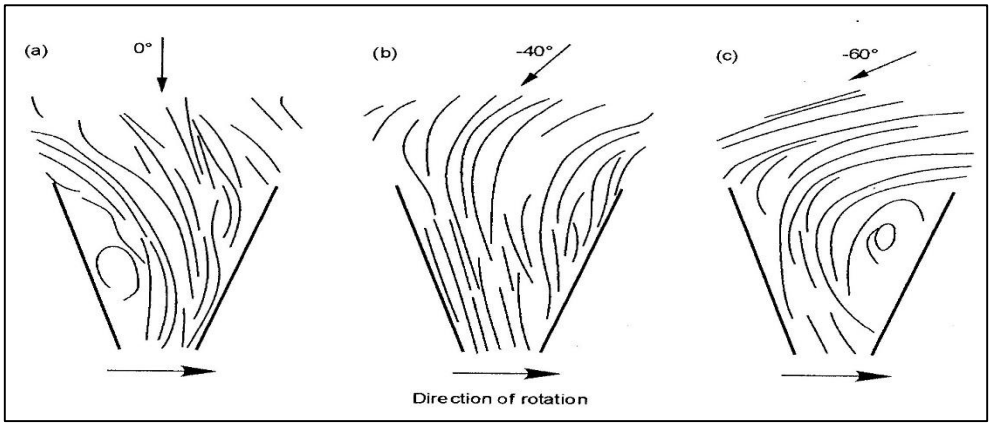

Figure 5.14 *Observed path lines in a radial flow rotor at various inlet flow angles [55].*

The flow visualisation by Woolley and Hatton [55] of Figure (5.14) can be useful to explain and understand the flow field at the inlet region. The fluid approaches a purely radial rotor with different angles: the most uniform flow pattern is achieved for an inlet angle of -40°. An approach angle of 0° comports the creation of strong recirculation in the suction face, which occupies the full extent of the surface without reattaching. In case of a more negative flow angle (-60°), appears a large recirculation area on the pressure surface, but in this case the flow is reattaching to the surface before reaching the trailing edge, becoming uniform again. Only in the case of an angle of -40° are occurring no fluid separation [12].

This behaviour is attributable to the large static pressure gradient that the blade loading produces across each passage, which tends to move the fluid from the pressure to the suction face against the direction of rotation. In this way, a secondary flow is set up in the blade passage, in the form of a recirculation in the opposite direction to the passage rotation [12].

The losses occurring in in the approach of the flow to the rotor are defined incidence losses. In fact, they refer to the work of turning the working fluid from the approaching direction to the one required by the blade passage. Even in a well-designed geometry and in a design point condition, but especially in a condition far from the optimum, some losses occur. The general approach of the models proposed by several authors (Futral and Wasserbauer [56], Todd and Futral [58]) is to assume that the kinetic energy associated with the change in relative tangential velocity is converted into internal energy of the working fluid, which manifests itself an increasing in entropy [12]. This phenomenon is modelled as if it would happen in an infinitely small extent. Following the formulation of the so called "Model NASA 2" by Wasserbauer and Glassman in [58], the losses can be expressed in terms of enthalpy decay as:

$$\Delta h_i = \frac{1}{2} W_4^2 sin^2(\beta_4 - \beta_{4,opt}) \tag{5.53}$$

Where $\beta_{4,opt}$ represents the angle at which any incidence losses occur.

The authors found out better agreement with experimental results when the exponent of the sine term was replaced by 3 at positive incidence, and kept at 2 for negative ones. Since in this work the incidence is always set as negative, the exponent will always be 2.

The problem is now the definition of the optimal approach angle $\beta_{4,opt}$. Futral and Wasserbauer in [56] adopted a simple approach, that consider the optimal angle equal to the rotor blade angle, so in our case of completely radial inlet as zero. Nevertheless, as said before, the optimum never occurs if the incidence angle is zero, but at some negative inclination. Following the empirical model of Stanitz [59] proposed for compressor slip factor correlation, is possible to calculate $\beta_{4,opt}$:

$$\beta_{4,opt} = tan^{-1}\left[\frac{-1.98\tan(\alpha_4)}{Z_B\left(1-\frac{1.98}{Z_B}\right)}\right] \tag{5.54}$$

Using this model, no energy dissipation due to incidence is supposed to be, if $\beta_4 = \beta_{4,opt}$.
Even if is the split of the rotor losses in incidence and in passage ones has physically no meaning, is useful to find the characteristic of the fictitious thermodynamic point 41, which concern the state of the fluid after the incidence zone. Hence:

$$h_{41} = h_4 - \Delta h_i \tag{5.55}$$

Considering the relative enthalpy conservation, is possible to calculate the relative velocity as:

$$W_{41} = \sqrt{2\left(h_4 - h_{41} + \frac{W_4^2}{2}\right)} \tag{5.56}$$

The incidence losses have a very low relative impact on the outputs of this code. This because the design procedure generates always an approach angle very close to the optimal one. This source of loss gain much more weight in an off-design simulation, where the variation of mass flow rate or the variation of inlet guided vanes for instance, can vary dramatically the approach angle β_4.

```
    %%%%%INCIDENCE LOSSES
beta4_opt=atand((-1.98*tand(alfa4))/(Zb*(1-1.98/Zb))); %[°]      optimal angle
Dh_il=.5*W4^2*(sind(beta4-beta4_opt))^2;  %[kJ/kg]    incidence losses

h41=h4-Dh_il;     %[kJ/kg]

W41=sqrt(2*(Dh_il+.5*W4^2));  %[m/s]
```

Code section 5.9 *Model of incidence loss.*

5.5.2 Passage losses

The term passage losses includes a wide spectrum of different phenomena occurring to the fluid crossing the rotor. In fact, after a rapid acceleration in the flow direction, the fluid is turned in the meridional plane along the camber line: this creates a complex pattern of secondary flows and cross-stream, which still today not completely known [11]. Moreover, this causes the growth of boundary layers with loss of kinetic energy and blockage. For these reasons a fully detailed model that takes into account separately all these loss sources, as the ones existing for the axial turbines, was not yet developed. In fact, in axial turbine cascades this can be done by a careful set up and measures, but this is not actually possible for radial turbine, due to the three-dimensionality of flow pattern, that does not permit to differentiate the losses [11].

Is not also very correct to distinguish the incidence losses from the passage losses. Indeed, a non perfect approach angle creates a mechanism whose effect is also a passage disturbance.

Anyway, a qualitative classification of the main sources of losses occurring in the rotor can be set up, and this consider [12]:

- Skin friction, caused by the viscous forces operating on the solid surface of the passage. It is usually expressed by a coefficient, which is a strong function of the surface roughness;
- Secondary flows losses, caused as said before by the complex fluid pattern in the rotor due to vortices, eddies, and multiple curvatures;
- Tip clearance losses, caused by the leakage of the fluid through clearance gaps between blade tips and shroud.

The model utilised in this work takes into account simultaneously both the skin friction losses and the secondary losses; the tip clearance ones will be analysed separately. It was proposed firstly by Futral and Wasserbauer [56], then checked by Benson [47] against test data, and finally developed by Wasserbauer-Glassman in [58]. It has the advantage that is quite simple to implement and showed results as correct as the ones of other more complex models [11]. Here, in particular, the passage loss is considered as a function of the mean of the relative kinetic energies at inlet and exit, in the following form:

$$\Delta h_p = K \frac{W_{41}^2 + W_{6s}^2}{2} \tag{5.57}$$

Where K is an experimental coefficient, that should be determined by comparison with experiment; is usually in the range of 0.2-0.44, and in this work was chosen $K=0.33$ according to [11].

All the values that in this part of the code are referred to the outlet, are studied at root mean square radius, $r_{6,rms}$.

At this point, however, the characteristics of the station 6 are not already known, while the pressure in p_{06} is an input datum of the design procedure; so, the equation (5.57) cannot be used yet, as far as the W_{6s} is not known. To avoid this problem a iterative loop was set up, in order to have a convergent value of p_6.

As first attempt, is set $p_6' = p_{06}$. This permits, using Refprop, to know the enthalpy of the isentropic state 6s:

$$\{p_{6s} = p_6, s_{6s} = s_{01}\} \xrightarrow{Refprop} \{h_{6s}\} \tag{5.58}$$

Considering then the rothalpy conservation between the points 41 an 6s ($h'_{041} = h'_{06s}$), it is possible to calculate:

$$W_{6s} = \sqrt{2(h_{41} - h_{6s}) + W_{41}^2 - U_4^2 + U_6^2} \tag{5.59}$$

This value can be now used in the relation of Wasserbauer and Glassman of Equation (5.57) in order to define the passage losses. The enthalpy of the state 6, is then obtained by the definition of passage losses:

$$h_6 = h_{6s} + \Delta h_p \tag{5.60}$$

$$\{h_6 \; ; \; p_6\} \xrightarrow{Refprop} \{\rho_6, s_6\} \tag{5.61}$$

The knowledge of the thermodynamic properties permits now to estimate the velocity triangles in the exducer, at the mean radius $r_{6,rms}$. Considering that the preliminary geometry design has already fixed the blade angle β_6, is possible to calculate the relative velocity W_6 as:

$$W_6 = \frac{m}{A_6 \rho_6 \cos(\beta_6)\,(1 - bk)} \tag{5.62}$$

Hence:

$$W_{u6} = W_6 \sin(\beta_6) \quad ; \quad C_{m6} = W_6 \cos(\beta_6) \quad ; \quad C_{u6} = U_6 + W_{u6} \tag{5.63}$$

$$C_6 = \sqrt{C_{m6}^2 + C_{u6}^2} \tag{5.64}$$

$$\alpha_6 = tan^{-1}\left(\frac{C_{u6}}{C_{m6}}\right) \tag{5.65}$$

This permits to define the total enthalpy at the station 06:

$$h_{06} = h_6 - \frac{C_6^2}{2} \tag{5.66}$$

Hence, using Refprop, the pressure p_{06} is obtained:

$$\{h_{06}\ ;\ s_{06} = s_6\} \xrightarrow{Refprop} \{p_{06,calc}\} \tag{5.67}$$

This value of pressure is now related to the one fixed as input of the code, in order to obtain a second attempt value for p_6'', to compare with the first attempt one, until convergence.

$$p_6'' = p_6' \frac{p_{06,input}}{p_{06,calc}} \tag{5.68}$$

Δp_6 is set as 1kPa, this means that for the most used range calculated for p_6 (200-300kPa), the error introduced by this loop in meanly 0.3-0.5%.

```
    %%%%%%PASSAGE LOSSES
p6_prec=10000;
p6=p06_prog;

while abs(p6-p6_prec)>1;
      h6s=refpropm('H','P',p6,'S',s01,'r245fa');      %[kJ/kg]
      p6s=p6;     %[kPa]
      U6_RMS=omega*r6_RMS;    %[m/s]
      W6s_RMS=sqrt(2*(h41-h6s)+W41^2-U4^2+U6_RMS^2); %[m/s]
      K=0.33;
      h6=h6s+K*(W41^2+W6s_RMS^2)/2; %[kJ/kg]    Futal-Wasserbauer
      Dh=h6-h6s;  %[m/s]
      h26s=refpropm('H','p',p6,'S',s2,'r245fa');      %[kJ/kg]
      Dh_pl=h6-h26s;    %[kJ/kg]
      [rho6,s6]=refpropm('DS','H',h6,'P',p6,'r245fa'); %[kg/m^3] [kJ/kgK]
```

```
%%%%%VELOCITY TRIANGLES AT (6)

    W6_RMS=m/(A6*rho6*cosd(beta6_RMS)*(1-bk));      %[m/s]
    W6u_RMS=W6_RMS*sind(beta6_RMS);                 %[m/s]
    Cm6_RMS=W6_RMS*cosd(beta6_RMS);                 %[m/s]
    Cu6_RMS=U6_RMS+W6u_RMS;                    %[m/s]
    C6_RMS=sqrt(Cm6_RMS^2+Cu6_RMS^2);          %[m/s]
    alfa6=atand(Cu6_RMS/Cm6_RMS);              %[°]

 %%%%%CARATTERISTICHE PUNTO 06

    h06=h6+.5*C6_RMS^2;     %[kJ/kg]
    s06=s6;                 %[kJ/kgk]
    [p06,rho06]=refpropm('PD','H',h06,'S',s06,'r245fa'); %[kPa] [kg/m^3]


  p6_au=p6*p06_prog/p06;    %[kPa]
  p6_prec_c=sqrt(p6_au*p6); %[kPa]
  p6_c=p6_au;               %[kPa]

end
```

Code section 5.10 *Passage losses model and calculation of velocity triangle and thermodynamic state at the rotor outlet.*

5.5.3 Tip clearance

A clearance gap must be provided between the blade tip and the shroud in order to permit a completely free rotation of the components. This clearance causes a leakage of fluid from pressure to suction surface, and that means that an amount of the total inlet flow rate does not have a useful effect in terms of power production.

Several empirical models tried have been proposed. Based on a large number of rotor test, Rodgers [60] proposed a simple correlation, where a total-to-total efficiency loss factor is expressed by:

$$\Delta\eta_{tt} = 0.1\frac{\epsilon_r}{b_6} \tag{5.69}$$

Where ϵ_r represents the radial gap as showed in Figure (5.15) and b_6 the blade height at the exducer.

This is model is simplified and takes into account just the effect of the tip clearance, but without studying the physical origin of the phenomenon [11]. Moreover, the axial gap is not considered; several authors showed how the effect of radial clearance is approximately one order of magnitude larger than the effect of axial clearance, as reported in Table ().

Percentage change in:	**Total-to-total efficiency**		**Mass flow rate**	
Due to:	**+1% axial clearance**	**+1% radial clearance**	**+1% axial clearance**	**+1% radial clearance**
Futral-Holeski	-0.15	-1.6	-0.1	+0.3
Ricardo	-0.2	-0.5	-0.1	+0.5
Ishimo et al.	-0.2	-1.2		+0.6
Krylov and Spunde	-0.1	-0.6	-0.1	-0.2

Table 5.2 *Comparison of reported effects of rotor tip clearance on radial turbine performance [11].*

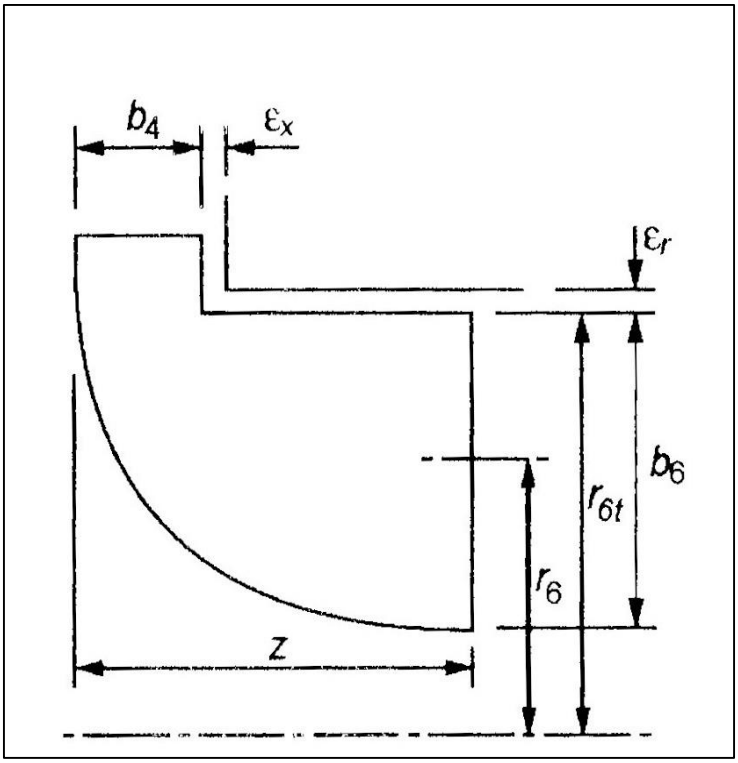

Figure 5.15 *Simplified tip clearance model*

In this work it was applied the relation proposed by Spraker in [61]: in its analysis a more fundamental investigation of the physical phenomenon is attempted. He modelled the leakage flow through the gap firstly as a flow through an orifice, using a finite elements analysis, and secondly as a shear flow where the velocity at the wall was supposed to be zero, with a linear variation until the local blade speed at the tip. Hence, the leakage flow rate is:

$$m_L = \frac{1}{2}\rho_6 U_{6s} \epsilon_r L Z_B K_L \tag{5.70}$$

Where L represents the length of the gap, U_{6s} the blade velocity at the tip and K_L is a coefficient whose value was determined as 1.5 by experiments.

The leakage loss was then determined by the mass flow rate multiplied by the fluid kinetic energy:

$$\Delta h_L = \frac{m_L}{m}\frac{U_6^2}{2} \tag{5.71}$$

In the code, moreover, is assumed that the leakage losses do not affect the thermodynamic state at the state 6; for this reason they were taken into account as a non-produced-power, which is deduct to the net power output:

$$\Delta P_L = m\, \Delta h_L \tag{5.72}$$

The main problem in considering the tip clearance losses is to define the radial gap. In fact, this value, evaluated as a certain percentage of the blade height can be considered as an inverse function of the size of the expander.

To model this peculiar aspect, a function called "gap_radial" was implemented, whose input is identified in the size parameter *VH*; considering values from literature, a value of about $\frac{\epsilon_r}{b_6} = 0.06$ is considered for the small size turbomachines (*VH≈0.05*), and $\frac{\epsilon_r}{b_6} = 0.01$ for the larger size ones (VH≈0.3). The graph of the function in showed in Figure (5.16).

The values obtained for the radial gap are in accord, with the typical ones, $\epsilon_r = 1 \div 1.5mm$.

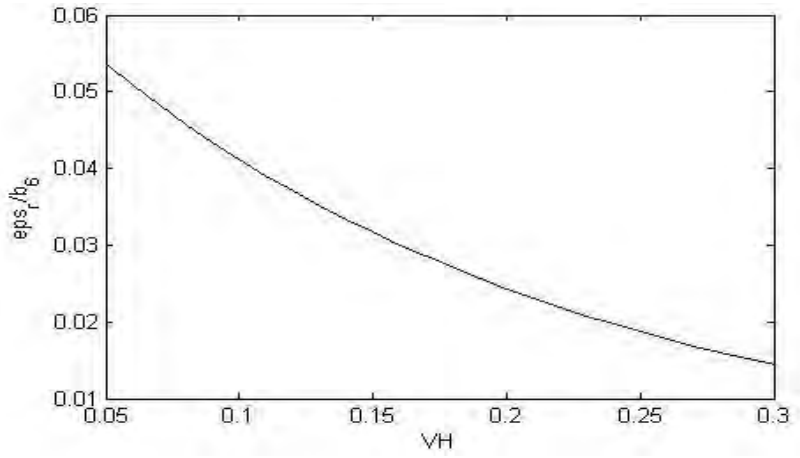

Figure 5.16 *Gap to blade height ratio, as a function of size parameter.*

```
      %%%%%TIP CLEARANCE LOSSES


U6s=r6s*omega;                %[m/s]
eps_r=(gap_radial(VH))*b6;    %[m]
ml=.5*rho6*U6s*(2*pi*r6s)*1.5*eps_r; %[kg/s]    Spraker (1987)
Dh_ll=.5*(ml/m)*U6s^2;        %[kJ/kg]
DP=Dh_ll*m;                   %[kW]
```

Code section *5.11 Tip clearance losses model for radial turbine.*

```
%%%%%FUNCTION: GAP RADIAL


function [ eps_r ] = gap_radial( VH )
sample_VH=[.01; .03;.07; .1; .3; .5];
sample_eps_r=[.07; .06; .05; .03; .02;.01];
fit_curve=fit(sample_VH,sample_eps_r,'exp1');
eps_r=fit_curve(VH);


end
```

Code section 5.12 *Function "gap radial"*

5.5.4 Disk friction

The only external loss that is usually taken into account in radial turbine modelling is that of disk friction. This occurs because of the fluid leakage between the rotor disc and the stationary back plate, where the windage flow causes quite strong friction. Depending on the expander installation, this leakage could also be recirculated into the turbine annulus, or taken away [11].

The most common model used for this kind of losses is the one proposed by Daily and Nece [62] (also analysed in [63]), which considers the rotation of a disk in an enclosed casing. They identified four different kinds of flow regimes, but for radial turbine this can be simplified to two regimes determined by the Reynolds number referred to the inlet radius condition, expressed as:

$$Re = \frac{U_4 r_4}{\nu_4} \tag{5.73}$$

Where ν_4 represents the dynamic viscosity in [Pa s].

The limiting value for *Re* is identified in $Re_{lim}=10^5$, so that if the calculated *Re* is inferior to this value the flow is considered laminar, otherwise turbulent. It must be said that mostly the flow condition was laminar.

Is also important to say that the model of Daily and Niece considers the friction loss as power loss, to be subtracted to the net power output.

The expression of the power loss is then:

$$\Delta P_F = \frac{1}{4} K_f \rho_4 \omega_4^5 r_4^3 \tag{5.74}$$

Where the friction coefficient K_f depends on the flow regime in the following way:

$$K_f = \frac{3.7\left(\varepsilon_f / r_4\right)^{0.1}}{Re^{0.5}} \quad (Re < 10^5) \tag{5.75a}$$

$$K_f = \frac{0.102\left(\varepsilon_f / r_4\right)^{0.1}}{Re^{0.2}} \quad (Re > 10^5) \tag{5.75b}$$

ε_f represents the radial interspace between the rotor disk and the static back plate. As project condition it is set as a fix percentage of the inlet blade height, so that $\varepsilon_f = 0.02 b_4$.

The results will show that the friction losses have a relative large influence on the general losses breakdown. The designer has anyway the possibility to operate some variations on the input parameters such as the ratio ε_r/b_4, in order to fit in the best way model to empirical data.

```
    %%%%%DISC FRICTION LOSSES
eps_f=0.02*b4; %[m]  radial gap
Re=U4*r4/(ni4);

      if Re>10e5
        K_fric=0.102*(eps_f/r4)^0.1/Re^0.2;
      else
        K_fric=3.7*(eps_f/r4)^0.1/Re^0.5;
      end

DP_fric=K_fric*rho4*omega^3*r4^5/4;
Dh_fric=DP_fric/m;
```

Code section 5.13 *Model of disc friction losses for radial turbines.*

5.6 Exhaust diffuser

Even if this component is not strictly part of the expander itself, in this work its evaluation was considered as worthy for a more understandable knowledge of the turbine behaviour, considering the flow from the inlet of the volute until the outlet of the diffuser. Indeed, it is common that a turbine for electrical production is provided of a component, the diffuser, whose aim is to recover the exhaust kinetic energy of the fluid, flowing out from the rotor. Even if a proper diffuser is not provided, the flow has to be delivered to another location, so that also the exit pipe becomes a very important component [11].

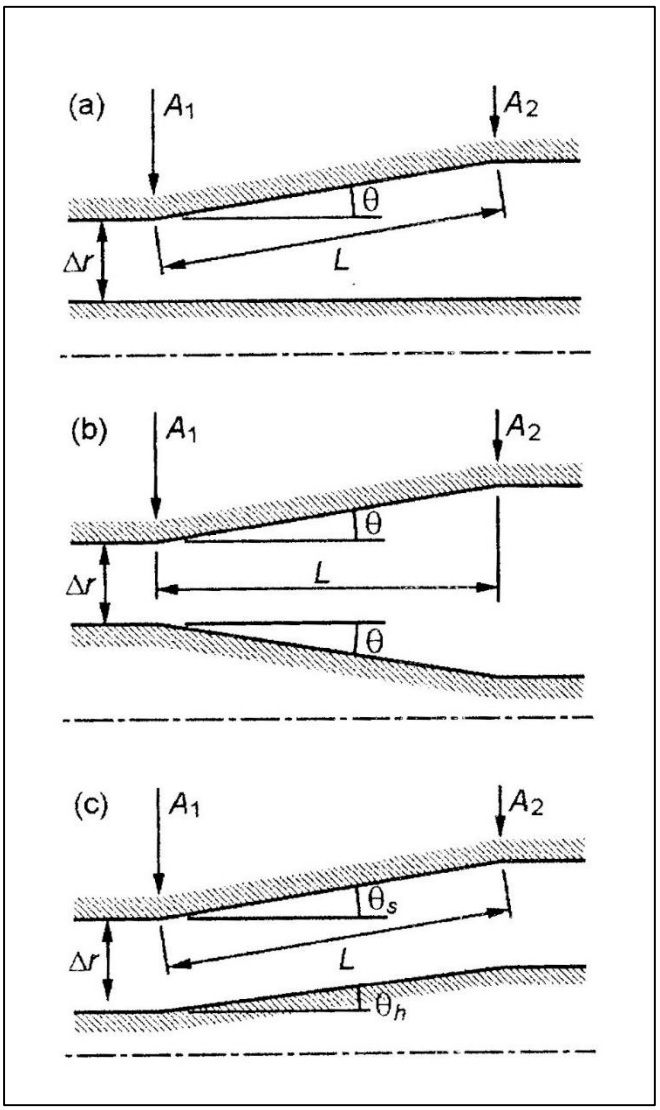

Figure 5.17 *(a) Straight hub annular diffuser*
(b) Equiangolar annular diffuser
(c) Radially divergent annular diffuser

Normally the most common shapes used are the conic and the annular, straight sided or profiled depending on the installation. Despite of an apparently simple geometry, the flow pattern results as

extremely complex and influenced by a large number of parameters, both geometrical and fluido dynamic [11]. Moreover, a mean line analysis is based on the hypothesis that the fluid characteristics are considered as constant in the flow perpendicular plane: in real machines instead, they are rarely constant across the rotor exit, and this aspect plays a key role in the definition of diffuser performance. The rotor outlet condition is also characterised by secondary flows and eddies, which are in this analysis phase not completely known [12].

For all these reasons, the analysis proposed in the code can be considered as a preliminary step, which can provide a mean evaluation of the expander performance.

Is also important to remember that one of the first project decision was to design an expander without exit swirl, so that $\alpha_6 = 0$.

The pressure recovery coefficient for any kind of diffuser is defined as:

$$C_p = \frac{p_7 - p_6}{p_{06} - p_6} \tag{5.75}$$

Where the state 6 represents the outlet of the turbine or inlet of the diffuser, and 7 the diffuser outlet. The meaning of this parameter is to establish the fraction of kinetic energy that is converted to static pressure gain. This is possible, according to Bernoulli's equation, because of an area increase, which reduces the meridional velocity.

In a common way, can be defined also the ideal pressure recovery coefficient:

$$C_{pi} = \frac{p_{7s} - p_6}{p_{06} - p_6} \tag{5.76}$$

Which is obtained assuming a completely loss free flow which follows the diffuser surfaces and exits without any blockage and distortion. For a diffuser without swirl it can also be expressed, with combination of mass conservation and Bernoulli's equation, as:

$$C_{pi} = 1 - \frac{1}{AR^2} \tag{5.77}$$

Where $AR = A_7/A_6$.

At this point several geometrical hypothesis have been done, following the annular diffuser studied by Japikse and Pampreen in [64], exposed in the Table (5.3).

Θ_i [°]	Θ_i [°]	L/Δr	AR	r_{1h}/r_{1t}
10	15	7.0	2.4	0.75

Table 5.3 *Characteristics of adopted diffuser, proposed in [64].*

This permits to estimate, using the Figure (5.18), a pressure recovery coefficient for zero swirl of $C_p = 0.6$.

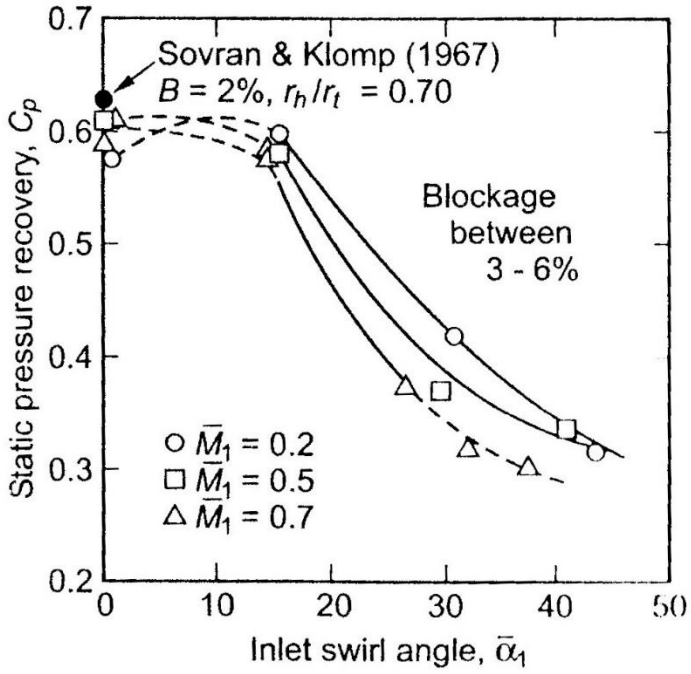

Figure 5.18 *Recovery coefficient for diffuser of Table (5.3), as a function of inlet swirl [64].*

From equation (5.75) is possible to calculate p_7 and from equation (5.76) p_{7s}. The thermodynamic properties at this stations can be calculated using Refprop:

$$\{p_{7s}\ ;\ s_{7s} = s_6\} \xrightarrow{Refprop} \{td.properties_{7s}\} \tag{5.78}$$

$$\{p_7\ ;\ s_7\} \xrightarrow{Refprop} \{td.properties_7\} \tag{5.79}$$

This permits also to define the outlet velocity as:

$$C_7 = C_6 \frac{\rho_6}{\rho_6} \frac{1}{AR} \tag{5.80}$$

The kinetic energy associated to the outlet condition is then considered as wasted, because it can be anymore recovered. The kinetic loss at the diffuser is expressed as:

$$\Delta h_k = \frac{1}{2} C_7^2 \tag{5.81}$$

```
    %%%%%EXHAUST DIFFUSER
%the code follows the model proposed by Japikse-Pampreen (1979)

AR=2.4;
A2=A6*AR;   %[m^2]

Cdi=1-1/AR^2;
Cd=0.6;     %from graphic relation, no swirl conditions
p7=Cd*(p06-p6)+p6;
p7ss=Cdi*(p06-p6)+p6;
s7ss=s6;
[T7ss, h7ss, rho7ss, Q7ss, a7ss]=refpropm('THDQA','P',p7ss,'S',s7ss,'r245fa');
[T7s, h7s, rho7s]=refpropm('THD','P',p7s,'S',s7,'r245fa');
C7=C6*(rho6/rho7s)*(1/AR);
Dh_kin=.5*C7^2;
```

Code section 5.14 *Model of exhaust diffuser for radial turbine*

Output generation and re-iteration

The last part of the code proposed has the purpose of generating the output values. Not only, as said in the initial part of this chapter, the code has implemented an inner iteration based on the calculated efficiency. This means that, starting from input values of load coefficient, flow coefficient, rotational speed, and a first attempt value of total-to-total efficiency; the code generates a main geometrical aspect of the expander, and this aspect is then analysed using losses correlation, evaluating a performance prediction, whose output is again a value of total-to-total efficiency, as showed in Figure (5.2). The first and the second attempt values should be compared, because their convergence is a fundamental passage that permits to achieve a satisfactory design prediction.

In this way, the total-to-total efficiency considered as an output of the performance prediction is calculated as:

$$\eta_{tt,calc} = \frac{h_{01} - h_{06}}{h_{01} - h_{06s}} \tag{5.81}$$

The convergence method fixes a maximum gap of $\Delta\eta_{tt} = 0.001$. This means that if the convergence is not achieved, a second attempt value of iterative efficiency must be provided. In the code was chosen to calculate it as the square mean:

$$\eta''_{tt} = \sqrt{(\eta''_{tt})^2 \cdot \left(\eta_{tt,calc}\right)^2} \tag{5.82}$$

Once that the convergence is completely achieved, the design procedure can be definitely considered concluded. This means that other important evaluation can be now provided, in order to have a complete idea of the behaviour of the expander.

A different value of efficiency is calculated in the code at this point: the total-to-static efficiency. Differently from the total-to-total one, the enthalpy gap considered as comparison term is not the total one; for the outlet ideal thermodynamic point is considered the static enthalpy h_{6s}, as result of an isentropic expansion. This is expressed in the following formula:

$$\eta_{ts} = \frac{h_{01} - h_{06}}{h_{01} - h_{6s}} \tag{5.83}$$

The gross power output is one of the most descriptive parameter, and it can be calculated in two ways, which should give the same results (except for a little percentage error):

- Using the energy balance as:

$$P_{g,eb} = m(h_1 - h_6) \tag{5.84}$$

- Using the Euler's work equation for turbomachines:

$$P_{g,Eu} = m(U_4 C_{u4} - U_6 C_{u6}) \tag{5.85}$$

Moreover, from the gross power output is now necessary to subtract the losses calculated as power losses. These sources as explained before, do not affect the thermodynamic state of the fluid at the turbine outlet, but they are supposed to subtract useful power. Thus, the net power output can be calculated subtracting the disk friction and the leakage losses:

$$P_n = P_g - \Delta P_L - \Delta P_F \tag{5.86}$$

In addition, the values of efficiency must be affected by this kind of losses, so that they have to be recalculated one more time at the final convergence. At this point it is also worthy to consider the recovery of kinetic energy provided by the exhaust diffuser, which clearly increase the value of total-to-static efficiency. These values are now obtained from the net power output in the following way:

$$\eta_{tt} = \frac{P_n}{m(h_{01} - h_{06s})} \tag{5.87}$$

$$\eta_{ts} = \frac{P_n}{m(h_{01} - h_{7s})} \tag{5.88}$$

This last calculated value gives a final evaluation of the behaviour of the expander. In fact, it takes into account all the components and the sources of losses that are typical of the turbine model, from the inlet of the volute to the outlet of the exhaust diffuser. As suggested by papers and books from many authors, this value will be in the post processing analysis considered as the most typical one, so useful to be compared among different inputs and design procedures.

```
          %%%%%TURBINE INDEXES
eta_tt=(h01-h06)/(h01-h06s);
eta_ts=(h01-h06)/(h01-h6s);
eta_ts_rec=(h01-h7ss)/(h01-h7s);
P_TDV=m*(abs(U4*Cu4)-abs(U6_RMS*Cu6_RMS))/1000;      %[kW] Euler's power output
P=m*(h01-h06)/1000;           %[kW] Gross power output
P_l=P-(DP+DP_fric)/1000;      %[kW] Net power output
eta_tt_l=P_l/(m*(h01-h06s)/1000);
eta_ts_l_rec=P_l/(m*(h01-h7s)/1000);

V06ss=m/(refpropm('D','P',p06,'H',h06ss,'r245fa'));  %[m^3/s]
Ns=(omega*V06ss^.5)/(h01-h06ss)^.75;
Ds=(2*r4*(h01-h06ss)^.25)/V06ss^.5;
R=(h4-h6)/(h1-h6);

eta_tt_prec=sqrt(eta_tt*eta_tt_hp);
```

Code section 5.15 *Calculation of the output characteristic of a radial turbine.*

Chapter 6

Results analysis

A full analysis of the output data obtained from the model is studied in this chapter. The results will be showed in a progressive way, starting from design procedures where many variables are considered as fixed parameters, to more complex ones. The aim is to evaluate the goodness of the proposed model, focusing limiting aspects and flexible applications. Moreover, an evaluation of the performances is illustrated, as functions of the size and volume expansion ratio of the expander. Lastly, the characteristics of turbines that do not operate at ideal specific speed I are analysed.

6.1 Introduction to outputs analysis

In this chapter, a full analysis of the results of the model will be provided. There are many steps at different levels of depth, in which the designer can study the characteristics of the expander. It depends firstly on the aim of the application, and secondly on the possibility of variation of the input parameters of the model. In particular, this means that to consider a characteristic as a fixed value or as a range of possibility can affect the goal of the whole analysis.

For these reasons, in this work are carried out different levels of analysis that the model proposed can provide. In a first level examination, a design procedure where all the input values are fixed is focused. In particular, this concerns size parameter, volume expansion ratio, flow and load coefficients: this has the main aim to focus the geometrical and thermodynamic output that the code calculates. In the second step analysis, the total-to-static efficiency is investigated varying the main input design

parameters, flow and load coefficients. In fact, it is showed that they can completely change the expander characteristic, in geometry, thermodynamic and performance features.
Then a fulfil study is carried out considering the variation of size and of volume expansion ratio: this part can be considered as the most significant one because provides a performance prediction of the maximum achievable efficiency for each couple of *VH* and *VR*. In a design procedure of a complete ORC plant, this could permit to choose the cycle parameters able to maximize the efficiency of the whole system.
The last analysis focus the efficiency of expanders working in non-ideal condition, and in particular for specific speed not corresponding to the one of maximum efficiency.

6.2 Analysis at fixed *VH, VR, ψ, φ, N*

The study of the expander characteristics through the proposed Matlab code, permits the variation of input design parameter. To prove the goodness of proposed relations, anyway, it appears as important to consider the output values that are here calculated. Clearly, as also explained in previous chapters, they are strongly influenced by several assumptions and constrains, which were necessary fixed in the code implementation. Their variation can in fact change the output characteristic, and for this reason, the influence of the most important ones will be evaluated.
The parameters considered as fixed in this first section are:

- Size parameter *VH*, which is considered as the index that mostly influence the size of the turbo-machine. In fact, it sets up the mass flow rate for a fixed isentropic enthalpy drop.
- Volume expansion ratio *VR*: this parameter fixes the inlet-outlet thermodynamic characteristic. For instance, for a fixed inlet condition in temperature and pressure, to set *VR* means also to fix the isentropic outlet conditions, and vice versa.
- Flow and load coefficients φ and ψ are the input parameters that mostly affect the geometry of the turbomachines. When they are fixed, also the velocity triangles are known. They can also be considered as indexes of characteristic aspect of the machines.
- Rotational speed *N* is another fixed value, necessary as input of the design. It is chosen in order to achieve a specific number N_s included in the ideal range of 0.3-0.8 [12]. Because this range is quite large, the variation of *N* will be one of the first aspects that will be subsequently evaluated.

6.2.1 Case study

In order to give an easier understanding of the results proposed, it can be worthy to refer us to a practical case study. The fixed characteristic of this are summarized in the Table (6.1). The fluid considered is R245fa.

VH [m]	VR	N [rpm]	Φ	Ψ	p01 [kPa]	T01 [K]	p06 [kPa]	N_s	N_t
0.1	5.71	9000	0.215	0.918	1000	369.9	178	0.415	1.529

Table 6.1 *Main input values for the case study considered*

These case study characteristics were chosen because they are near to the mean of the analysed values range, considering *VH* and *VR*. The values chosen for φ and ψ are the ones suggested by the graph proposed by Chen and Baines, reported in figure (3.1), where this couple of value is related to the maximum achieved efficiency for radial turbines (circa 90%). These values were also chosen by Sauret and Rowlands in [15], so that this could be a comparison between results.

Also the thermodynamic input parameters are shown in the Table (6.1). They provide the inlet and outlet characteristics, being directly linked to the other design values. In this way, the constrains of the analysis are fixed.

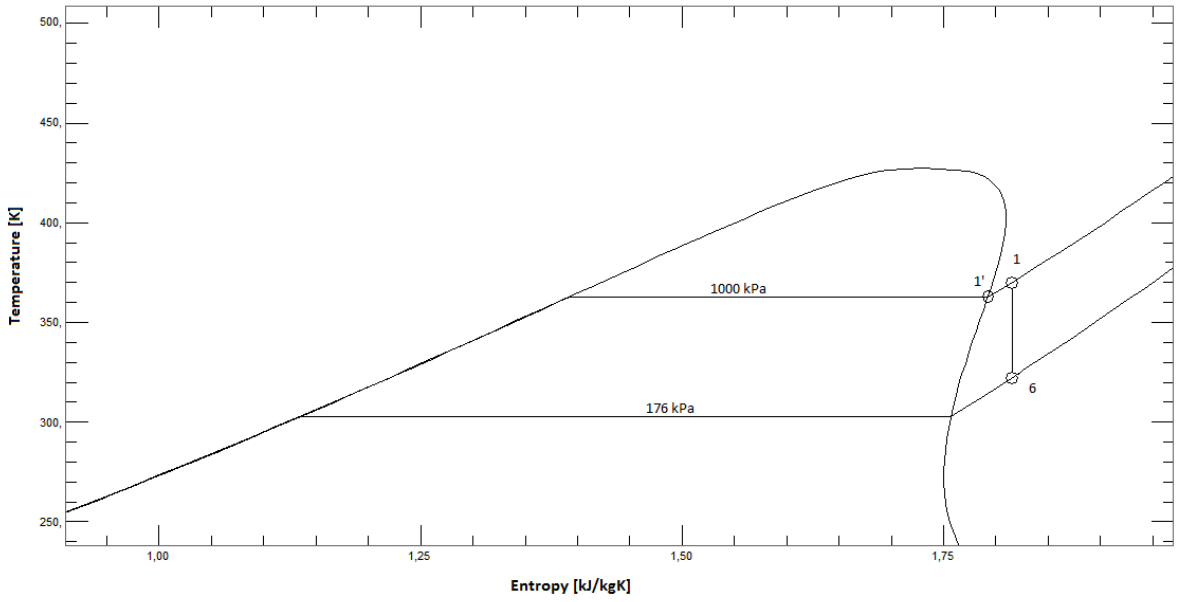

Figure 6.1 *Thermodynamic inlet and outlet states of the considered case study, in T-s diagram.*

In this case the inlet pressure was fixed as $p_{01} = 1000$ kPa, then was supposed an overheating of 7°C respect the saturation conditions, so that $T_{01} = T'_{01} + 7$. In this way, the inlet thermodynamic

state is fully defined. The outlet pressure is then obtained considering a typical condenser temperature of 35°C, so that $p_{06} = p_{cond,T_{cond}=35°C}$. They are also showed in Figure (6.1), which gives an idea of the isentropic expansion in the *T-s* diagram of R-245fa.

The rotational speed is chosen, as said, in order to achieve a specific speed in the ideal range suggested for radial turbines. In fact, fixing *VH* and *VR* the only remaining value that can vary *Ns* is *N*. Certainly other values of *N* could have been chosen in this range, but this will be an aspect that is going to be discussed in the following chapters, where the efficiency will be evaluated for several values of *Ns*.

The code is then run referring to this hypothesis. The designer is provided of some instruments that can help to understand in the better way the generated output. First of all a table that summarize the thermodynamic states is created, as the one of Table (6.2). The table refers the characteristics of the total points (01, 02, 06), of the static points (1, 2, 3, 4, 6, 7), and their relative isobaric states on the line of isentropic expansion (2s, 6s, 7s).

With the hypothesis of no-losses occurring in the interspace between stator and rotor, it can be noticed that the states 2 and 4 present the same thermodynamic characteristics.

STATE	T [K]	p [kPa]	rho [kg/m^3]	h [J/(kg)]	s [J/(kgK)]	Title	a [m/s]
O1	369,89	1000,00	53,88	476,77	1,809	1,03	130,30
O2	368,04	902,24	47,75	476,77	1,815	1,04	132,69
O6	326,60	178,15	9,25	449,14	1,825	1,08	141,55
1	369,75	995,88	53,64	476,70	1,809	1,10	130,37
2	354,62	585,37	30,69	468,50	1,815	1,09	132,69
4	354,62	585,37	30,69	468,50	1,815	1,09	137,21
6	325,74	171,81	8,94	448,47	1,825	1,12	141,53
7	326,45	177,05	9,19	449,02	1,825	1,12	141,54
2s	352,95	585,37	30,61	466,65	1,809	n	n
6s	320,36	172,08	9,13	443,26	1,809	n	n
7s	321,06	177,05	9,39	443,80	1,809	n	n

Table 6.2 *Thermodynamic properties of the most important states characterising the expansion process of the case study*

These informations can be also visualized in the *T-s* diagram, that the code automatically generates, Figure (6.2). In this case, the calculated degree of reaction is *R=0.709*, and it belongs to the typical range of this kind of turbomachines.

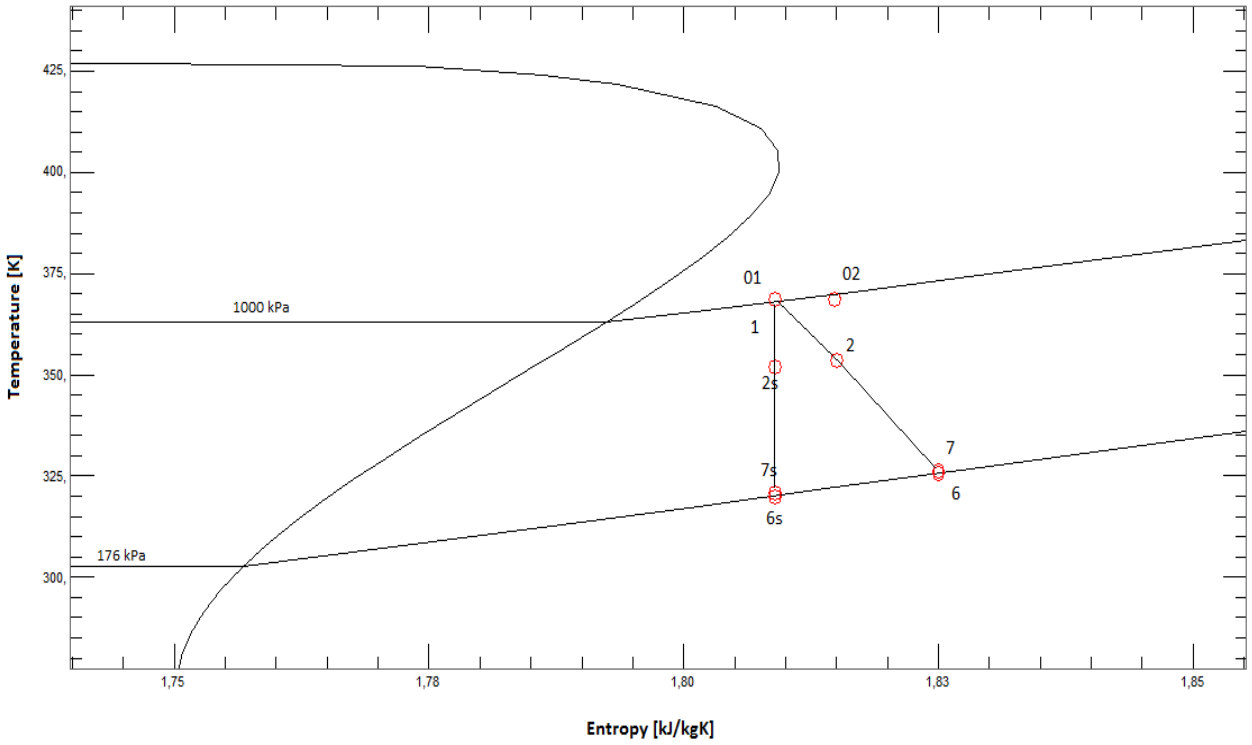

Figure 6.2 Expansion process of the case study.

Subsequently, it is possible to analyse the velocity triangles and the geometrical aspects of the expander: these parameters must be carefully examined, because is not uncommon that a computational program gives as output values, whose physical significance is impossible or not acceptable. In this way, in the code is implemented a procedure of output printing, as showed in the Table (6.3). In this case, all the values showed have a correct interpretation. In particular, they can be summarized as:

- Design parameters, which are the ones also reported in Table (6.1);
- Geometric parameters, as crossing sections, radii and angles. These values are reported for all the sections of the expander: nozzle vanes inlet (1), nozzle vanes outlet (2), rotor inlet (4), and rotor outlet (6);
- Velocity triangles, with absolute, relative and blade velocity. In particular, for the rotor exit, they are referred to the root-mean-square radius;
- Absolute and relative Mach numbers;

EXPANDER PERFORMANCE-FIXED INPUT	[m] r6s= 0.1169
	[m] r6h= 0.0539
DESIGN PARAMETERS	[°] beta6_RMS= -64.0532
[kPa] p01= 1000.0000	
[K] T01= 369.8924	**VELOCITY TRIANGLES**
[rpm] N= 9000.0000	
[m] VH=0.1	[m/s] U4= 169.2690
[adim] VR=5.71	[m/s] C4= 142.2656
[adim] phi=0.215	[m/s] W4= 44.7003
[adim] psi=0.918	[°] beta4= -43.4682
	[°] beta4_opt= -27.8216
GEOMETRY PARAMETERS	[°] alfa4= 76.8186
[m^2] A1= 0.0167	
[m] r1= 0.2335	[m/s] U6_RMS= 74.8327
	[m/s] C6= 36.5380
[m^2] A2= 0.0811	[m/s] W6_RMS= 83.5064
[m] r2= 0.1811	[°] beta6= -64.0532
[m^2] A2_throat= 0.0024	[°] alfa6= -0.4018
A2_throat/A2= 0.0296	
[m] blade_thikness= 0.0020	**MACH NUMBERS**
[m^2] A4= 0.0129	Ma1= 0.0950
[m] r4= 0.1796	Ma2= 1.0369
[m] b4= 0.0114	Ma4= 1.0369
[°] alfa4= 76.8186	Ma4_r= 0.3258
	Ma6= 0.2582
[m^2] A6= 0.0338	Ma6_r= 0.5900
[m] r6_RMS= 0.0794	

Table 6.3 *Output values for the considered case study. The designer should carefully check this table in order to avoid code mistakes.*

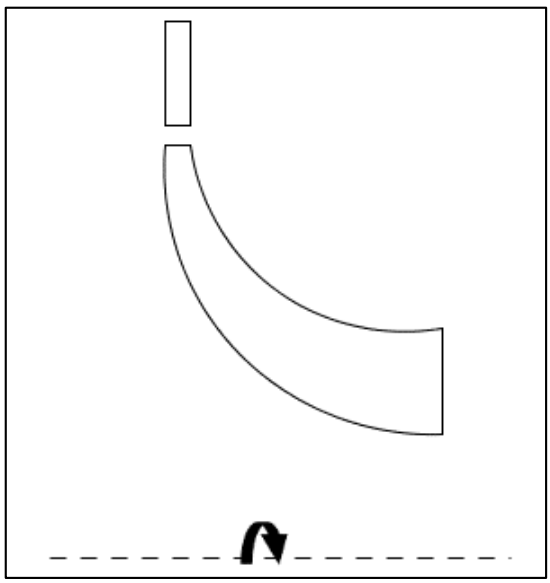

Figure 6.3 *Meridional section generated for the case study.*

The inlet and outlet sections are influenced by the choice of the meridional velocity ratio E defined in Equation. (3.22). In this simulation (as in all the simulations run with this model) was chosen as $E=1$, so that the flow parameter was a constant in section 4 and 6.

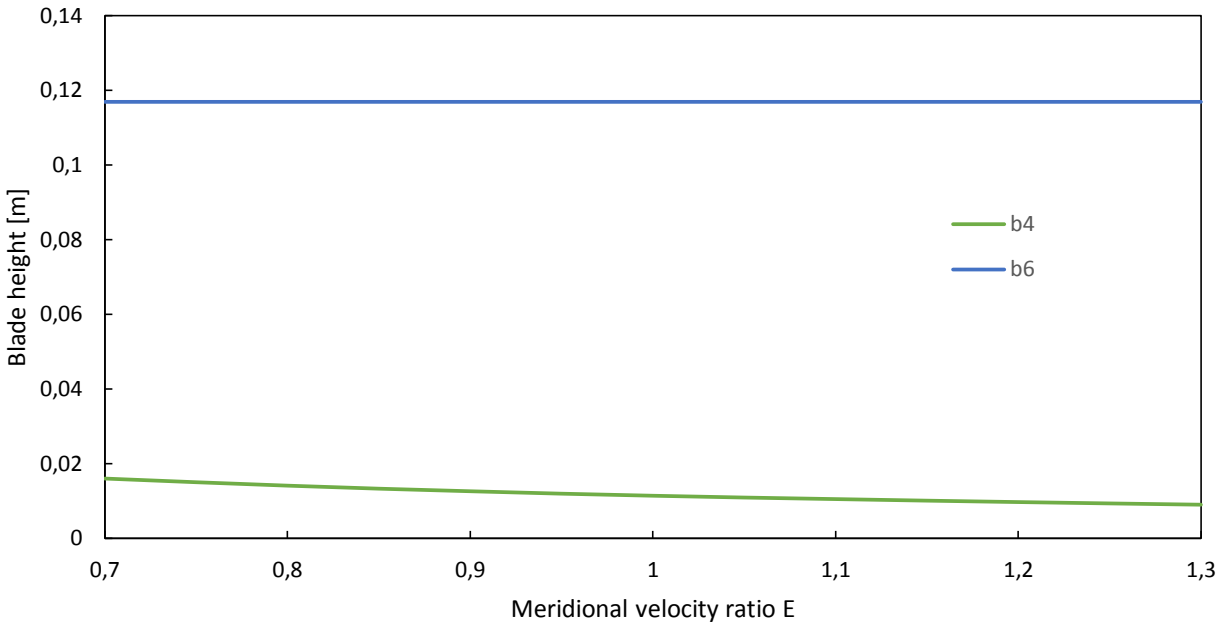

Figure 6.4 *Blade height at the rotor inlet and outlet, as functions of the meridional velocity ratio E. While b4 shows variations, b6 is a constant.*

E has a direct influence on the blade height of the inlet section, while the one of the outlet is constant because is defined by other parameters, as Φ. The trends are shown in Figure (6.3). Anyway the choice of $E=1$ permits in most of the cases to provide a non-choked inlet section, where $Ma_4 \approx 1$.

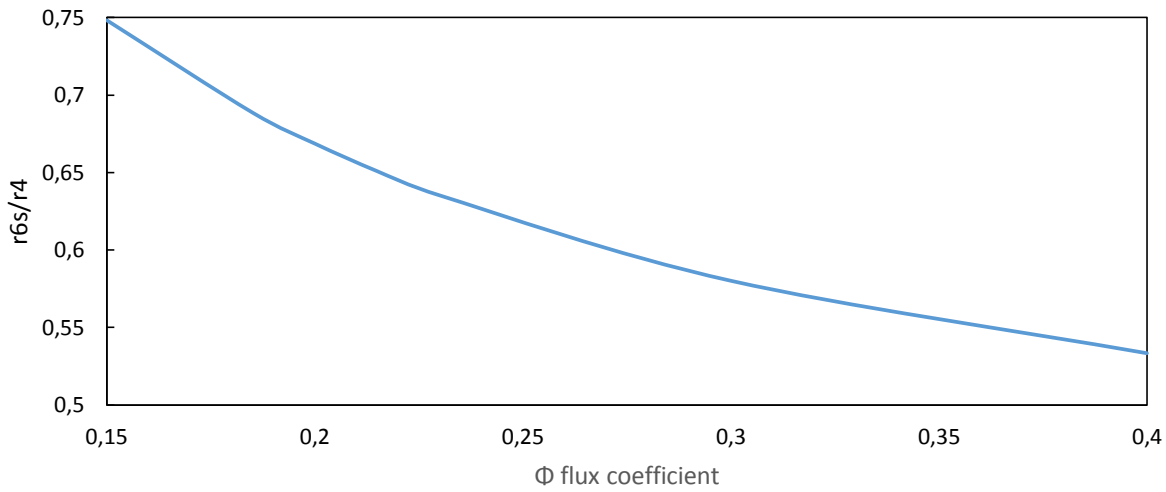

Figure 6.5 Radius ratio r4/r6s as a function of flux coefficient

Another geometrical aspect important to focus is the radius ratio r_4/r_{6s}. This characteristic defines the curvature on the profile at the shroud, which is an aspect that can influence the capacity of the turbo machine to extract useful work from the fluid.

To fix the hub radius at the outlet as $r_{6h}=0.3r_4$, as explained in §5.3, means that an increase of the flux coefficient leads to narrower areas A_6. In this way, the outlet radius at the tip (r6s) is reduced. This can be a good solution in case that the design procedure leads to non-optimal radius ratio r_{6s}/r_4, especially when it exceeds 0.8, value which is considered as the limit for an optimal fluid deviation [11].

It is also worthy for the designer to evaluate at this step the velocity triangles, which are a direct index of goodness of the design procedure. Indeed, the code is created considering several constrains and ideal values for angles, which should be respected.

The rotor inlet velocity triangle is characterized by an angle fixed by the preliminary geometry procedure, α_4. This angle determines the swirl given by the inlet vanes. The procedure then calculates their thickness, and the vane throat area, which are the values that determine the magnitude of the meridional velocity C_{m4}. This is done, in order to achieve a value of the relative flow angle β_4 as close as possible to the one predicted in the preliminary geometric design. The predicted one in fact, is calculated, basing only on evaluation linked to N, Φ, and Ψ.

Figure (6.5) represents the velocity triangles calculated in the design procedure with the hypothesis considered.

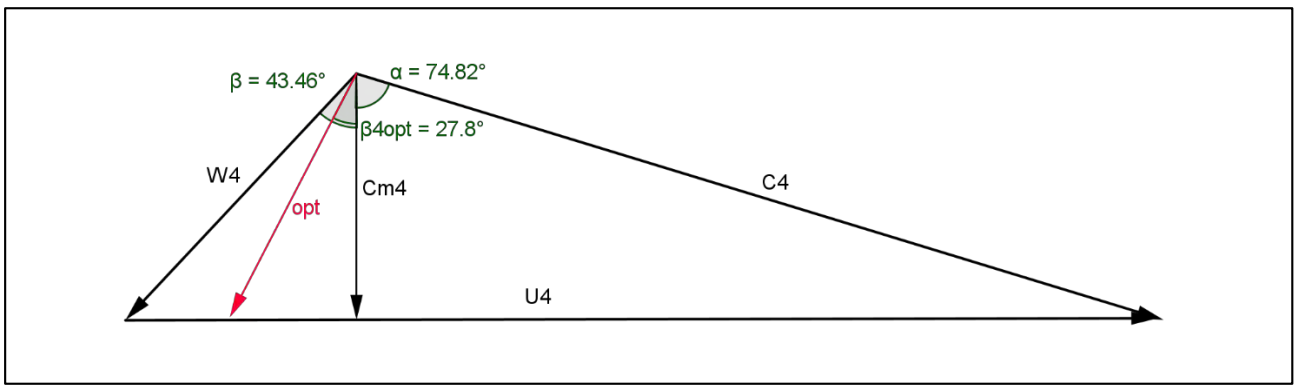

Figure 6.6 *Inlet velocity triangles for the case study.*

It is possible to note that the angle β_4 and $\beta_{4,opt}$ are not exactly the same: the first in fact represent the calculated value of the design, which is achievable with the defined thickness of the inlet blade vane. The second one instead is calculated by the empirical equation of Stanitz, expressed in Equation (5.54). The fact that β_4 was not externally imposed, but calculated as a consequence of the deviation given by the nozzle, implies the introduction of some incidence losses. This is the reason why, even

if the works refers to a study of design conditions (any off-design applications are taken here into account), there is not a perfect match between the ideal and the actual inlet velocity triangle. In other studies, the incidence losses are totally not evaluated (see [27]), because it is set a priori as the ideal one. It is also to say that the calculated values are so close to the ideal one, that the incidence losses will have a little relative weight on the total losses evaluation.

The designer should also analyse the velocity triangles at the exducer section of the rotor. As the geometry design procedure has the constrains to generate a flow without swirl in the exhaust diffuser, the absolute velocity should be here completely axial, so that the absolute flow angle α_6 must be close to 0° in all the section of the blade height, from the hub to the tip. Because of the radius variation, however, also the blade velocity varies along the blade height, so that the angle β_6 is not constant in all the section. This gives to the rotor outlet its typical curved shape.

Figures (6.6) the velocity triangles are shown in correspondence of hub, shroud and mean square radius. As shown in the results exposed in Table (6.3) the design procedure in this application gave an angle $\alpha_6=0.402°$, value that can be considered largely acceptable.

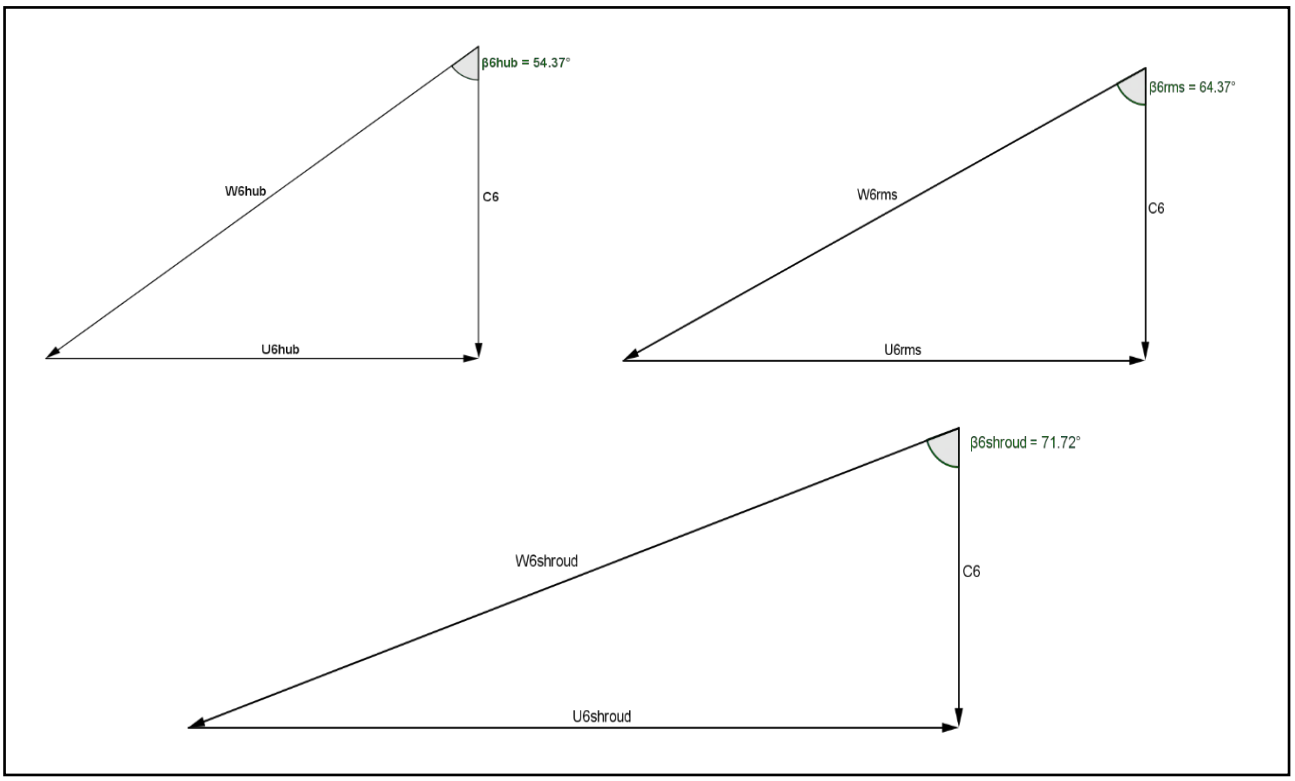

Figure 6.7 *Velocity triangles at the rotor outlet. Staring from top-left, clockwise: at the hub radius, at the root-mean-square radius, at the tip radius*

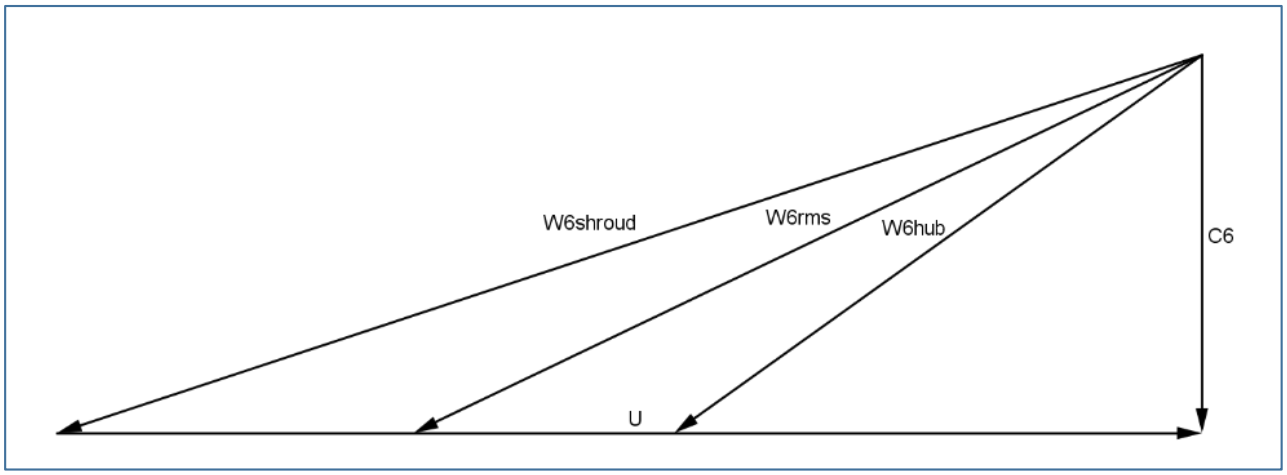

Figure 6.8 *Comparative visualization of velocity triangles at the rotor outlet, calculated for three different sections.*

The study of different losses weight is also an important step that allows the designer to consider the way the turbine is working. It is important to say that every loss model is strongly influenced by assumption and simplification done [27]. Indeed, all of them are calculated by using equations where many empirical coefficients play a fundamental role in the results. They clearly affects also the efficiency calculation, that will be the most important term of comparison in following sections, to give and study satisfactorily the best design conditions.

The Figure (n° figure) has the aim to show graphically the different impact that they have on the analysed model.

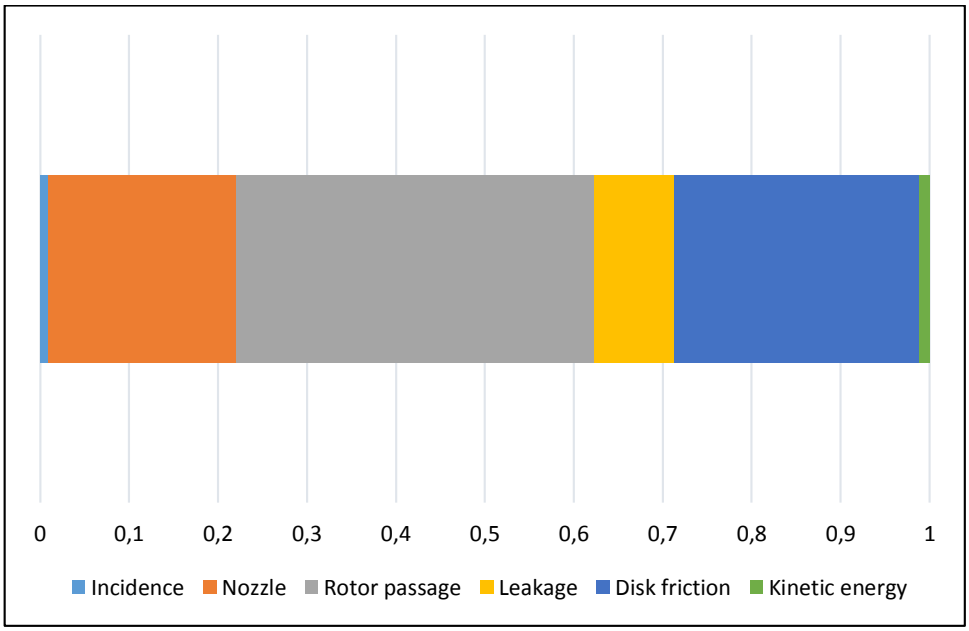

Figure 6.9 *Losses relative weight, in the considered case study.*

The graphic elaboration shows that more than 60% of losses is due to the passage of the fluid in stator and rotor. Incidence loss, as said before, has a low impact, as the kinetic energy at the exhaust outlet. The reason of this phenomenon can be the presence of the diffuser, which is able to recover large part of static pressure coming out from the expander.

It can be useful for a better understanding, to analyse the rotor losses varying the empirical coefficient K presented in Equation (5.57).

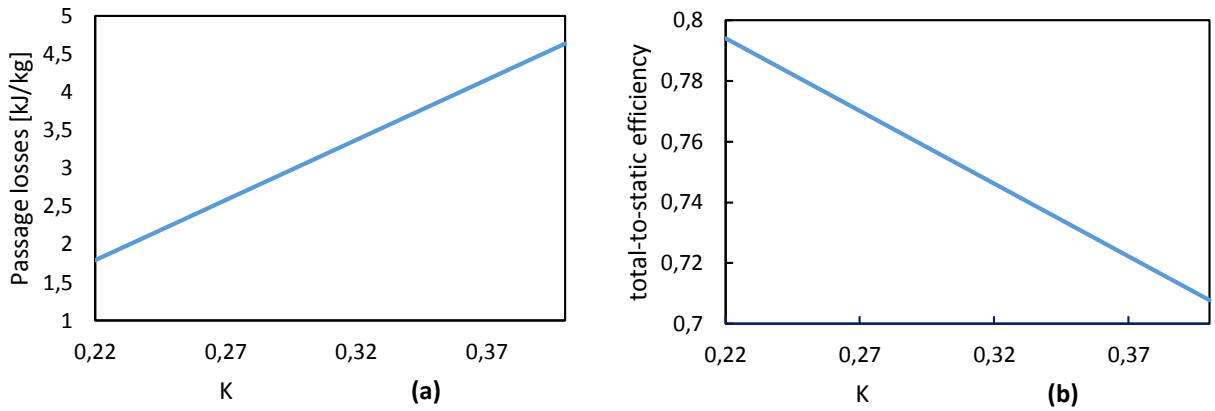

Figure 6.10 *In (a) the rotor passage losses are showed as a function of K coefficient. Depending on the same parameter, the achieved efficiency is showed in (b). The more the parameter K grows, the more efficiency penalty increases.*

The graphic relations showed in Figure (6.10) express the variation of passage losses and of efficiency related with the choice of the empirical coefficient K. In [11] and [12] is suggested that this value should vary in a range between 0.22 and 0.4, advising that some experimental studies found a good match for $K=0.33$, which is the value utilised in this work. As can be seen, anyway, this choice constrains strongly the analysis, because there is a variation of total-to-static efficiency related to the range of K of eight percentage points. Therefore, the range of variation of K implies a range of variation for the considered passage losses. This is to say that the model proposed should be always compared and modified, taking into account the experience of empirical experiments.

A similar reasoning can be expressed for other source of loss. In figure (n fig) are analysed the disk friction losses related to different values of axial gap between the rotating disk and static back casing. An important aspect is here to estimate the physical meaning of the value of the interspace, which must be in reasonable accord with the technical feasibility. This means that is worthy to define a range of acceptable value for ε_f, according to literature between 0.3 mm and 1.5 mm. In the study proposed, the radial gap was chosen as a percentage of the inlet blade height b_4 as $\varepsilon_f / b_4 = 0.02$, this lead to $\varepsilon_f = 1.2\ mm$, acceptable value. In Figure (6.11) a study of variation of efficiency related to this gap

is exposed, showing that the definition of it can lead to incorrect prediction of total-to-static-efficiency, around one percentage point.

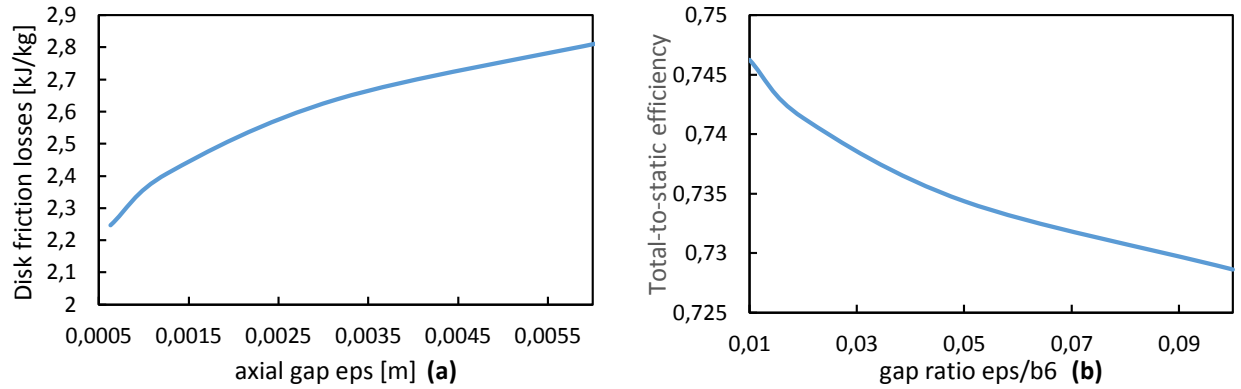

Figure 6.11*Variation of disk friction loss as a function of the gap between rotor disc and back plate (a). Variation of efficiency as a function of gap to radio ratio (b).*

In Figure (6.12) is also presented the variation of the leakage loss: the more the radial gap ε_r between the blade tip and the shroud is large, the more the leaking mass flow rate m_L (5.70) grows. In this way, the power los due to this phenomenon subtract more and more power to the turbine outlet. This can lead to efficiency penalty in the order of circa 1.5%, considering the main acceptable range of ε_r between 0.7mm and 2mm.

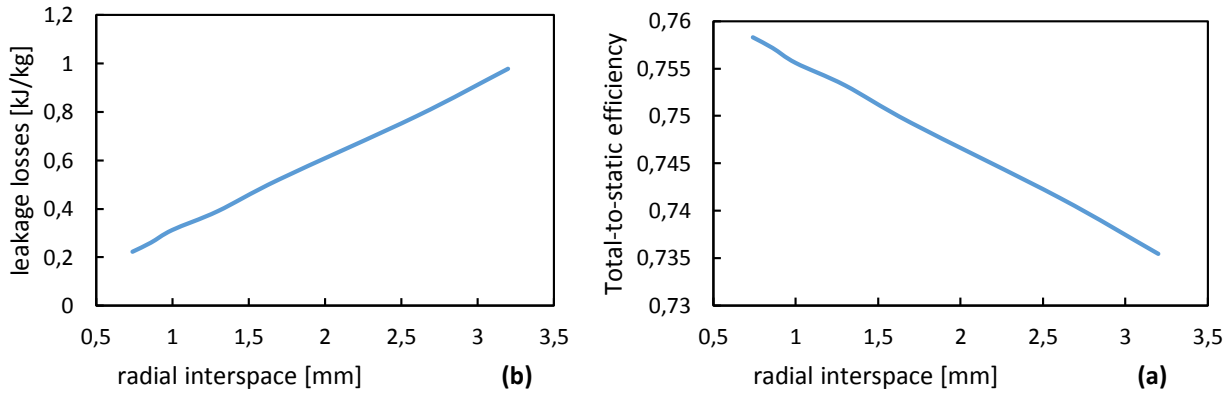

Figure 6.12 *Variation of leakage loss as a function of the radial gap (a). Variation of efficiency as a function of radial gap (b).*

After considering the effect of each separate loss, it is possible to show and compare the output of the model considering different losses coefficient. This example is worthy to show the flexibility that the model can assume, in order to represent in the best way experimental data from real turbines. In Figures (6.13) and (6.14) is compared the division of losses based on the study case, against two similar cases where the main empirical coefficients have been varied. One of them can be considered

as an example of a high quality turbine, in the meaning that the radial gaps, both related to friction and leakage losses are narrow. Also the rotor presents a lower parameter *K*. The other instead is the opposite, with larger gaps and a worst rotor loss coefficient. The only component considered as constant is the exhaust diffuser. The parameters are represented in Table (6.5).

	"High quality turbine"	**"Case study turbine"**	**"Low quality turbine"**
Rotor loss coefficient *K*	0.28	0.33	0.36
Radial gap, leakage loss [mm]	0.74	2.60	3.20
Rotor-Backplate gap, friction losses [mm]	0.63	1.26	3.15
Total-to-static efficiency	77.4%	74.1%	69.9%

Table 6.5 *Characteristics and coefficients utilised in the comparison analysis between three generalised kinds of radial turbines.*

The graphical results are shown in Figures (6.13) and (6.14). They show respectively the relative division of losses (6.13) and the absolute one (6.14) for tree different cases. A large efficiency penalty is calculated between the high quality and low quality one (circa 7%). Although the aim of the designer is always to design the turbomachines as best as possible, the low quality case could be considered as a limiting case. Here the device could be conditioned by production costs, which suggest choosing less expensive solution and mechanical machining.

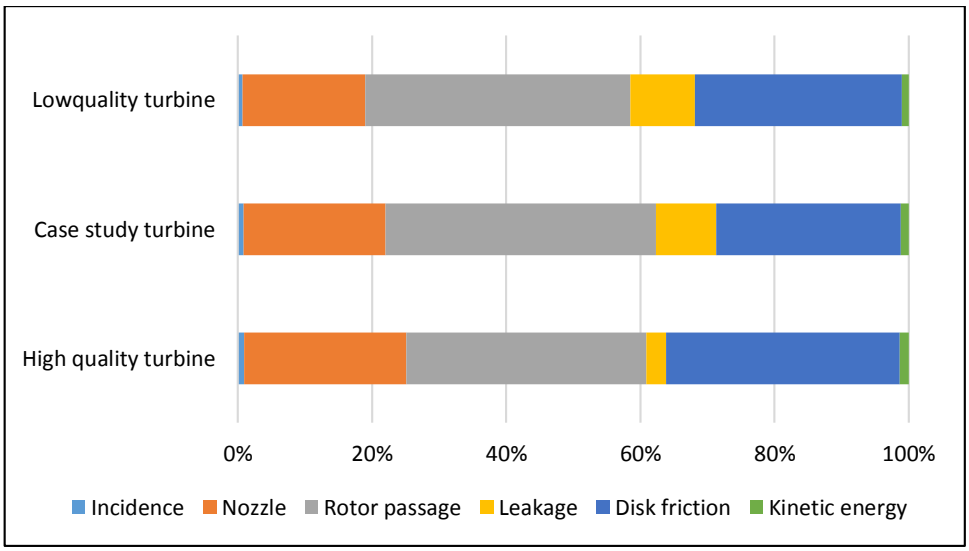

Figure 6.13 *Relative division of losses, for three different "quality" of turbines.*

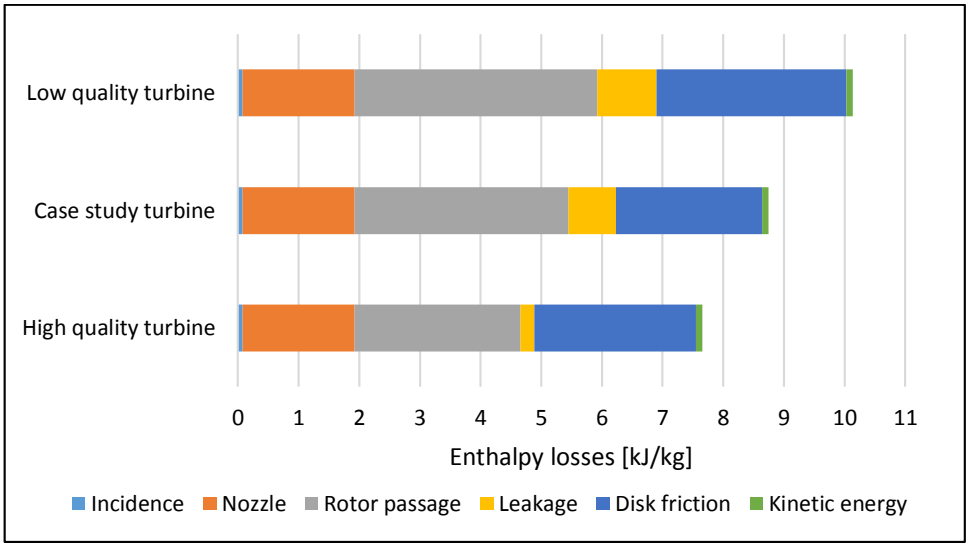

Figure 6.14 *Absolute division of losses, for three different "quality" of turbines.*

6.3 Analysis at variable Φ and Ψ

Flow and blade loading coefficients play a key role in the definition of velocity triangles at inlet and outlet sections of the expander. Not only, they clearly affect and determine the geometrical aspects of the main sizes of radii, blade height and areas, being in the proposed code a design procedure input. Considering this, it seems extremely important to define which are the coefficients that allow to reach the best design condition. Other main design input are instead considered as constants (size parameter, volume expansion ratio and rotational speed).

The Figure (3.1) proposed in Chen and Baines in [14]is based on several statistic sources. The total-to-static-efficiency is correlated with values of Φ and Ψ: this suggest that there should be ideal values that allows to design a radial turbomachine with optimal characteristics. The limit of this study, that hardly fits with the proposed method, is that these ideal values were statistically calculated, basing on expander operating with ideal gases (air, combustion exhaust gases).

Indeed, other studies concerning the design of radial expanders for Organic Rankine applications showed that best efficiency design condition are obtained starting from different values, as explained in §4.4.2 (in particular in [30]). For this reason, even if they can be considered surely as a good starting point for designing, an evaluation of efficiency based on the combination of other values of Φ and Ψ is here carried out.

This implies to implement in the code a double "for" cycle, which permits to analyse the expander characteristic, calculated starting from different couples of values.

The results are graphically expressed in following figure: for fixed condition of VH, VR and N a three-dimensional surface is created, linking efficiency to each combination of load and flow parameters.

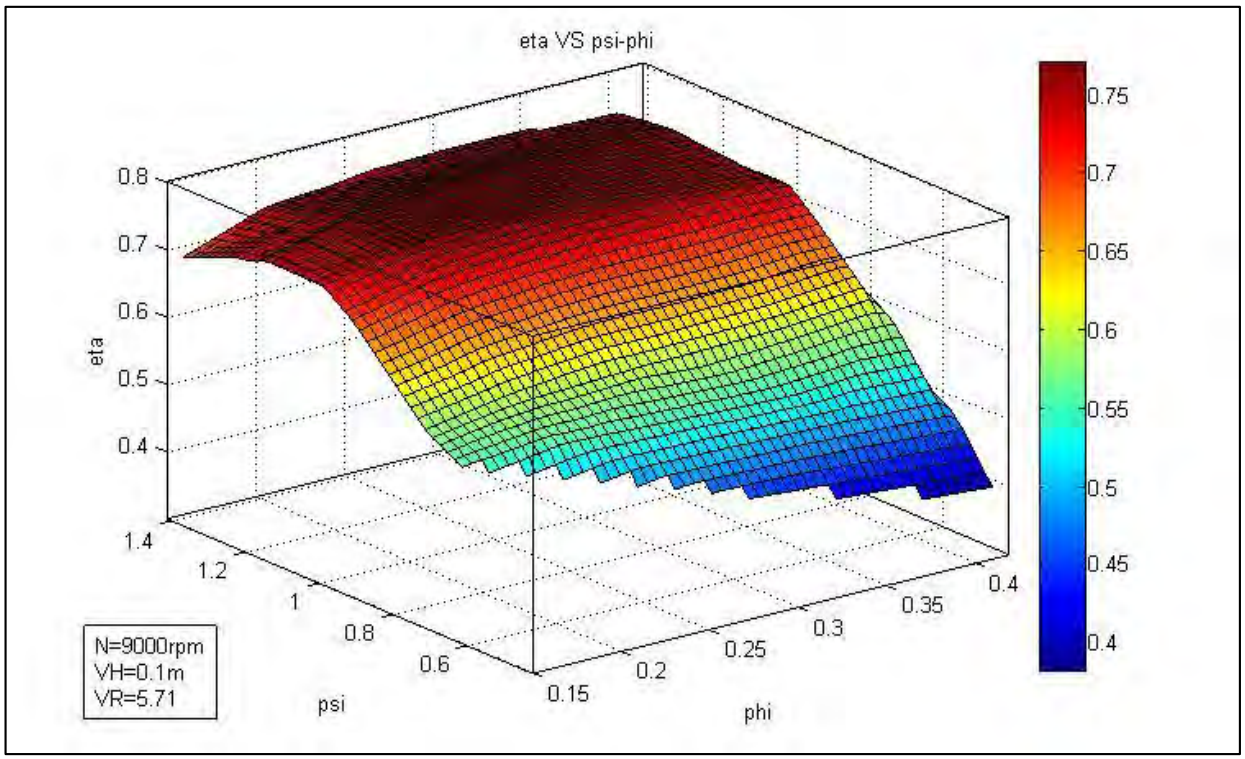

Figure 6.15 *Surface fiting of the calculated total-to-static efficiency, as a function of Φ and ψ The case refers to the following design parameters: VH=0.1 m; VR=5.71; N=9000 rpm.*

The surface fitting permits to evaluate the trend of total-to-static efficiency, so that the best combination of design parameter can be chosen. In Table (6.6) a comparison is expressed between the best efficiency solution, and the characteristics of the expander designed using values of Φ and Ψ suggested as optimal in Chen-Baines. Both cases refer to the following design parameters: VH=0.1 m; VR=5.71; N=9000 rpm.

	Φ	**Ψ**	**η_{ts}**	**Ns**	**Nt**	**P [kW]**	**R**
Best efficiency turbine	0.275	1.20	0.770	0.41	1.371	277	0.65
Chen-Baines turbine	0.215	0.918	0.741	0.41	1.52	267	0.71

Table 6.6 *Main characteristics of two turbines, whose design conditions are fixed for VH=0.1 m; VR=5.71; N=9000 rpm. Instead, flow and load coefficients are different.*

The working condition in this way shows an increase of three percentage points in efficiency, with a net power output higher of 10kW, comparing with the expander designed following the Chen-and Baines design conditions. Table (6.7) points out the different division of generated losses for the

different solutions. A graphic interpretation of this aspect is showed also in Figure (6.16).The losses are directly linked to geometrical aspects, which are collected in Table (6.8). From Figure (6.17) it can be seen that the geometries generated are quite similar, because the optimum coefficients and the ones suggested by Chen and Baines are similar.

	Incidence [kJ/kg]	Stator loss [kJ/kg]	Rotor loss [kJ/kg]	Leakage [kJ/kg]	Disk frict. [kJ/kg]	Leaving kin. En. [kJ/kg]
Best efficiency turbine	0,145	2,221	3,274	0,559	1,53	0,134
Chen-Baines turbine	0,072	1,847	3,530	0,782	2,40	0,104

Table 6.7 *Losses for the considered design conditions.*

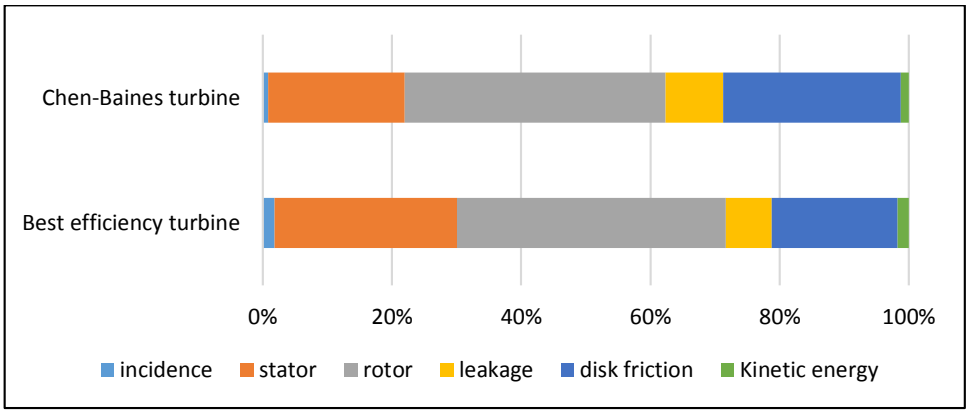

Figure 6.16 *Relative losses division for the considered design conditions.*

	A4[m^2]	r4[m]	b4[m]	alfa4[°]	A6[m^2]	r6$_{rms}$[m]	r6$_s$[m]	r6$_h$[m]
Best efficiency turbine	0,0138	0,1605	0,0137	76,5514	0,0299	0,0724	0,1088	0,04815
Chen-Baines turbine	0,0129	0,1796	0,0114	76,8186	0,0338	0,0794	0,1169	0,05389

Table 6.8 *Geometric characteristic of the considered turbines.*

The first solution presents higher values of Φ and Ψ and this aspect permits to a have a more compact rotor geometry, as reported in Figure (6.17). This lead to a reduction in leakage and disk friction losses, whose variation is the aspect, which has more influence in increasing efficiency, added to a little decrease of rotor losses. The only loss source that presents an opposite trend is the stator one, because an increase of Φ and Ψ involves an increase of mass flow rate. Utilizing the exposed Benson relation of Figure (5.5) about stator characteristic, this aspect produces an increase of losses in this component.

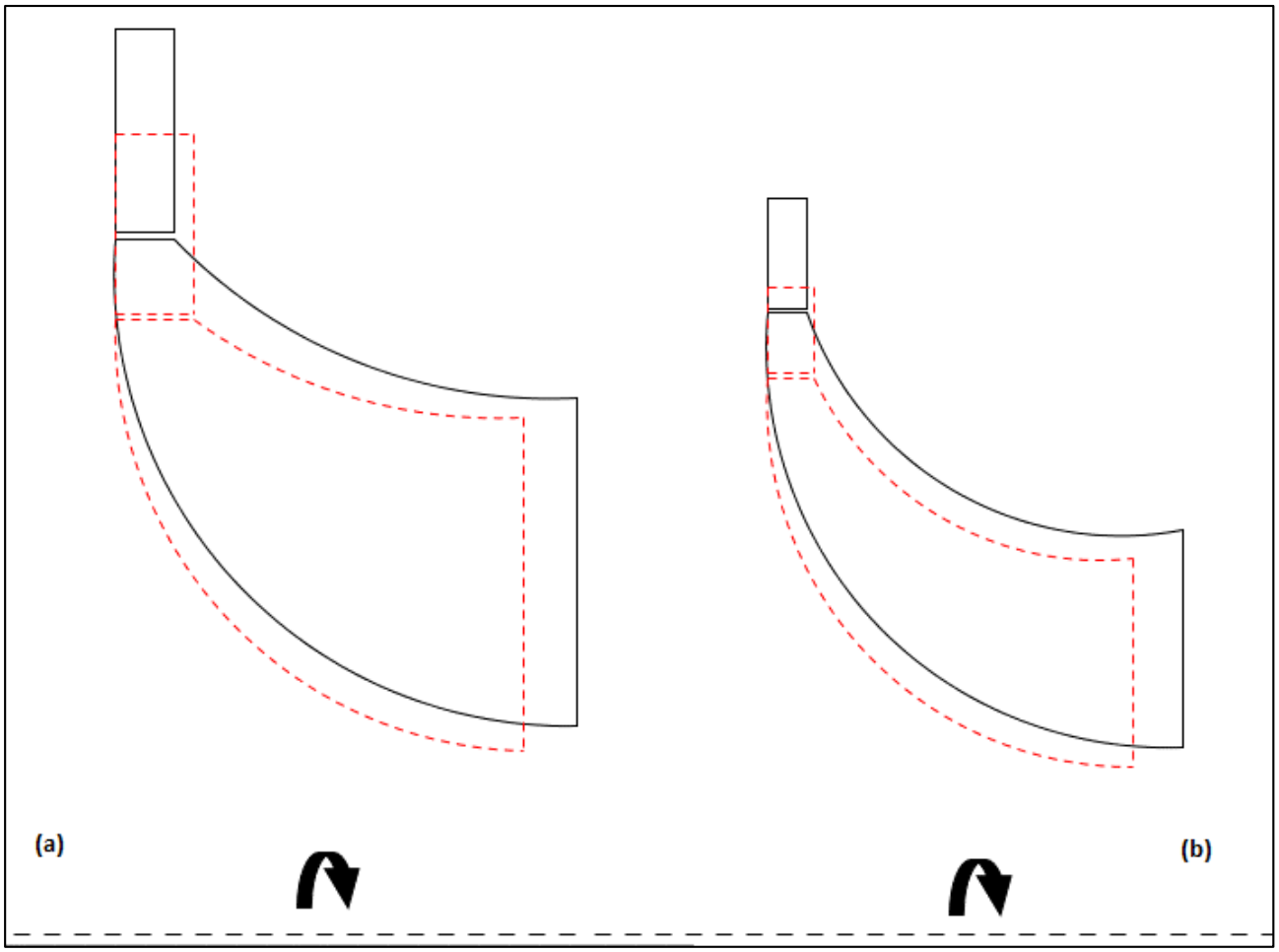

Figure 6.17 *(a) Comparative representation of rotor meridional section. In dashed red line the geometry optimized by the proposed code, with Φ=0.250 and Ψ=1.20. In black continuous line, the geometry obtained using different flow and load coefficients,: Φ=0.211 and Ψ=0.924. The second configurations shows an efficiency decrease of 5%. (VH=0.3 m; VR=6.80; N=9000 rpm).*
(b) Comparative representation of rotor meridional section. In dashed red line the geometry optimized by the proposed code, with Φ=0.275 and Ψ=1.20. In black continuous line, the geometry obtained using the coefficients suggested by Chen and Baines: Φ=0.215 and Ψ=0.918. (VH=0.1 m; VR=5.71; N=9000 rpm).

It is also important to understand that this new ideal parameters found do not maximise the efficiency in all the design conditions, but a new couple of ideal values can be express for different ones. For this reason, we report a graphical comparison between two-dimensions, which link Φ and Ψ with efficiency, Figure (6.18). First of all, the achieved maximum efficiency completely changes in different cases. In fact, as will be showed in next section, it is strongly a function of *VH, VR, N*.
Anyway. it is possible to note that also flow and load coefficients linked to maximum efficiency condition are an aspect that cannot be considered as constant in different situation.

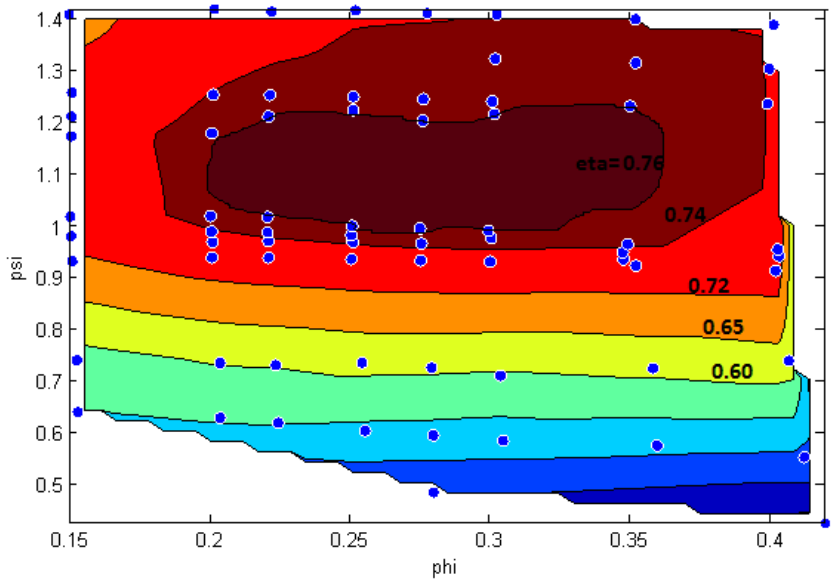

(a)

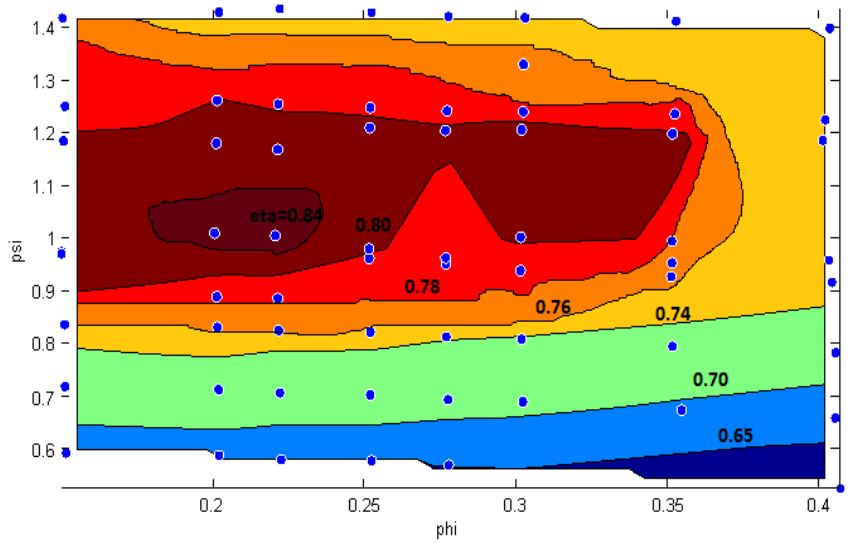

(b)

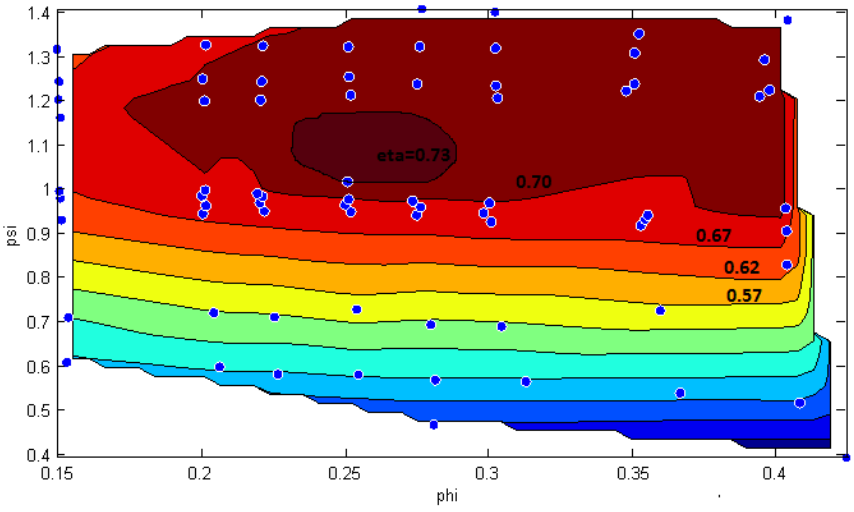

(c)

Figure 6.18 *In these graphs is showed the total-to-static efficiency calculated as a function of the couple ψ and Φ. The aim is to give a graphical idea of how the optimum values of ψ and Φ change, depending on input parameters VH, VR and N.*
Blue points refers to calculated point, used as input data for the elaboration.
In (a): VH=0.1 m, VR=5.71, N=9000.
In (b): VH=0.3 m, VR=2.94, N=5000.
In (c): VH=0.008 m, VR=6.80, N=17000.
This has a particular importance if compared to Chen and Baines [14]

An elaboration of the best design conditions for each couple of value *VH* and *VR* is then rported in Figure (6.19). Here is showed how the optimal flow coefficient is a function both of the size and of the compressibility of the working fluid. The data were interpolated by a second degree polynomial function. For higher expansion ratios and smaller sizes, the flow coefficient suggested can reach values around 0.34, which are quite far away from the ones suggested in Chen Baines [14].

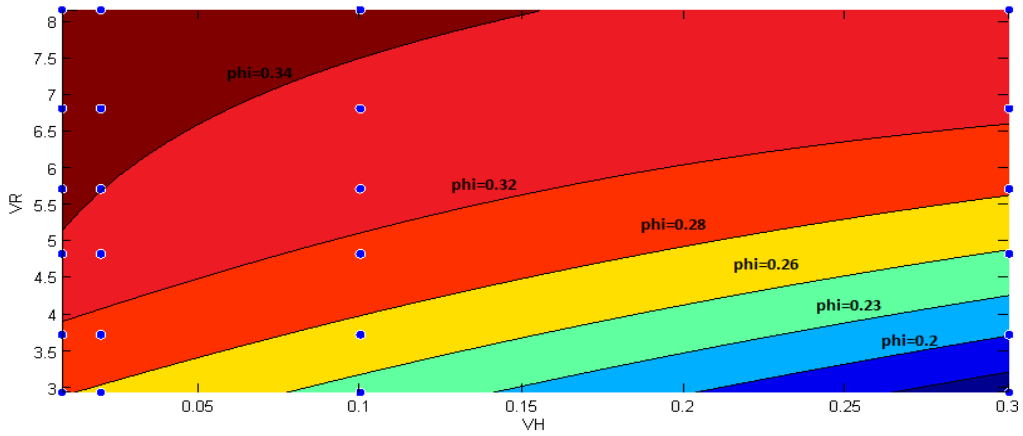

Figure 6.19 *Variation of flow coefficient Φ related to the best design conditions (higher total-to-static efficiency), as a funcion of VH and VR.*

A similar elaboration was done also for the load coefficient, Figure (6.20). In this case, it can be seen that the variation of the parameter as a function of VH and VR is more limited, if compared to the one of Φ. In fact, the range observed for this parameter is between 0.98 and 1.15, (15% of variation), while the range of Φ is between 0.20 and 0.34 (41% of variation). Largest values of ψ are required for the best design of small scale turbines. The behaviour of respect the volume expansion ratio shows a maximum around VR=5.50.

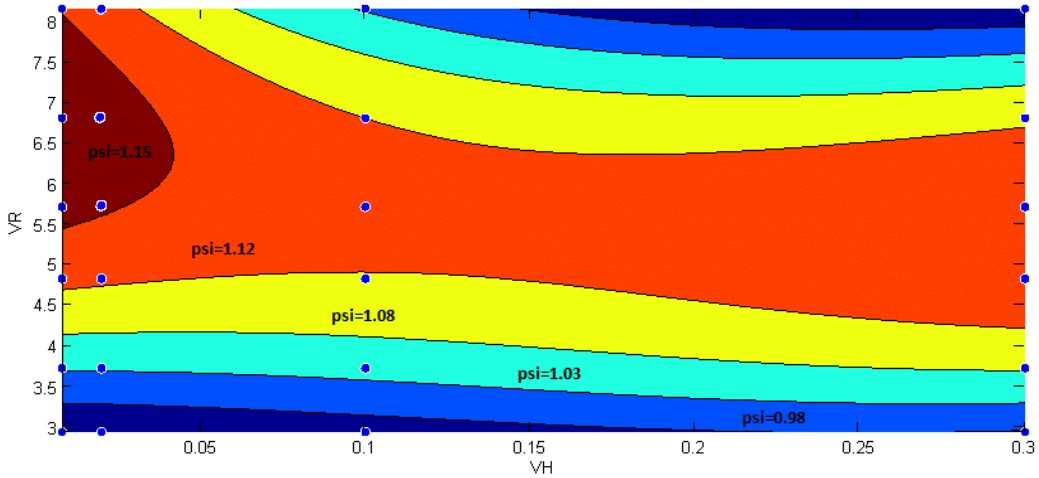

Figure 6.20*Variation of flow coefficient Φ related to the best design conditions (higher total-to-static efficiency), as a funcion of VH and VR.*

6.4 Ideal design efficiency prediction

In this section, the maximum achievable efficiency for several design input parameters is analysed. For this reason, this part can be considered the most important one of the whole work. It can give to designers a useful tool, which can help them to estimate the isentropic efficiency of the expander. Indeed, studies as [10] showed that to consider a constant isentropic efficiency for the turbine in an ORC system model can lead to erroneous evaluations, in particular relating to the optimization of the whole cycle characteristic parameters.

The two different level of studies showed in sections §6.2 and §6.3 can be considered as necessary and preparatory units, because their repeated utilisation provides the necessary evaluation required in this more general analysis.

Following this idea, the model was performed in order to find how the maximum achievable efficiency varies, relating to size parameter *VH* and volumetric expansion ratio *VR*. This means that for each couple of *VR* and *VH*, simulations have been run with several combinations of load and flow coefficient, for a fixed rotational velocity. This was then varied, changing in this way the specific velocity and the typical number, recording in this manner the parameters offering the highest total-to-static efficiency η_{ts}. Thus, the best efficiency condition has been studied as showed in the previous parts as the result of five different parameters:

- Size parameter *VH*;
- Volume expansion ratio *VR*;
- Load coefficient Ψ;
- Flow coefficient Φ;
- Rotational speed *N*;

As expressed in Equation (3.21), a turbine design where *VH, VR* and *N* are fixed implies that the specific speed *Ns* is also fixed. This parameter plays in the design a key role to achieve the maximum efficiency, being one of the most used non-dimensional parameter that characterise the component. For this reason, the first data elaboration consist in the analysis of the *Ns* linked to the best design configuration, for each couple of *VH* and *VR*, as showed in Figure (6.21).

The graphic relation obtained is similar to the one achieved by Perdichizzi and Lozza in [27], which has been already reported in Figure (4.14). To obtain a comparable value for *Ns,* is necessary to multiply the values of Figure (4.14) by 2π. The range suggested for *Ns* in [27] is between 0.52 and 0.75, while in the proposed optimization is between 0.42 and 0.52. The trend, anyway, is similar, and the differences could be caused by different assumptions in the models.

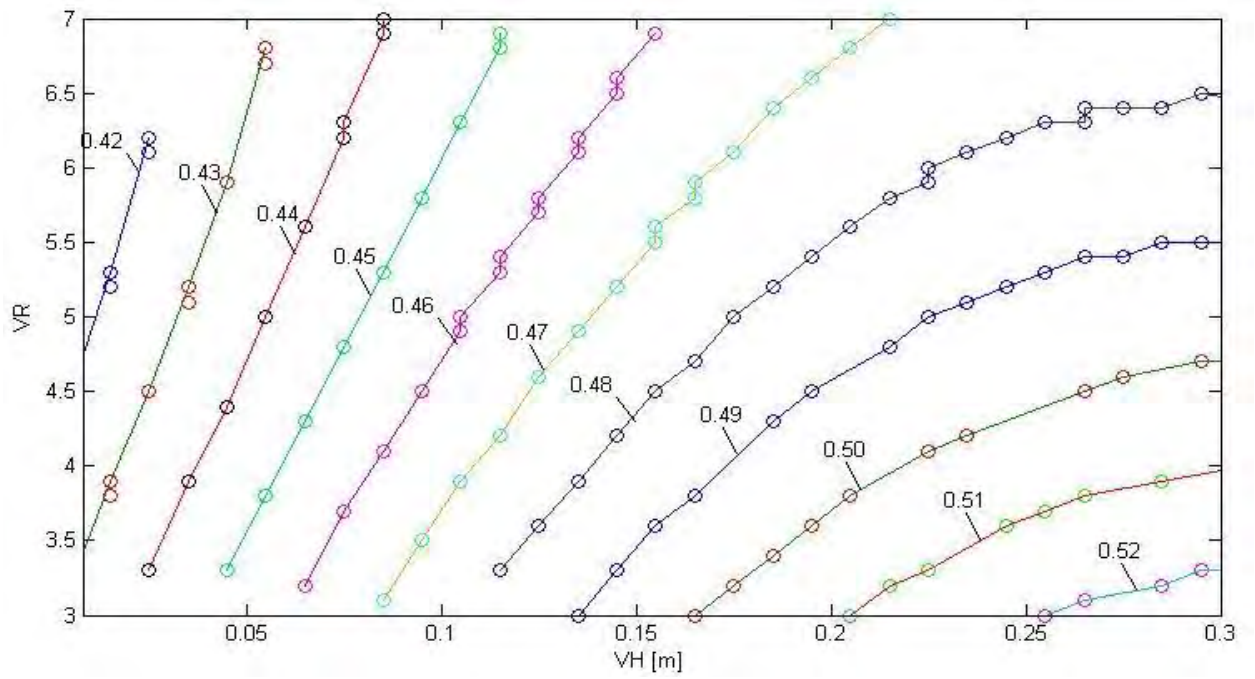

Figure 6.21 *Optimal specific speed for a radial stage, as function of size parameter and volume expansion ratio.*

The graph shows how *Ns* is influenced by the size of the machine and the compressibility of the operative fluid. Having lower *Ns* for high values of *VR* allows to achieve a geometry with larger radii and relatively lower speed of rotation. This characteristic permits a reduction of the disk friction losses, which, as showed in Equation (5.74), depend by the 3rd power of radius and 5th power of ω. Also for small turbines (*VH<0.1*), it is shown that is better to design expanders with low specific speed, because in this design range the leakage losses are increasing strongly with *N* and therefore with *Ns* as showed in Equation (5.70). For larger size parameters, the optimal *Ns* seems to have an asymptotic trend, so that Ns_{opt} could be in a certain way independent from VH.

Figure (6.22) expresses the trend of the maximum achievable efficiency for each couple of design parameters *VH* and *VR*, as obtained for the best specific number.

Large efficiency penalties are showed for low scale turbine, up to seven or eight percentage points. This clearly represent, as was expected, that the scaling down of the machine does not respect practically the principle of geometrical similarity: even if the expanders are characterized by the same non-dimensional parameters in fact they are not able to achieve the same maximum efficiency. This can be explained, remembering that the similarity principles clearly states, that all the geometrical characteristic must be scaled down of the same percentage. This aspect cannot be practically achieved due to technical production limits, such as clearance between blades and chasing, and between back rotor disk and chasing, besides the surface roughness of the components.

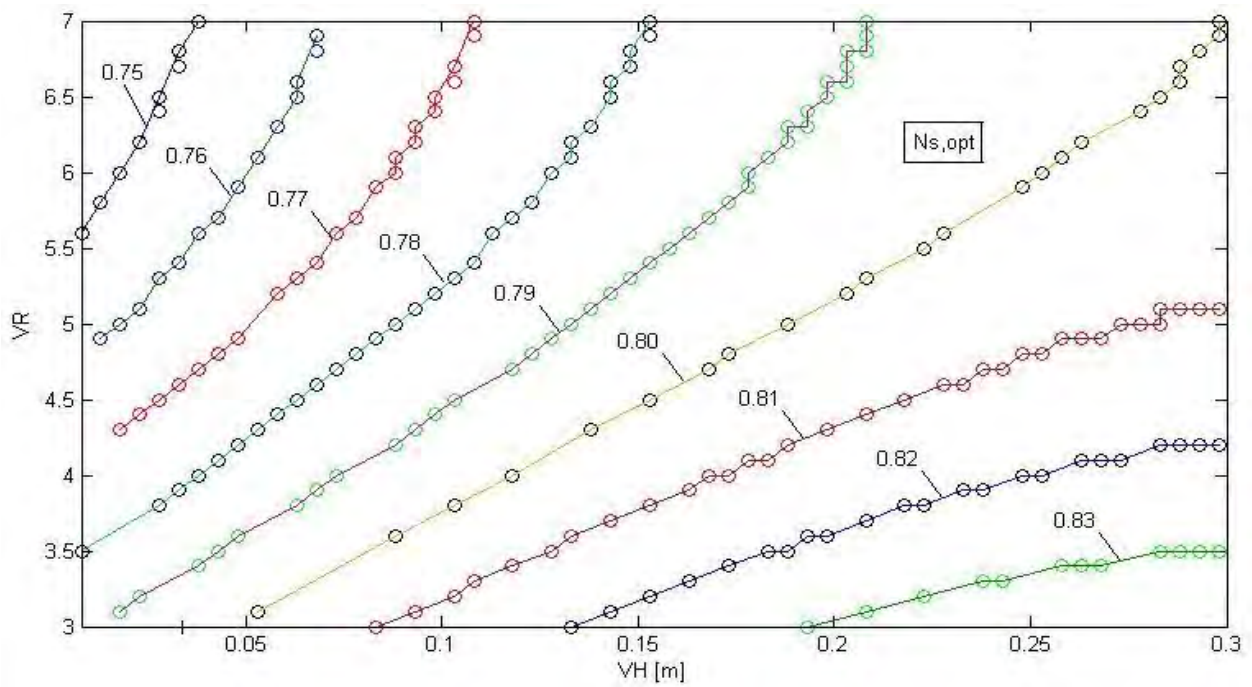

Figure 6.22 *Maximum achievable efficiency for a radial stage, at optimum specific speed condition*

It is also shown that several efficiency penalties occurs at large VR, and this manly due to very small blade height at the inlet section of nozzle and rotor, if compared to outlet section. The very low volume flow rate at the state 4 respect to the state 6 implies high value of the blade height ratio b_4/b_6, and this aspect is showed in figure (6.23), where b_4/b_6 is obtained for several VR and fixed VH ($VH=0.1\ m$).

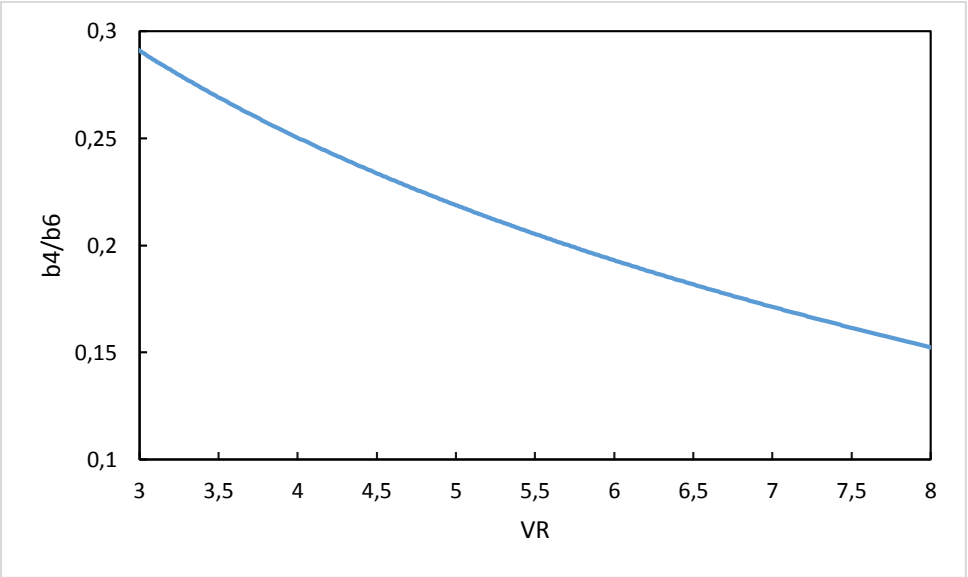

Figure 6.23 *Trend of the blade height ratio, as a function of the volume expansion ratio, for a fixed value of size parameter (VH=0.1 m)*

Stator losses, using the Benson's relation of Figure (5.5), increase with *VR*, because this implies lower mass flow rate crossing the nozzle. In this way, expanders designed with low value of *VR* can achieve up to five percentage points more in efficiency.

The trends of losses evaluated firstly at fixed *VH* and then at fixed *VR* are analysed in the following graphs.

In Figure (6.24) and (6.25) the trends of losses source at optimum *Ns* and fixed *VH* are represented, both as cumulative trends and stand-alone trends.

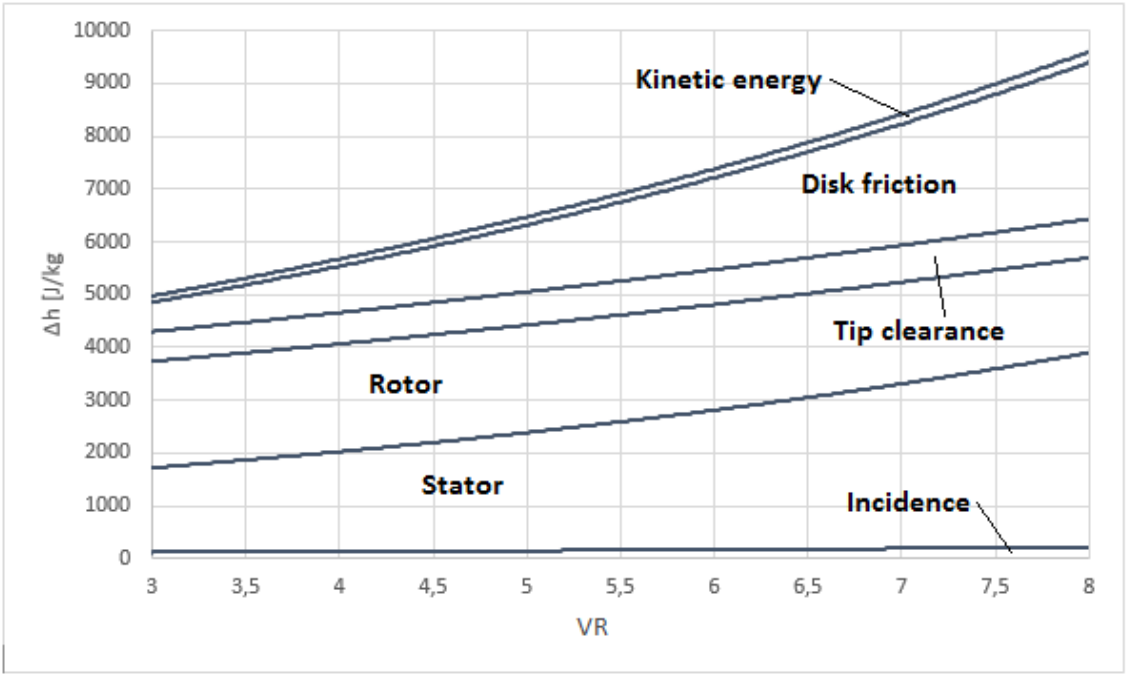

Figure 6.24 *Cumulative losses trends, as functions of volume expansion ratio, for a fixed value of VH=0.01 m.*

Some considerations can be exposed:

- Incidence losses: being in a design condition, they are largely considerable as constant and with quite low importance;
- Stator losses: they increase with *VR*, being a function inversely proportional of the mass flow rate. In fact, an increase of VR implies a larger enthalpy drop through the expander. For a fixed size VH, the required mass flow rate will be in this way smaller.
- Rotor losses: they present a decreasing trend with increasing *VR*;
- Tip clearance losses: they are quite constant because the radial gap ε_r is considered as a function of the size of the expander, which here is a constant (*VH=constant*); the same consideration can be made for the outlet radius r_{6s};

- Disk friction: they have a clear increasing with VR because of the higher density of the fluid at the inlet section, maintaining constant the outlet pressure; moreover is required a larger inlet radius r_4 and a smaller inlet blade height b_4. Considering the radial gap between the rotor disk and the back plate as a fixed percentage of b_4, the ratio $(\varepsilon_f/r_4)^{0.1}$ creates a larger friction parameter (5.75);
- Leaving kinetic energy: it mainly as a constant because of the fixed outlet parameters and the presence of the diffuser.

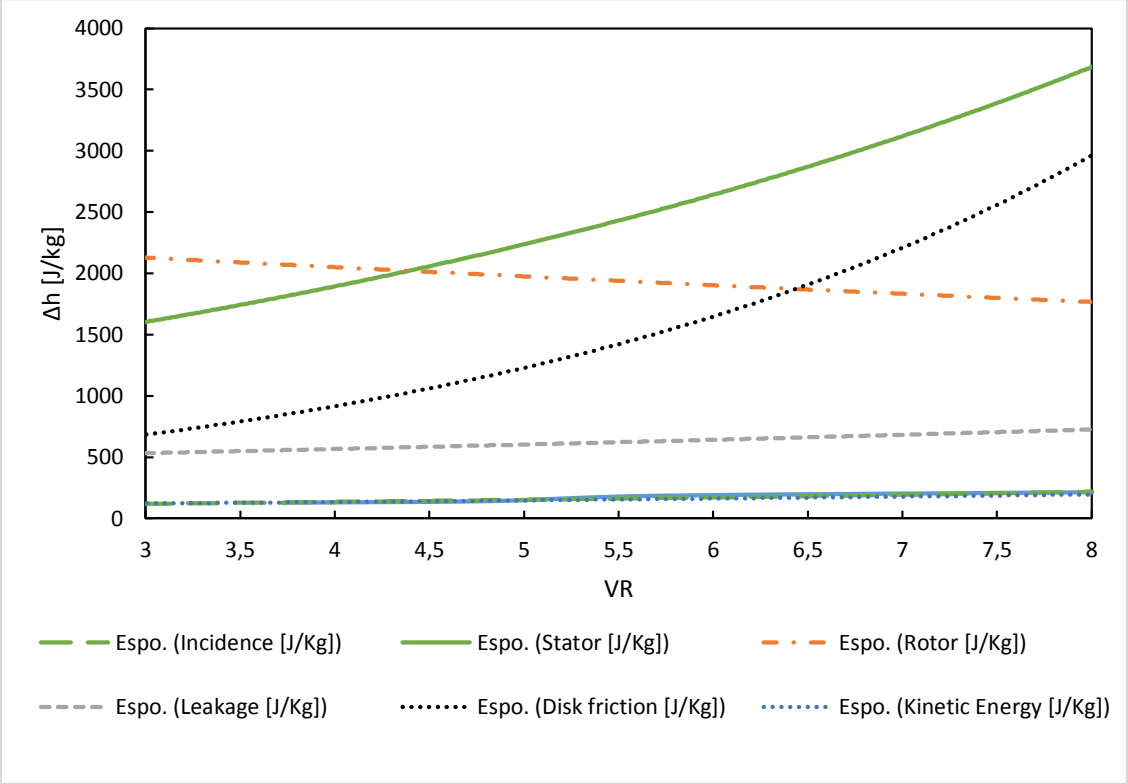

Figure 6.25 *Single losses trends, as functions of volume expansion ratio, for a fixed value of VH=0.01 m.*

In Figures (6.26) and (6.27), instead, it is analysed the losses trends for a constant condition of *VR* (*VR=5.71*) for the considered optimal specific speed.

Almost all the analysed sources of loss present an increase for small size expanders, and in particular:

- Incidence losses: being in a design condition, they are largely considerable as constant and with quite low importance;
- Stator losses: they show a little decrease, with augmenting of *VH*, because of the reduction of secondary losses taken into account in Benson's model, which decrease in larger size machine;
- Rotor losses present a decrement with *VH* increase;

- Tip clearance losses: they are considerable quite constant because the density is a function of *VR*, which is in this constant; moreover, also the blade speed at the outlet shroud U_{6s} is a quite constant parameter, because large diameter machines presents low rotational speed, and vice versa;
- Disk friction losses, for a reason similar to the tip clearance losses, there is a good balance between ω and r_4, so that in machine where the first is high the second one is small (low *VH*), and vice versa; however, due a stronger dependence of the friction to ω, the losses show a decreasing trend at higher *VH*;
- Leaving kinetic energy: it mainly as a constant because of the fixed outlet parameters and the presence of the diffuser.

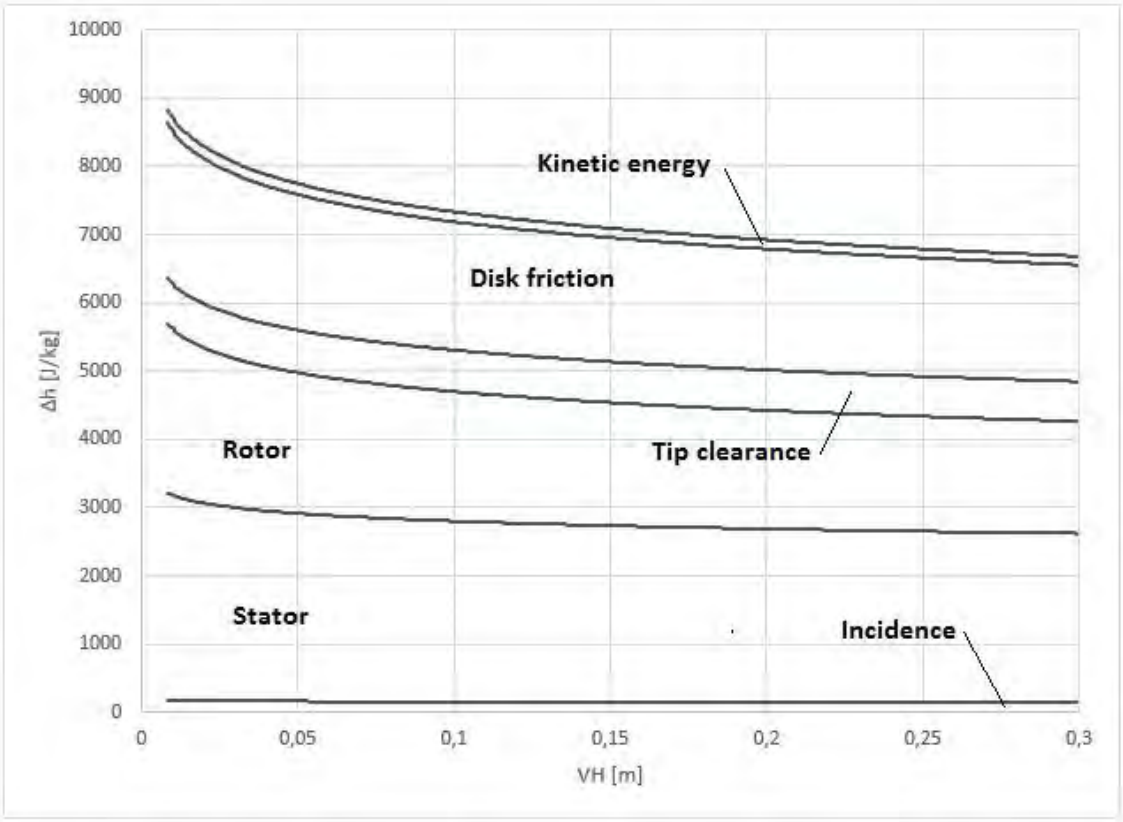

Figure 6.26 *Cumulative losses trends, as functions of size parameter, for a fixed value of VR=5.71.*

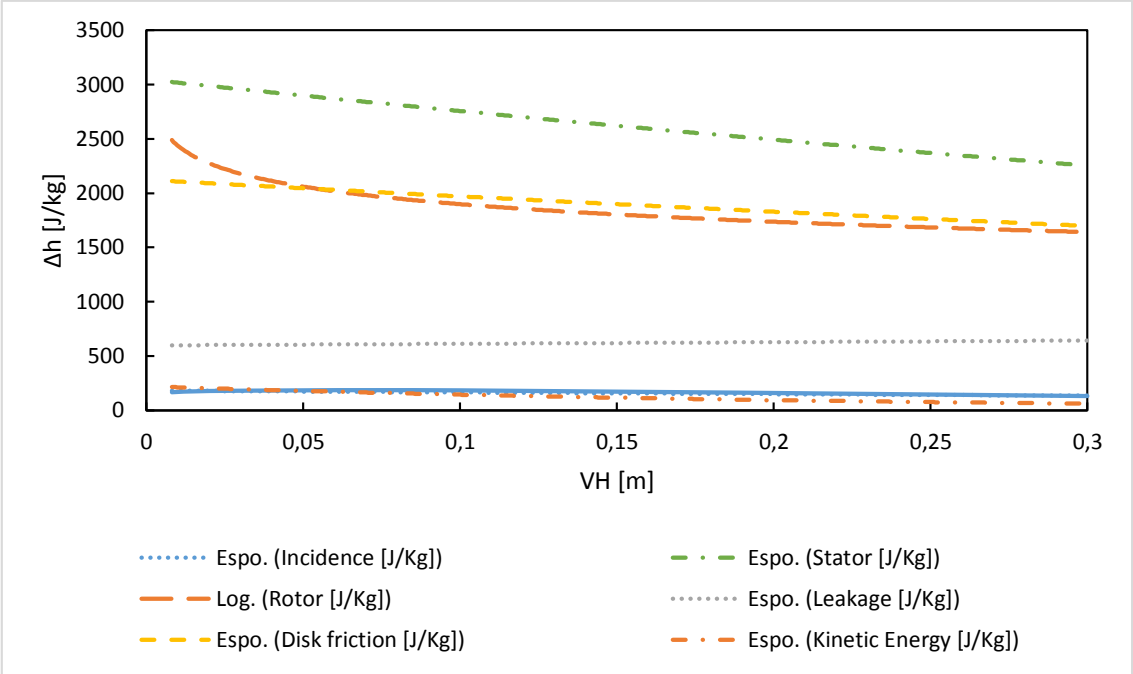

Figure 6.27 *Single losses trends, as functions of size parameter, for a fixed value of VR=5.71.*

Figures (6.24) and (6.26) can be compared to the result exposed in [27], and represented in Figure (6.28). It can be noticed that the trends are quite similar, but a few differences should be focused: in [27] incidence losses have been not considered, while here they are present even if with a little weight (see §6.2.1). The presence of the diffuser is considered in the proposed model. This reduces largely the weight of the leaving kinetic energy, which is a strong loss source in [27].

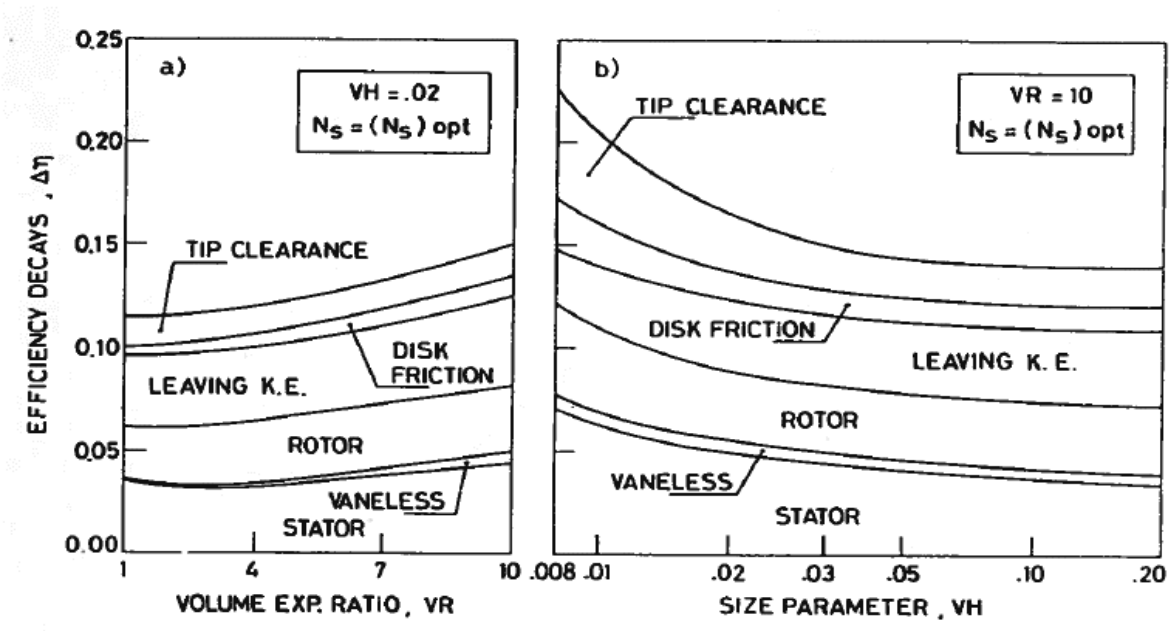

Figure 6.28 *Efficiency penalties as a function of VR and VH at optimum specific speed [27].*

In Figure (6.29) is exposed the maximum total-to-static efficiency achievable for several values of *VR* at optimal specific speed. This representation be considered as an explicative section of figure (6.22). In addition, here it can be seen the effects of expander size and compressibility, and how they affect the achievable efficiency η_{ts}.

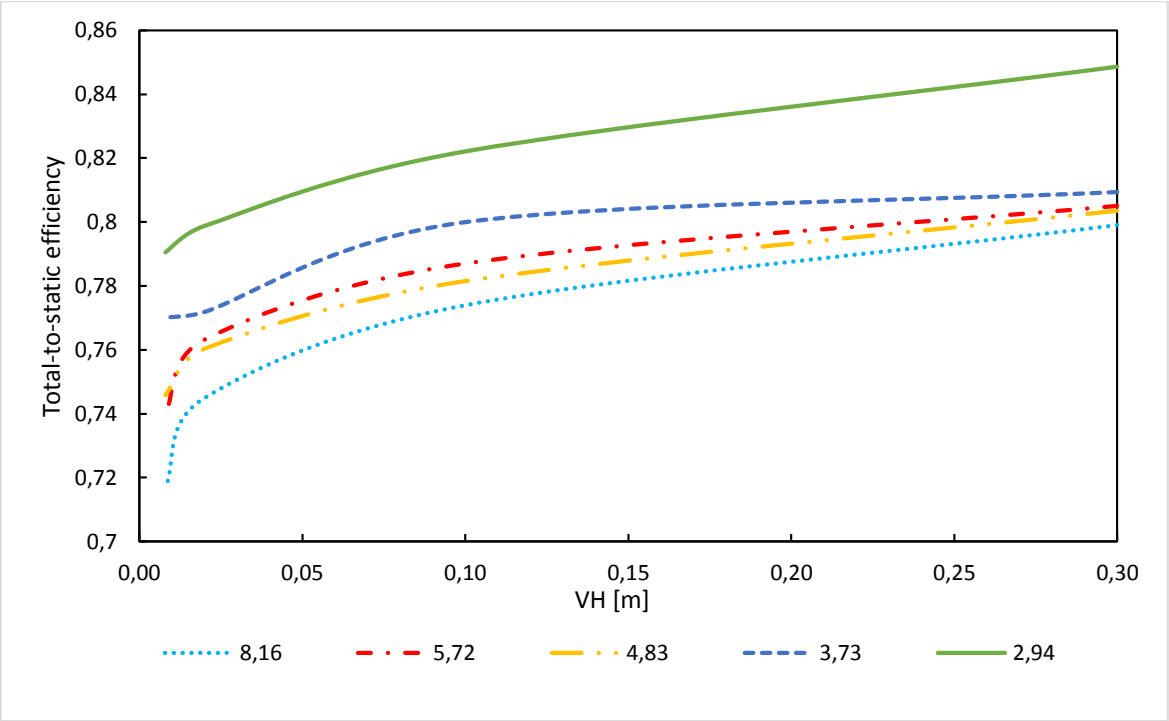

Figure 6.29 *Maximum achievable efficiency, as a function of size parameter, calculated for several values of volume expansion ratio.*

Analysis at non-optimum *Ns*

The procedure of design of radial turbo-expander had permitted to generate a large amount of data, not only in the best efficiency conditions, but also generally in different conditions linked to design parameters. Actually, in order to find the best design condition, many expander models based on different factors were simulated. This means that is now possible to expose an analysis of components, in not optimal design condition, when the specific speed is not the ideal one.

In fact, in real application, design constrains may impose non optimal specific speed: some of the classical reasons could be coupling with electric generator, or that the revolution speed derived by optimum *Ns* can be substantially higher than the maximum one imposed by technological constrains [65].

This analysis should be considered anyway as a design study, and not an off-design one. This means that the efficiency prediction at non-optimal *Ns* represent a procedure where the machine geometry

is created following the mean-line design proposed, but the constrictive condition does not allow to reach the maximum achievable efficiency condition.

In Figure (6.29) the total-to-static efficiency is shown calculated for a range of specific speed, for several design conditions of *VH* and *VR*.

The more the size is small (*VH* decreasing) and the more the best efficiency value occurs for smaller specific speed *Ns*, in particular for high volume expansion ratio. By these graphs is possible to note that in the range of *Ns* usually suggested by classical turbo-machines literature, the achievable efficiency can be largely penalized by the choice of a non-ideal *Ns*.

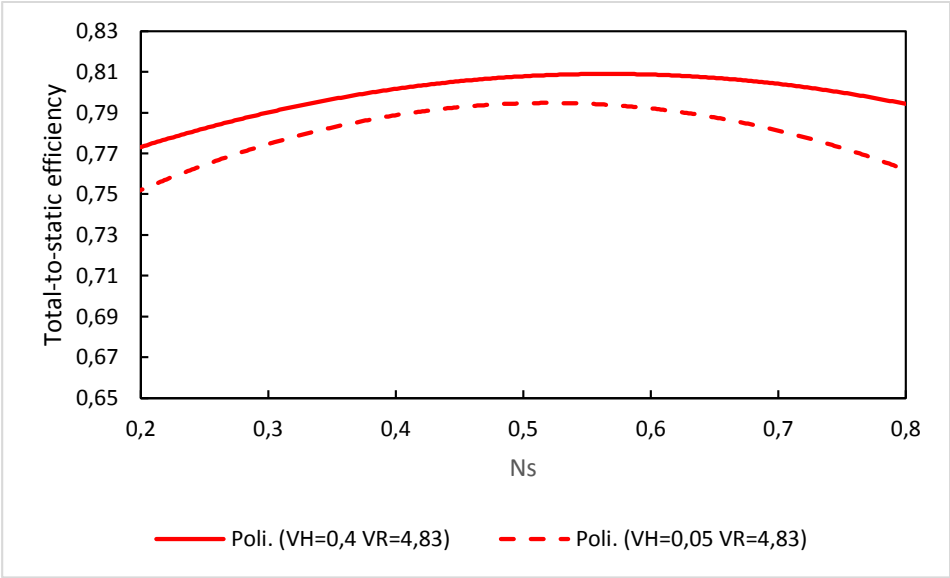

(a)

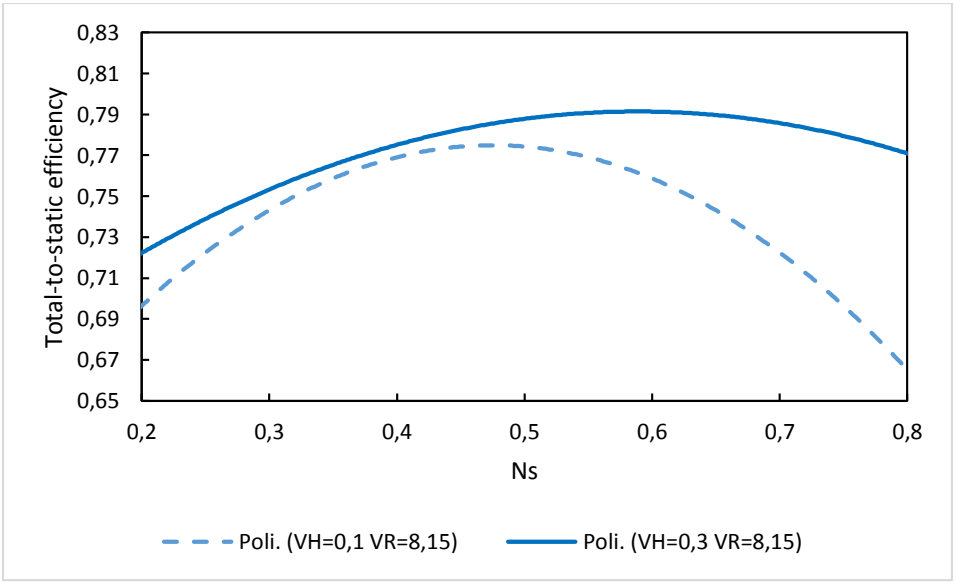

(b)

Figure 6.30 *Efficiency prediction for specific speed s different from optimum. In (a): VH=0.4, VR4.83 and VH=0.05, VR=4.83. In (b): VH=0.1, VR=8.15 and VJ=0.3, VR=8.15.*

The graph of Figure (6.31) has the aim to point out the incidence that each loss source presents at several specific speed, for a fixed design condition: *VH=0.3 m*, *VR=8.15*.

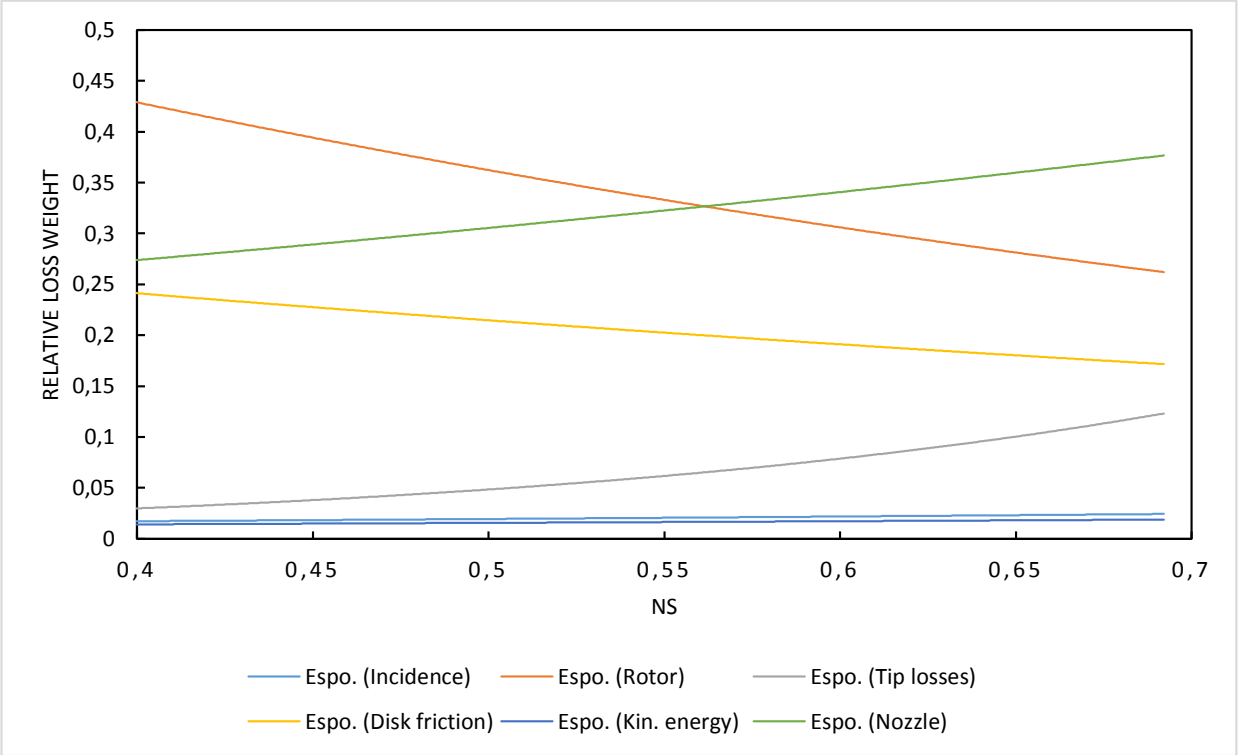

Figure 6.31 *Relative weight of loss sources, as a function of specific speed. The design parameters are VH=0.3m and VR=8.15.*

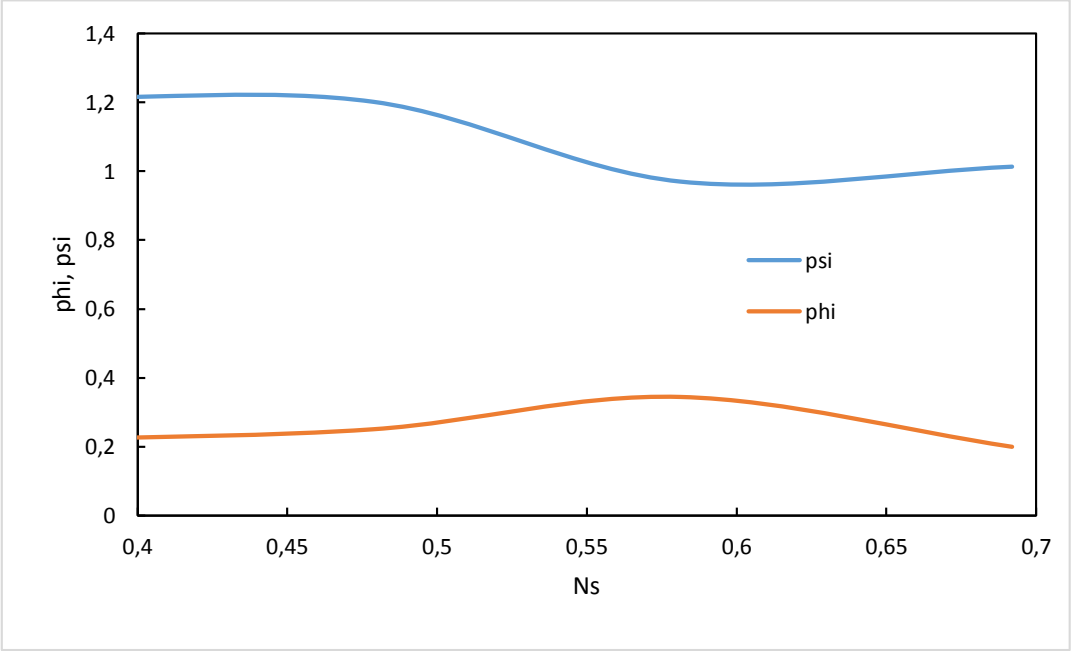

Figure 6.32 *Flow and load coefficients as functions of specific speed. The design parameters are VH=0.3m and VR=8.15.*

As shown, losses of kinetic energy and incidence have just a little weight related to the other sources; while nozzle and leakage losses increase at larger Ns, rotor and disk friction ones have a decreasing trend at larger *Ns*.

Smaller specific speed parameter leads to larger diameters, characterizing the expander geometry and performance. Indeed, with large r_4, the rotor loss, linked to the dissipation of relative kinetic energy, is supposed to decrease. On the other hand, in this condition, also the leakage mass flow rate has a lower weight in general losses definition; disk friction, instead, increases with *Ns* because of the higher speed of rotation.

Figure (6.32) shows for the same design conditions the variation of load and flow coefficients as functions of specific speed. It is to notice that reducing Ns, leads to expander with high ψ and small Φ. This permits in fact to avoid large diameters, aspect related to the already mentioned friction losses.

Chapter 7

Conclusions

A step-by-step design model of radial inflow turbines for Organic Rankine Cycles has been implemented in fluid dynamic computer-aided design code. An innovation over the traditional approach, which generally considered fluids as perfect gases, was the evaluation of real fluid properties in the expansion model. This is a focal point in preliminary design of ORC radial expanders, to evaluate the most appropriate geometry and to predict the achievable performances.

The analysis had the aim to make a step forward in project development compared to the classic similitude theory of turbomachines. In this direction, size parameter and volumetric flow rate ratio have been particularly considered as fundamental values, which strongly affect the geometry characteristics and the performances of the turbo expanders.

Considering *VH* and *VR*, it has been showed that in the analysed expanders' field, total-to-static efficiency ranges from 0.75 for highly loaded small turbines, to 0.89 for large turbines with small expansion ratios. In a similar way, also optimum specific speed has been evaluated, and it was noticed that it ranges from 0.42 to 0.52.

Optimum condition for flow and load coefficients has been demonstrated to be function of *VH* and *VR*. This can be considered an innovation, as many publications proposed design procedures where the suggested values of Φ and ψ were not optimized for heavy fluids, but elaborated for different applications.

An analysis of turbine performances in design condition at non-optimum specific speed has been also pointed out, analysing the efficiency decreases that occurs far from optimum *Ns,* and the dependence of this trend to expander size and compressibility.

The proposed model was performed considering as working fluid the Refrigerant 245fa, but can be easily extended to other fluids, provided that the required peripheral speed is within the technological

limitation imposed by centrifugal stresses; in fact, in order to obtain more general results, no peripheral speed limit was imposed in the investigation.

At the end of the performed analysis, three further studies can be suggested:

- An extension of the analysis to other fluids, especially heavy ones suitable for ORC applications;
- An experimental validation of the model proposed, which analyses in a more practical way the theoretical evaluation proposed. As it has been showed, the code is very flexible to modifications, as many relation are based on empirical coefficients that an experimental setup could improve;
- An implementation of the results in a model to predict the performances of a whole ORC plant utilising radial expanders; in this way it would be possible to evaluate a true turbine efficiency, variable depending on *VH* and *VR*. This would provide a more precise cycle optimization.

Bibliography

[1] Quoilin S. - Sustainable Energy Conversion Through the Use of Organic Rankine Cycles for Waste Heat Recovery and Solar Applications. PhD Thesis. University of Liège, Belgium; 2011

[2] Bao J., Zhao L. - A review of working fluid and expander selections for organic Rankine cycle. Renewable and Sustainable Energy Reviews 2013, 24: 325-342

[3] Bianchi M., De Pascale A. - Bottoming cycles for electric energy generation: parametric investigation of available and innovative solutions for the exploitation of low and medium temperature heat sources, Applied Energy, 2011, 88: 1500-1509

[4] Turboden web site, < http://www.turboden.eu/it/home/index.php>, last access 04/2014

[5] Branchini L., De Pascale A., Peretto A. – Systematic comparison of ORC by means of comprehensive performance indexes, Applied Thermal Engineering, 2013

[6] Karellas S., Schuster A., Leonaritis A.D. - Influence of supercritical ORC parameters on plate heat exchanger design, Applied Thermal Engineering, 2012, 33: 70-76

[7] Schuster A., Karellas S., Kakaras E., Spliethoff H., Energetic and economic investigation of Organic Rankine Cycle Applications, Applied thermal engineering, 2009, 29:1809-1817

[8] Vescovo R. – ORC recovering industrial heat, Cogeneration and On-Site Production, 2009, 53-57

[9] Wang D., Ling X., Peng H., Liu L., Tao L. – Efficiency and optimal performance evaluation of ORC for low grade waste heat power generation, Energy, 2013, 50: 343-352

[10] Lazzaretto A., Manente G. – A criterion to optimize ORC design performance taking into account real turbine efficiencies, Proceedings of ECOS, Guilin; RC, 2013

[11] Moustapha H., Zelesky M.F., Baines N.C., Japikse D., - Axial and Radial Turbines, Concepts NREC, 2003

[12] Whitfield A., Baines N.C. – Design of radial turbomachines, Longman Scientific and Technical, New York, USA, 1990

[13] Dixon S.L., Hall C.A., Fluid mechanics and thermodynamics of turbomachinery, Butterworth Heinemann, sixth edition, 2010

[14] Chen H., Baines N.C. – The aerodynamic loding of radial and mixed flow turbines, International Journal of Machanic Science, 1994, 36: 63-79

[15] Sauret E., Rowlands A.S. – Candidate radial-inflow turbine and high-density working fluids for geothermal power systems, 2011, Energy, 36: 4460-4467

[16] RITAL, Concepts NREC, <http://www.conceptsnrec.com/Solutions/CAE-CAM-Software/CAE-Software/Radial-Turbines.aspx>

[17] Baljè O.E. – Turbomachines: A Guide to Design, Selection, and Theory, Jhon Wiley and Sons, New York, 1980

[18] Macchi E. - Design criteria for turbines operating with fluids having a low speed of sound, Lecture Series 100, Von Karman Institute for Fluid Dynamics, 1977

[19] Macchi E., Perdichizzi A. - Efficiency prediction of Axial-Flow Turbines operating with non-conventional Fluids, ASME Journal of Engineering for Gas Turbines and Power, 1981, 103: 718-724

[20] Perdichizzi A. - Criteri di ottimizzazione di uno stadio di turbina assiale, Milano

[21] Angelino G., Gaia M., Macchi E. – A review of Italian activity in the field of Organic Rankine Cycles, International VDI-Seminar, Zürich, CH, 1984

[22] Cantore G. - Macchine, Progetto Leonardo, Bologna, 1999

[23] Pini E., Persico G., Casati E., Dossena V. - Preliminary design of a centrifugal turbine for ORC applications, First International Seminar on ORC Power Systems, Delft, NL, 2011

[24] Kang S.H. - Design and experimental study of ORC (organic Rankine cycle) and radial turbine using R245fa working fluid, Energy, 2012, 41: 514-524

[25] Craig H.R.M., Cox H.J.A. – Performance estimation of Axial Flow Turbines, Proceeding of the Institution of Mechanical Engineers, 1971, 185: 407-423

[26] Baliè O.E., Binsley R.L. – Axial Turbine Performance Evaluation Part B; Optimization with and without Constraints, ASME Journal of Engineering for Gas Turbines and Power, 1968, 90: 341-348

[27] Perdichizzi A., Lozza G. – Design Criteria and Efficiency for Radial Inflow Turbines, Gas Turbine Conference and Exhibition, Anaheim CA, USA, 1987

[28] Civinkas K.C., Povinelli L.A. – Application of a Quasi-3D Inviscid Flow and Boundary Layer Analysis to the Hub Shroud Contouring of a Radial Turbine, AIAA/SAE/ASME Joint Propulsion Conference, 1984

[29] McLallin K.L., Haas J.E. – Experimental Performance and Analysis of 15.04 Tip Diameter Radial Inflow Turbine with Work Factor of 1.126 and Thick Blading, NASA Tech., 1980

[30] Fiaschi D., Manfrida G., Maraschiello F. – Thermo-fluid dynamics prelminary design of turbo-expanders for ORC cycles, Applied Energy, 2012, 97: 601-608

[31] F-Chart Software. <http://www.fchart.com/ees/>

[32] Marcuccilli F., Zouaghi S. – Radial Inflow Turbines for Kalina and Organic Rankine Cycles, Proceedings European Geothermal Congress, Unterhaching, DE, 2007

[33] Bambang Teguh P., Suyanto, Taufan Surana, Panca Kurniawan, Euis Djubaedah, Kornel Ola - Design of n-Butane Radial Inflow Turbine for 100 kW Binary Cycle Power Plant, International Journal of Engineering and Technology, 2011, 11: 55-59

[34] Aungier R.H. - Turbine Aerodynamics-Axial flow and Radial Flow Turbine Design, New York, 2006

[35] Kang S.H. - Design and experimental study of ORC (organic Rankine cycle) and radial turbine using R-245fa working fluid, Energy, 2012, 41: 514-524

[36] Saleh B., Koglbauer G., Wendland M., Fischer J. - Working fluids for low temperature organic Rankine cycles, Energy, 2007, 32: 1210-1221

[37] Tchance B.F., Papadakis G., Lambrinos G., Frangoudakis A. - Fluid selection for a low temperature solar organic Rankine cycle, Applied Thermal Engineering2009, 29: 2468-2456

[38] Wang X.D., Zaho L. - Analisys of zeotropic mixtures used in low temperature solar Rankine cycles for power generation, Solar Energy, 2009, 83: 605-613

[39] Sun J., Li W. - Operation optimization of an Organic Rankine cycle heat recovery power plant, Applied Thermal Engineering, 2011, 31: 2032-2041

[40] Zhang N., Cai R., - Analytical solution and typical characteristic of a part-load performances of single shaft gas turbine and its cogeneration, Energy Conversion and Management, 2002, 43: 1323-1337

[41] Aspen Plus, Aspentech, < https://www.aspentech.com/products/aspen-plus.aspx>

[42] Matlab, Mathworks, http://www.mathworks.it/products/matlab, version R2010a

[43] NIST Reference thermodynamic and transport properties database (REFPROP), www.nist.gov/srd/nist23.cfm, version 8.0

[44] Rodgers C. – Mainline performance prediction for radial inflow turbines, Lecture Series 1987-07, Von Karman Institute for Fluid Dynamics, 1987

[45] Rohlik H.E. – Radial inflow turbines, Turbine design and applications, NASA SP 290 vol. 3, 1975.

[46] Yeo J.H., Baines N.C. – Pulsating flow behavior in a twin-entry vaneless radial inflow turbine, Turbocharging and Turbochargers, IME, 1990

[47] Benson R.S. – A review of methods for assessing loss coefficients in radial gas turbines, Internal Journal of Mechanical Science, 1970, 18: 905-932

[48] Rodgers C., Geiser R. – Performance of a high efficiency radial/axial turbine, ASME Journal of Turbomachinery, 1987, 109: 151-154

[49] Barnard M.C.S., Benson R.S. – Radial gas turbines, Proceedings of IME, 1968, 183: 59-70

[50] Chapple P.M., Flynn P.F., Mulloy J.M. – Aerodynamic design of fixed and variable geometry nozzleless turbine chasing, ASME Journal of Engineering for Power, 1980, 102: 141-147

[51] Jansen W. – The design and performance analysis of radial inflow turbines, NREC Report 1067, 1964

[52] Hiett G.F., Johnston I.H. – Experiments concerning the aerodynamic performance in inward radial flow turbines, Proceeding of the Institution of Mechanical Engineers, 1963, 178: 28-42

[53] Japikse D., Baines N.C., - Introduction to Turbomachinery, Concepts ETI, 1997

[54] Lazzaretto A., Del Col D. – Modello monodimensionale di previsione delle prestazionei fuori progetto di una turbine radiale, 50° Congresso ATI, St. Vincent, IT, 1995

[55] Woolley N.H., Hatton A.P. – Viscous flow in radial turbomachine blade passages, Proceeding for Institution of Mechanical Engineers Conference, 1973

[56] Futral S.M., Wasserbauer C.A. – Off-design performance prediction with experimental verification for a radial-inflow turbine, NASA TN D-2621, 1965

[57] Todd C.A., Futral S.M. – A FORTRAN IV program to estimate the off-design performance of radial-inflow turbines, NASA TN D-5059, 1969

[58] Wasserbauer C.A., Glassman A.J. - FORTRAN program for predicting the off-design performance of radial-inflow turbines, NASA TN 8063, 1975

[59] Stanitz J.D. – Some theoretical aerodynamic investigations of impellers in radial and mixed flow centrifugal compressors, trans. ASME, 1952, 74: 473

[60] Rodgers C. – A cycle analysis technique for small gas turbines, Proceedings of IME, 183 part 3N, 1968

[61] Spraker W.A. – Contour clearance losses in radial inflow turbines for turbochargers, ASME paper No 87-ICE-52, 1987

[62] Daily J.W., Nece R.E. – Chamber dimension effects on induced flow and frictional resistance of enclosed rotating disks, ASME Journal of Basic Engineering, 1960, 82: 217-232

[63] Nemdili A., Hellmann D.H. – Development of an empirical equation to predict the disc friction losses of a centrifugal pump, Proceedings of the 6th International Conference on Hydraulic Machinery and Hydrodynamics, Timisoara, RU, 2004

[64] Japikse D., Pampreen R. – Annular diffuser performance for an automotive gas turbine, ASME Journal of Engineering for Power, 1979, 101: 358-372

[65] Lozza G., Macchi E., Perdichizzi A. – Investigation on the efficiency potential of small steam turbines of various configurations, Proceedings of the 21st IECEC, San Diego CA, USA, 1986

Acknowledgements

I would like to thank Prof. Andrea Lazzaretto, who gave me the opportunity to start this Thesis and provided constructive advices along the work. Thanks to his agreement with Professor George Tsatsaronis from TU-Berlin, which gave me the occasion to develop large part of the Thesis in Germany, spending six wonderful months in Berlin.
I am also grateful to Ing. Giovanni Manente, for his fundamental help and support during the whole period of this work. I wish to thank him for the numerous hours spent discussing together, mainly via Skype, about theoretical issues, and for the precious help in reviewing the Thesis.
Thanks also to Prof. Tatjana Morozjuk from TU-Berlin, for her warm welcome in Berlin and for her helpful suggestions and constructive criticism.

This Thesis signs the end of a long period of my life, the period of scholar formation. But every End, takes with it a new beginning, and I feel myself ready to face every kind of new challenges.

Nothing would have never been possible without the unconditional support of my parents, who with their love and suggestions gave me the best means and conditions to face life and studies. Thanks to all my family, and in particular to my grandmothers, because their strength is an inspiration.
Thanks to Rita, who seven years ago choose to share her life with me. Being always by my side, she gave me the force to grow, and she is still doing. Thanks to her family, for their precious suggestions and for accepting me as a son. Thanks to Chiara and Attilio, more than friends, who gave me the chance to learn the importance of the work.
Thanks to the friends of yesterday and of today, hoping that our ways will be intertwined in the future too. The guys of the Contrada San Giacomo, friends from longer time, with who I spent most of my youth: Alessandro, Fabio, Giuseppe, Luca, Andrea (Tony) and all the others. Thanks to the Friends, with capital F, the one I cannot miss in my future, Eleonora, Filippo, Gianluca and Stefano. Thanks to my flatmates in Berlin, Francesco, Manuel and Cielo, and all the new friends I found in that incredible city, for the magic moments we spent together. And last but not least, thanks to Michele and Daniele, for their help in these two years of hard study in Padova.
Thanks. And rock on.